





**UNIVERSITÀ DEGLI STUDI DI PARMA**

Dipartimento di Chimica

Ph.D. in Science and Technology of Innovative

Materials

XXVI Cycle

**Supramolecular materials for  
sensing**

Jakub Waldemar Trzciński



Coordinator: **Prof. Enrico Dalcanele**

Supervisor: **Prof. Enrico Dalcanele**

Tutor: **Dr. Roberta Pinalli**

Author: **Jakub Waldemar Trzcíński**



*Mojej Miłości - Paulinie*  
*dziękując za wsparcie i bezgraniczną miarę*  
*oraz mej Rodzinie*



## Contents

# Chapter 1

## General Introduction: Supramolecular sensors

1.1. Chemical sensors.....	1
1.2. The stand-alone mini-GC system for VOCs detection.....	4
1.3. Fluorescent chemical sensors .....	8
1.4. The Metal Oxide transducers .....	11
1.5. The Photo Ionization Detector .....	12
1.6. Cavitand as supramolecular receptors .....	14
1.6.1. Phosphonate-bridged cavitands.....	15
1.6.2. Quinoxaline-bridged cavitands .....	17
1.7. References .....	21

# Chapter 2

## Design and synthesis of novel QxBox receptors for Benzene detection in air

2.1. Introduction.....	26
2. 2. Selective recognition event within tetraquinoxaline cavitands.....	27
2.3. Design and synthesis of new rigid QxBox receptors .....	30
2.3.1. Synthesis of the 2,3-dichloro-5,8-dimethoxy quinoxaline bridging unit.....	30
2.3.2. Synthesis of conformationally blocked QxBox cavitands .....	32
2.4. X-ray Crystallographic Studies .....	36
2.5. Analytical measurements .....	45
2.5.1. The thermo gravimetric analysis of the QxBox receptors.....	45



2.5.2. The SPME measurements .....	47
2.6. The stand-alone mini-GC system for VOCs detection.....	56
2.7. Fluorescent measurements .....	61
2.8. Conclusions and perspectives.....	63
2.9. Acknowledgments.....	64
2.10. Experimental part .....	65
2.10.1. Synthesis of the QxBox receptors .....	65
2.10.2. X-Ray analysis .....	69
2.10.3. Solution preparation.....	71
2.10.4. SPME Sampling.....	71
2.10.5. GC-MS analysis.....	71
2.11. References .....	73

## Chapter 3

### **QxCage: The ultimate approach for Benzene detection in air**

3.1. Introduction .....	76
3.2. Synthesis of new QxCage receptor .....	77
3.2.1. Synthesis of 2,3-dichloro-6,7-dimethoxyquinoxaline bridging unit .....	78
3.2.2. QxCage cavitand synthesis: the direct approach.....	79
3.3. X-ray crystallographic studies.....	83
3.4. The thermo gravimetric analysis.....	85
3.5. Conclusions and perspectives .....	86
3.6. Acknowledgments .....	87
3.7. Experimental part.....	88

# Chapter 4

## Water soluble Phosphonate cavitands

4.1. Introduction.....	94
4.1.1. Water-soluble cavitands .....	95
4.2. The complexation properties of tetrakisphosphonate cavitands .....	100
4.3. Design and synthesis of water-soluble Tiiii cavitands .....	104
4.3.1. The TEG-tetrakisphosphonate cavitand .....	105
4.3.2. Synthesis of TEG-phosphonic dichloride .....	106
4.3.3. Bridging reaction between TEG-phosphonic-dichloride and the resorcinarene .....	107
4.4. The tetraamino-tetrakisphosphonate cavitand .....	111
4.5. Conclusions and perspectives .....	116
4.6. Acknowledgements .....	116
4.7. Experimental part .....	117
4.8. References .....	122

# Chapter 5

## Lanthanides inclusion in molecular containers

5.1. Introduction.....	126
5.2. Principles of luminescence .....	126
5.2.1 The Lanthanide ions properties .....	128
5.2.2. The antenna effect.....	131
5.2.3. The supramolecular approach .....	133
5.3. Results and discussions.....	136
5.3.1. Hydrophobic driven encapsulation .....	137
5.3.2. The phosphonate cavitands as potential ligands for lanthanide complexation.....	141
5.3.3. Solvent free encapsulation in coordination cages .....	150

5.4. Conclusions.....	155
5.5. Acknowledgements .....	157
5.6. Experimental section.....	158
5.7 References.....	164
Appendix A.....	169
The author .....	173



General Introduction:  
Supramolecular sensors

*1*

## 1.1. Chemical sensors.

Sensors were created by Nature well before humans appear on Earth, both those converting the external physical signals into a chemical one further transferring them into a living organism like: light, temperature or touch, or those based on the “lock-and-key” molecular recognition taking place into a living systems like: enzymes or antibodies. Nowadays, chemical sensing is a hot topic because of the many different monitoring demands of under which chemical sensor can be defined as a device that transforms chemical informations, ranging from the concentration of a specific sample component to total composition analysis, into an analytically useful signal.<sup>1</sup> In Figure 1 the basic principles of chemical “sensing” is shown.

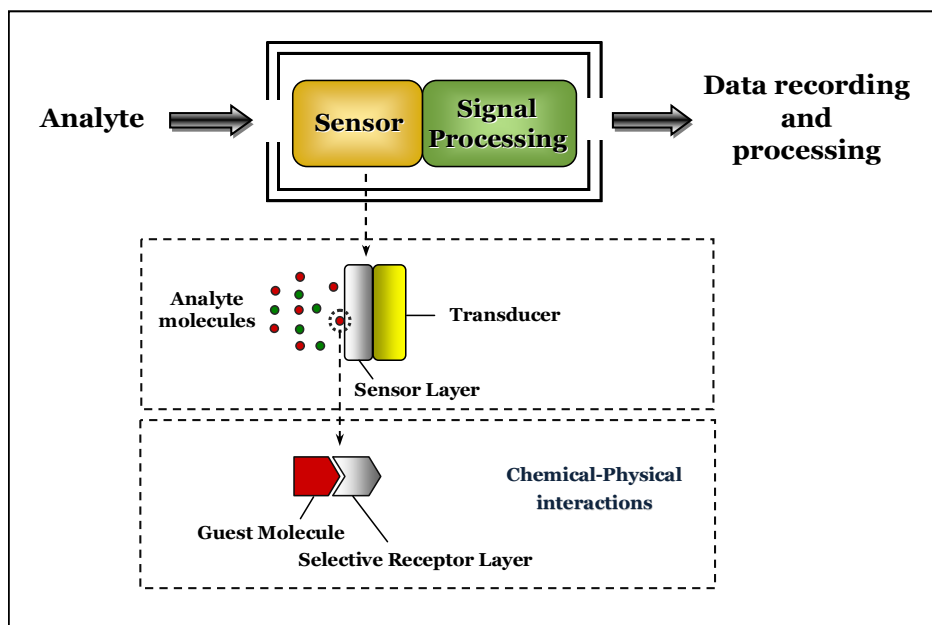


**Figure 1.** The sensing process based on a chemical sensor. The lower part highlights the “supramolecular sensing” approach.

The transform of the chemical information is part of process named “acquisition” where informations on the chemical composition of a system are obtained in real time. The acquisition process, itself, can be divided in two

separated steps: (1) recognition - which is carried by a sensing material that presenting affinity toward desired analyte and (2) amplification - which is provided by a transducer, and which transforms the chemical information into an analytically useful signal. Is worth to mention, that chemical signal transducers are often separated from the sensing layer by the analytical instruments like GC columns etc.. The recognition process is based on specific interaction between two or more molecules through non-covalent bonding such as: hydrogen bonds, metal coordination, hydrophobic forces, van der Waals forces,  $\pi$ - $\pi$  interactions, halogen bonding, electrostatic and/or electromagnetic effects. Each sensor can be characterised by three properties: *sensitivity*, *selectivity* and *reversibility*.

*Sensitivity* - is correlated with the magnitude of the change in the sensor signal upon a certain change in the analyte concentration represented by the change of the slope of the analytical calibration curve.<sup>2</sup> "Cross sensitivity" hence refers to the contributions of other than the desired compound to the overall sensor response.

*Selectivity* - is instead, the ability of a sensor to respond primarily to only one chemical species in the presence of other species (usually denoted interferents). The bigger selectivity can be achieved by the use of molecules characterised by the affinity toward specific targets like: enzymes or antibody-antigen complex.<sup>3</sup>

*Reversibility* - is the sensor ability to return to its initial state after exposure to the analyte. The reversibility requires the involvement of weak interactions, since the formation of covalent or ionic bonds would result in an irreversible saturation of the sensing layer.<sup>4</sup>

These entire characteristic (*selectivity*, *sensitivity* and *reversibility*) are determined by the thermodynamics and kinetics of sensor material-analyte interactions. The sensitivity with the selectivity are characteristic to the strong interactions between sensor and the analyte, while reversibility is associated to the weak,

reversible, interactions ( $\sim 60 \text{ kJ mol}^{-1}$ ).<sup>4</sup> Therefore, it is necessary to find a compromise in receptor design balancing between high selectivity and reversibility.

The conventional “lock-and-key”<sup>5</sup> approach for selective chemical sensors design is based on the synthesis of a specific receptor wherein the analyte of interest is bound selectively.<sup>6</sup> To create this specificity is necessary to exploit molecular recognition between two species that complement one to another in size, shape and functionality. As the concepts of shape recognition and binding site complementarity for biological systems are fundamentals for effective molecular recognition in artificial host-guest systems while transferring them to the solid state is very difficult to remain with high binding constants. The “lock-and-key “ concept works successful in the liquid phase, therefore can not be automatically transferred to vapour and gas sensing due to two major obstacles:

- moving from the vapour to the condensed phase the analyte experiences a dramatic increase in aspecific dispersion interactions, negligible in liquid to solid transfer;<sup>7</sup>
- the entropic cost for binding to the receptor is not alleviated by solvent release in the bulk liquid phase.<sup>8</sup>

For these reasons achieving effective molecular recognition at the gas-solid interface is a demanding task, which requires a fresh approach, both in terms of receptor design and characterization tools.

## **1.2. The stand-alone mini-GC system for VOCs detection.**

The selective detection of benzene, the most dangerous of aromatic VOCs, due to its known harmful influence on human body; breathing high levels of benzene can result in death, while low levels can cause drowsiness, dizziness, unconsciousness, or until long-term exposition leukemia, is a difficult issue due to the big amount of interferences which entail use of high ended laboratory equipment in air quality control. Therefore, thanks to a cooperation with Dr. Stefano Zampolli from CNR-Bologna, a mini GC portable device was



designed<sup>9</sup> which contains: a pre-concentrator filled with the molecular receptor for selective complexation of analytes from sampled air, the mini GC column for entrapped analytes separation, the MOX or PID sensor as the transducers of the molecular recognition event, the zero-grade air supplier and the hi-end driver electronics. The disassembled prototype system with all the components is shown in Figure 2 together with a 1 euro coin, for size comparison.

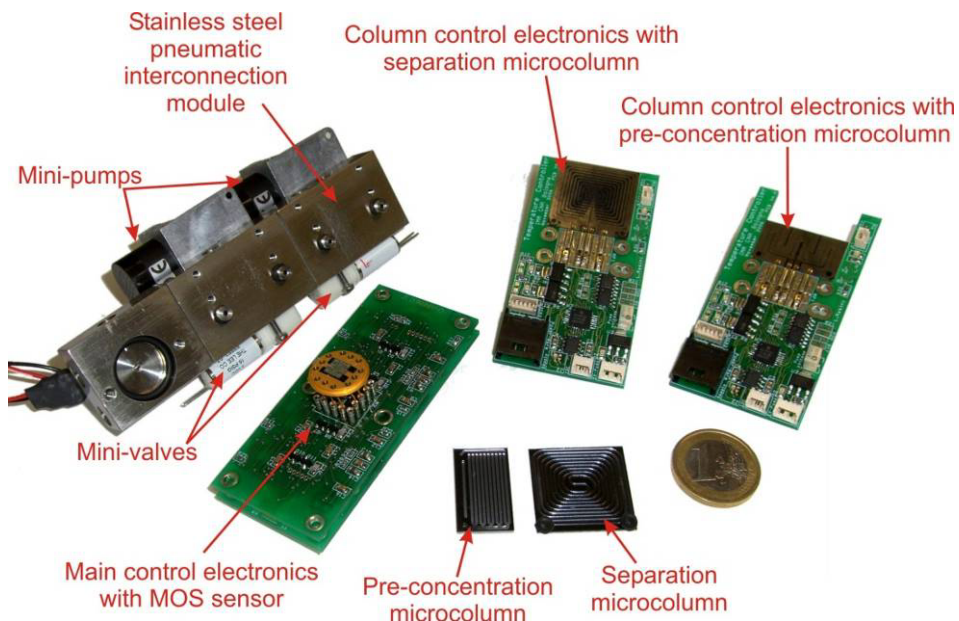


**Figure 2.** The setup of the mini-GC system for VOCs detection. The 1€ coin is included for size comparison.

The pre-concentration unit was made in silicon via Advanced Silicon Etching (ASE) technique and it consists of ten parallel columns; this geometry enables the best adsorption/desorption efficiency because the path of the analytes is shorter than in a single long column.

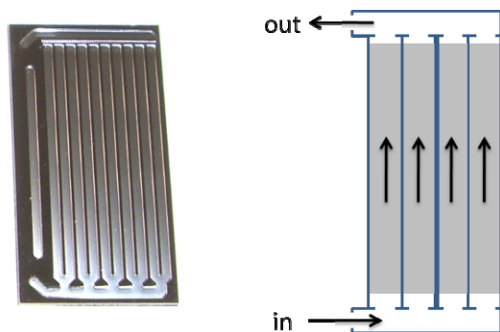


**Figure 3.** The pre-concentration unit (left) and its graphical representation (right).

The pre-concentration unit is attached to the platinum plate able to ramp conductive heating, controlled by the custom electronic interface directly connected to a PC. The pre-concentration principles are presented in Figure 4 below.

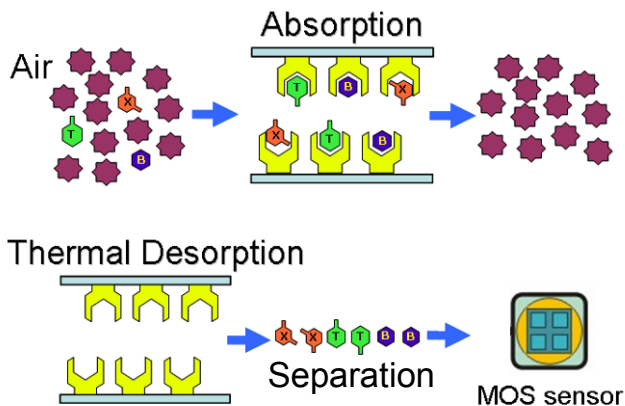


**Figure 4.** The schematic sensing protocol of the mini-GC system.

The air is pumped for a certain amount of time through the pre-concentration unit, filled with the molecular receptor. This promotes the selective host-guest recognition and the complexation of the target VOC molecules inside the receptor cavity. Afterwards, the pre-concentrator is heated in order to release

the entrapped analytes, which are consequently separated in the mini-GC column.

The mini-GC column, used for the separation step in presented in the Figure 5 below.

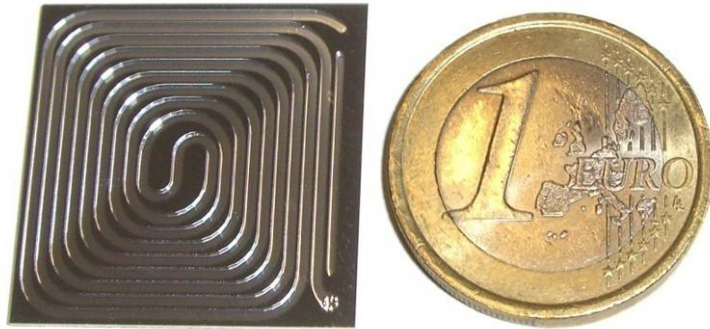


**Figure 5.** *The mini-GC column together with a 1€ coin for size comparison.*

The spiral-shaped channel of the mini GC column (cross sectional area of 0.8 mm<sup>2</sup> and length of 50 cm) was realized by ASE (850 μm of dept) on a 1 mm thin polished fused silicon wafer. The column, as pre-concentrator, was equipped with a platinum heater on the bottom side of the wafer for the desorption temperature control. The gas inlet and outlet was bonded to the Si wafer as Pyrex pre-formed drillings. For the operating mode the GC column was filled with a commercial packed gas chromatographic stationary phase.

The system was equipped with two pumps (KNF NMP09), a zero grade air generator (activated carbon mesh) and commercial 3-way microvalves for gas flow control. All these components were assembled on a stainless steel board and connected to specifically designed control electronics, fabricated using small footprint stacked SMD PCBs. The system does not require any external inert gas cylinder, since the carrier gas is generated directly on-board.

The MOX sensor is a Si-micromachined thin film, where the sensing layer was deposited by a sputtering process on a SiN<sub>4</sub> membrane using a thin gold

catalyst layer. A fixed voltage ( $U=1,2V$ ) and temperature ( $400^{\circ}C$ ), which was found to be the best temperature for aromatic VOCs detection, were used. The whole assembled system is reported in Figure 6.



**Figure 6.** Photograph of the complete monitoring system with a pencil for size comparison.

### 1.3. Fluorescent chemical sensors.

Among the different chemical sensors, those based on fluorescence presents many advantages: are very sensitive (even single molecule detection is possible, under special conditions), low cost, easily performed, versatile, offering subnanometer spatial resolution with submicron visualisation and submillisecond temporal resolution.<sup>10</sup> Its versatility originates from the wide number of parameters that can be tuned in order to optimise the convenient signal. The strict control of the excitation and emission wavelengths, the signal time window collection, and the polarisation of the excitation beam or of the emitted light can help to overcome even very complex analytical problem.

The main issue in effective chemosensor design is the association of a selective molecular recognition event which is further transduce into a highly sensitive physical signal.<sup>11</sup> Often, the chemical sensors work in the sense of dye displacement upon recognition event, therefore the receptor is required for selective binding of the substrate, while the fluorophore provides the means of signaling this binding, whether by fluorescent enhancement or inhibition. Simplifying, emission of a photon, fluorescence, follows HOMO to LUMO excitation of an electron in a molecule. Vibrational deactivation of the excited state prior to emission usually gives rise to a “Stokes shift” in that the wavelength of the emitted radiation is less than that of the exciting one. Various other interactions may also modify the emission process, and these are of considerable importance in regard to analytical applications of fluorescence.<sup>12</sup>

The substrate binding include the changes into a molecule like: photoinduced electron transfer (PET),<sup>13</sup> photoinduced charge transfer (PCT),<sup>12</sup> fluorescence (Förster) resonance energy transfer (FRET),<sup>12</sup> and excimer/exciplep formation or extinction which are the control mechanisms of the fluorophore response.<sup>12</sup>

The response in a PET sensor is induced upon excitation of the fluorophore, where one of its electron in the highest occupied molecular orbital (HOMO) is promoted to the lowest unoccupied molecular orbital (LUMO). This change enables photoinduced electron transfer from the HOMO orbital of the donor to that of the fluorophore and causes fluorescent quenching of the latter. Upon analyte binding the relevant HOMO of the donor becomes lower in energy than that of the fluorophore (Figure 7).

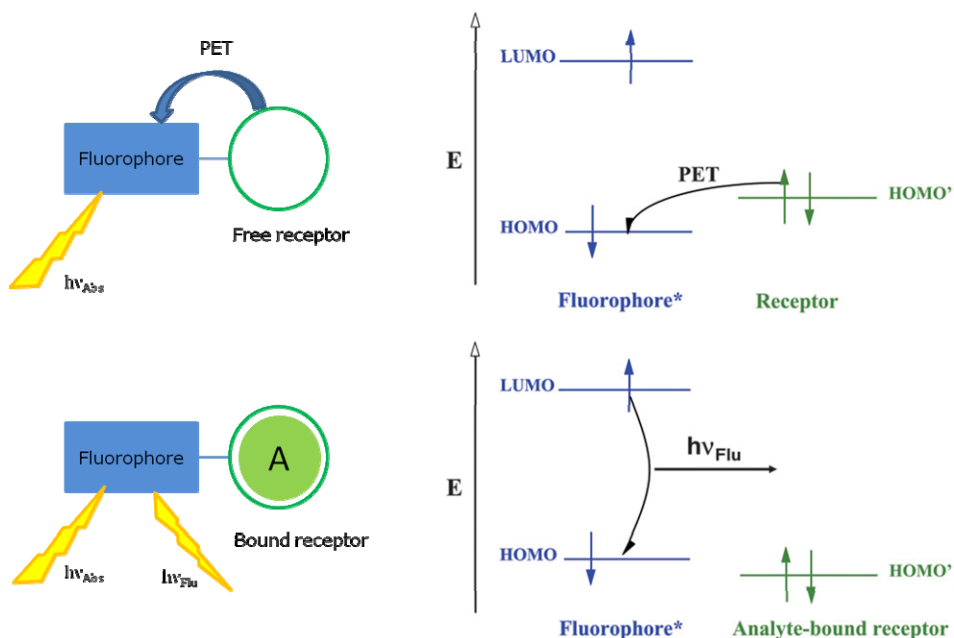


**Figure 7.** The photoinduced electron transfer (PET) mechanism.

Consequently PET is not possible anymore and fluorescent quenching is suppressed, in other words, fluorescent intensity is enhanced upon analyte binding.<sup>13</sup>

In the case of the PCT sensor, the fluorophore incorporate an electron-donating group, conjugated to an electron-withdrawing group. In fluorophores containing both electron-withdrawing and electron-donating substituents, the charge transfer may occur over long distances and can be associated with major dipole moment changes, making the process particularly sensitive to the microenvironment surrounding the fluorophore. Thus, it can be expected that analytes in close interaction with the donor or the acceptor moiety will change the photophysical properties of the fluorophore.<sup>12</sup>

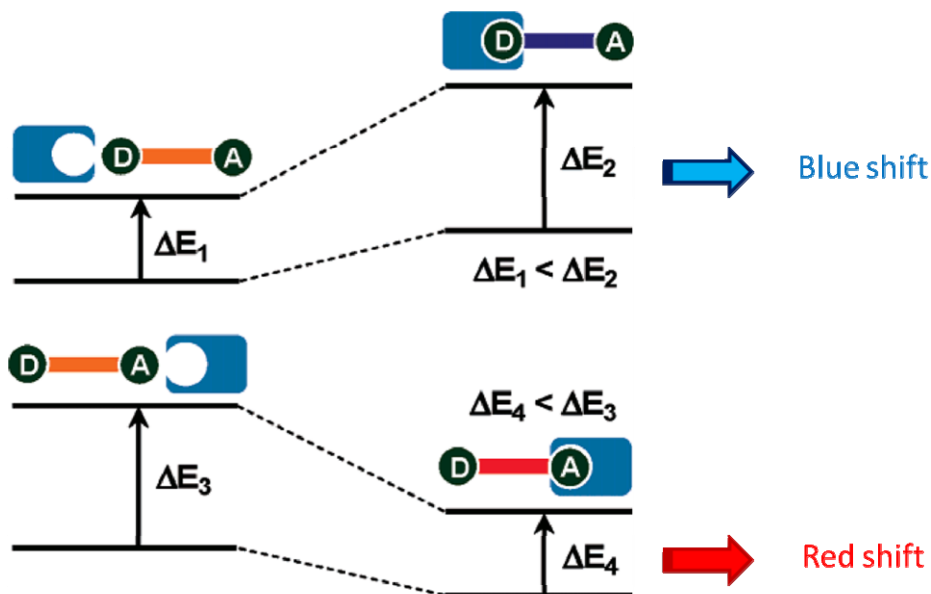


**Figure 8.** The photoinduced charge transfer (PCT) process.

As shown on the Figure 8, upon analyte complexation of an electron donor group within a fluorophore, the electron-donating character of the donor will be reduced, resulting in reduction of conjugation. This change causes a blue shift of the absorption spectrum together with a decrease of the molar absorptivity. In the case when analyte binds to the acceptor group enhances its electron withdrawing character the absorption spectrum is promoting a red-shifted with an increase in molar absorptivity. The fluorescence spectra should be shifted in the same direction as the absorption spectra, and in addition to these shifts, changes in the quantum yields and lifetimes can be observed.

#### 1.4. The Metal Oxide transducers.

Thin-film Metal Oxide Semiconductor (MOX) gas sensors are characterized by high sensitivity and fast response. As shown in Figure 9, the MOX sensor consists of an active layer of material oxide (usually  $\text{SnO}_2$ ) which is deposited on two metal electrodes which are able to perform the measurement of the active layer resistance. On the other side of the substrate a thin metal film

layer (platinum) is deposited, and by the resistance heats up the sensor to the desired operating temperature (commonly the range of 300-400°C).

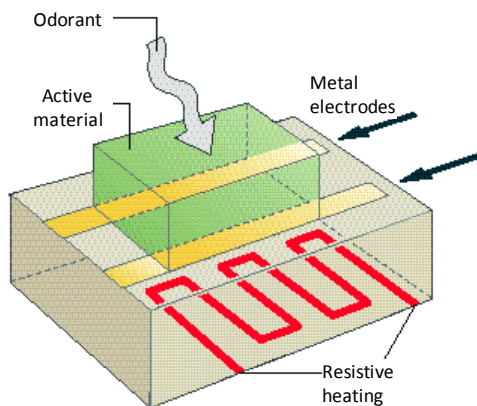


**Figure 9.** Schematic illustration of a metal oxide (MOX) sensor.

The change of the temperature promotes the chemical reactions on the surface of the active MO layer creating the variation of conductivity in presence of oxidizing and reducing gases. The adsorption and desorption of  $O^-$  and  $O^{2-}$  changes the electron density at the semiconductor surface. Adsorbed oxygen gives rise to potential barriers at grain boundaries and thus increases the resistance of the sensor surface. In the case of reducing gasses the oxygen ion surface concentration decrease is observed and therefore, the sensor surface resistance decrease as well. The magnitude of the response depends on the nature and concentration of the volatile molecules, and on the type of used metal oxide. Despite their well-established use, some potential applications of MOX are still out of reach due to low selectivity, the low steady state stability, and the temperature dependent behavior.

### 1.5. The Photo Ionization Detector.

A Photo Ionization Detector (PID) is the transducer which uses an Ultraviolet light (UV) source to break down chemicals to positive and negative ions (ionization) that can be easily counted with a detector (Figure 10).



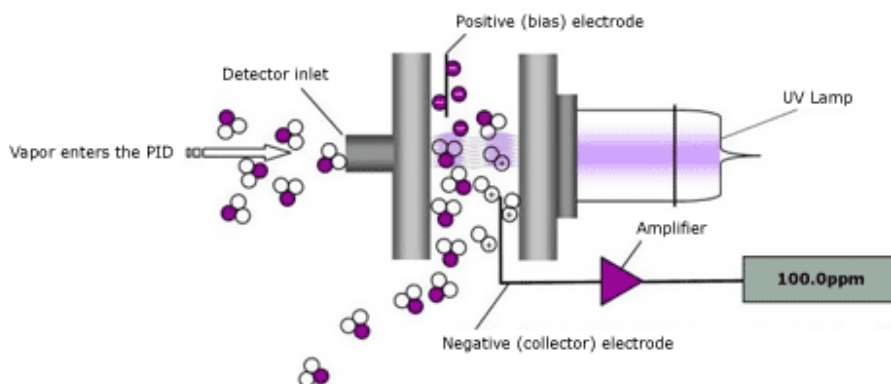


**Figure 10.** *The photo ionization detector (PID) sensor – principles of work<sup>14</sup>*

Ionization occurs when a molecule absorbs the high energy UV light, which excites it, resulting the temporary loss of a negatively charged electron and the formation of positively charged ion. It is worth to mention, that all elements and chemicals can be ionized, but they differ in the amount of energy they require. The energy required to displace an electron and ionize a compound is called its Ionization Potential (IP), measured in electron volts (eV). The light energy emitted by an UV lamp is also measured in eV. If the IP of the sample gas is less than the eV output of the lamp, then the sample gas will be ionized. When a gas molecule interacts with the UV irradiation becomes electrically charged. In the detector surface these charged particles produce a current that is then amplified to the ppm or ppb level. After ionization the ions quickly recombine after to their original molecule composition making PID analysis non-destructive technique. The PID detector can be used to “sense” wide range of the chemicals like: aromatic and aliphatic hydrocarbons, chlorinated compounds, amines, sulfur compounds, alcohols etc., being insensitive to the Air ( $O_2$ ,  $N_2$ ,  $CO$ ,  $CO_2$  etc.) methane and ethane, acid gases ( $HCl$ ,  $HF$ ,  $HNO_3$ ), etc.. Its big sensitivity is caused by the lack of the selectivity, because PIDs are able to detect just the amount of the ionized molecules in non-selective mode.

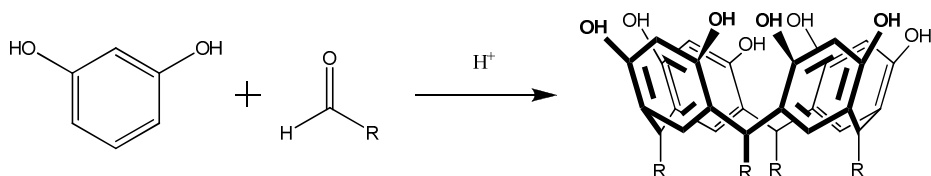
Therefore, like in the case of previously described MOX sensors, are still out of reach for some applications as stand-alone sensor.

## 1.6. Cavitands as supramolecular receptors.

Supramolecular chemistry may be defined as “chemistry beyond the molecule” bearing on the organized entities of higher complexity that result from the association of two or more chemical species held together by weak intermolecular forces. Its development requires the use of all resources of molecular chemistry combined with the designed manipulation of noncovalent interactions.<sup>15</sup>

The selective binding of a neutral substrate by a molecular receptor to form a complex involves molecular recognition, which is based on shape complementarity and the presence of specific weak interactions such as hydrogen bonding,<sup>16</sup>  $\pi$ - $\pi$  stacking,<sup>17</sup> and CH- $\pi$  interactions.<sup>18</sup>

In the field of supramolecular sensors cavitands were found to be interesting and versatile molecular receptors.<sup>19</sup> The name “cavitand” was given in 1982 by Cram<sup>20</sup> and refer to a resorcinarene-based open-ended host molecule formed in acidic condensation between resorcinol and aldehyde (Scheme 1), which being conformationally blocked at the upper rim by four bridging agents forming enforced cavity (Figure 11).



**Scheme 1.** General procedure for resorcinarene synthesis.

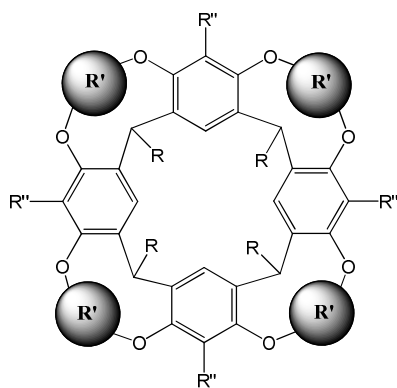


**Figure 11.** General scheme of the cavitand with marked possible functionalization sides.

The complexation properties of these molecules have been extensively studied in the solid state,<sup>21</sup> in solution,<sup>22</sup> and in the gas phase.<sup>23</sup>

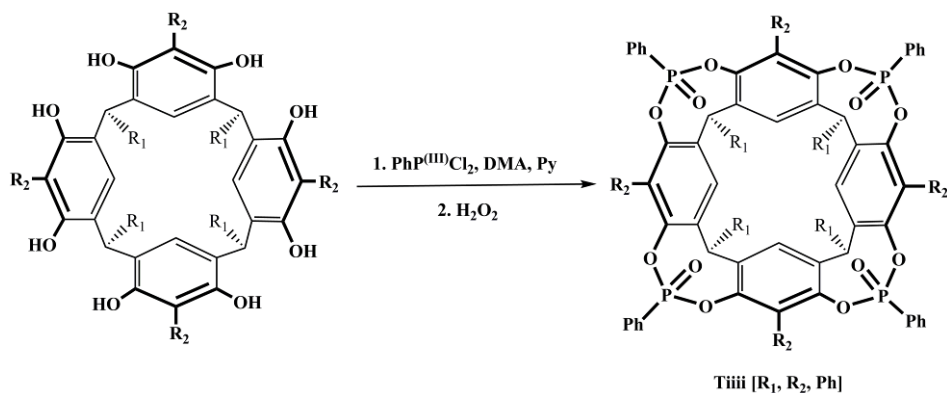
In the design of cavitands (Figure 11) the choice of the bridging groups connecting the phenolic hydroxyls of the resorcinarene scaffold is pivotal, since it determines shape, dimensions and complexation properties of the resulting cavity.

### 1.6.1 Phosphonate-bridged cavitands.

The resorcinarene-based cavitands with phosphonate bridging groups were found to be very efficient in cationic guest complexation and also as good hydrogen-bond acceptors.<sup>24</sup> This preorganized structure functionalised by the **P=O** units may form a specific interactions like H-bonding, CH- $\pi$ , and cation-dipole interactions with entrapped guest, making them fundamental for sensing events.

Phosphonate cavitands, presenting one to four H-bonding acceptor **P=O** groups at the upper rim of the cavity, are particularly appealing for the complexation of molecules based non-covalent host-guest interaction. Therefore, the high yields synthesis of phosphonate cavitands with all **P=O** groups oriented inward the cavity (**Tiiii**) have been developed in our group (Scheme 2).<sup>25</sup> Reaction of resorcinarene with dichlorophenylphosphine in the presence of pyridine

affords formation of the  $4P^{3+}_{iiii}$  cavitand. Its subsequent *in situ* oxidation with  $H_2O_2$  provides, in a single step, the **Tiiii** cavitand formation.



**Scheme 2.** The synthesis of tetraphosphonate (**Tiiii**) cavitand.

The presence of P(V) stereocenters affords configurational changes, since the relative orientation of the  $P=O$  groups with respect to the cavity determines the number of possible stereoisomers. In the case of tetrabridged phosphonate cavitands the presence of four stereogenic centers gives six possible diastereomeric cavitands. The inward (i) and outward (o) configurations are defined relative to the different orientation of the  $P=O$  moieties in respect to the receptor cavity, therefore a clear nomenclature for P(V) bridged cavitands has been proposed by our group.<sup>20</sup> It summarizes in a single acronym number and relative position of  $P=O$  bridges, their stereochemistry, type of substituents respectively at the lower rim, at the apical positions and on the phosphorus bridges. In Figure 12 all possible structures with their acronym below are shown. The first capital letters define number and position of bridges, the second lower case letters define the in-out stereochemistry at each P(V) center,  $R_1, R_2$  and  $R_3$  in brackets define respectively the substituents at the lower rim, in the apical positions and on the P(V) moiety.

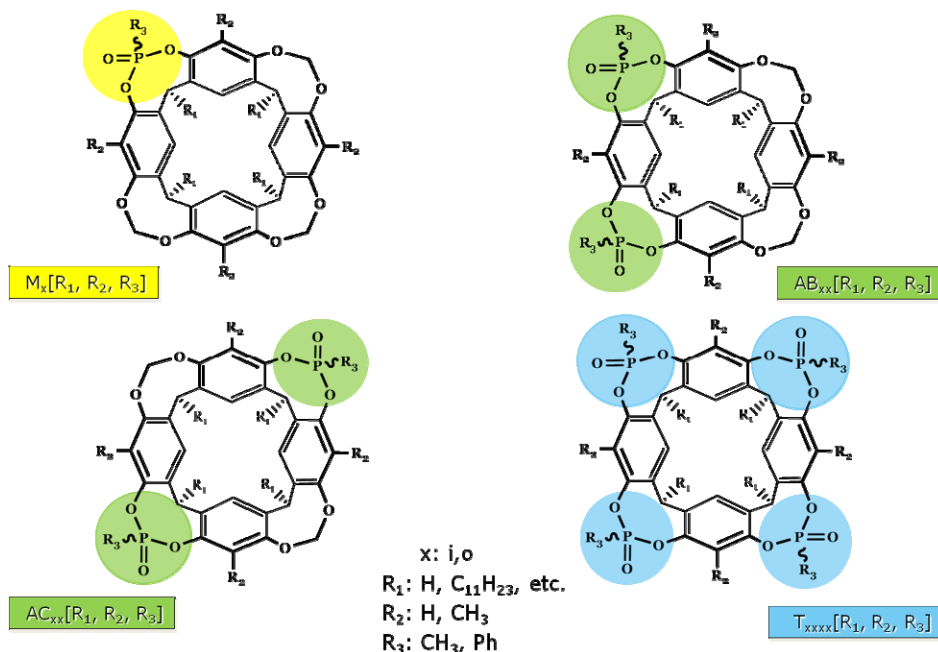


**Figure 12.** *Phosphonate cavitands nomenclature.*

The strong binding forces, especially toward charged methylated ammonium species like lysine or sarcosine, has been found involving cavitand with four  $P=O$  units orientated inward in respect to the cavity, making the **Tiiii** cavitands promising receptors.

### 1.6.2 Quinoxaline-bridged cavitands.

This heterophenylene cavitands are formed by bridging resorcinarene phenolic oxydryl groups in nucleophilic aromatic substitution with dichloroquinoxaline moiety.<sup>26</sup> This type of resorcinarene functionalization leads to a deep, hydrophobic and electron rich cavity, by the presence of electron rich quinoxaline units. The presences of four “walls” which occupy either axial or equatorial positions influence the receptor symmetry, therefore, the systems is able to perform reversible switching between a closed “vase” conformation

with a deep cavity, capable to guest complexation, and an open “kite” conformation with a flat extended surface (Figure 13.).<sup>27</sup>

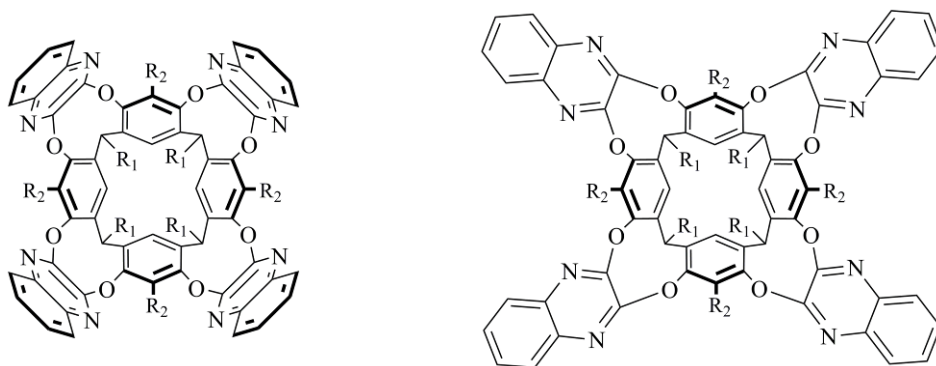


**Figure 13.** Structure of quinoxaline cavitand vase conformer (left) and kite conformer (right).

The extended studies on quinoxaline-cavitands by Cram,<sup>28</sup> shows that in solution, the cavitand presents high functionality: when they are in the fully axial conformation (aaaa) resemble a vase, with a large interior cavity, while, when they are in the fully equatorial conformation (eeee), the model looks like a kite.<sup>29</sup> This equilibrium can be obtained only in the case when resorcinarene scaffold is without methyl groups in apical position. At room temperature, in apolar solvents, only the close vase conformation can be detected by the <sup>1</sup>H NMR. Upon cooling, the population of the open and less symmetric kite form increases, until all cavitands are fully transformed at  $\approx 230$  K. This behaviour is due to the different solvation of the cavitand in its two geometrically conformations. In the open kite form, the solvent-accessible surface is much larger than in the close one, so that much more solvent molecules can stabilize this molecule by non-covalent interactions. This kind of stabilization is effective only at low temperature. In fact, interactions between solvent and cavitand result in a reduced solvent translational freedom, which determines an entropic loss that becomes too unfavourable at higher temperatures ( $\Delta G = \Delta H - T\Delta S$ ).

Changing the pH is another effective method to exert dynamic control over the kite-vase equilibrium.<sup>30</sup> Since the quinoxaline nitrogen atoms are weakly basic ( $pK_a$  293 K = 0.56), addition of a strong acid, such as  $CF_3COOH$  ( $pK_a$  293 K = 0.52) protonates them, inducing repulsive forces that lead the cavita $\text{nd}$  to assume the kite conformation, where the positive charges are moved apart from each other.

In the “vase” conformer the quinoxaline bridging units touch each other via their  $\alpha$ -hydrogens while forming a box like cavity with  $C_{4v}$  symmetry which is approximately 7 Å wide and 8 Å deep.<sup>31</sup> The cavity is open at the top and closed at the bottom by the cavita $\text{nd}$  itself. Tetraquinoxaline cavita $\text{nd}$ , in the vase conformation present strong affinity toward aromatic guests inclusion. The solid state measurements by the surface plasmon resonance (SPR) measurements confirmed the QxCav domination in aromatic guests coordination over cavita $\text{nds}$  presenting smaller cavities.<sup>32</sup> The cavity effect of tetraquinoxaline cavita $\text{nd}$  (Figure 14 A) was explored by the SPR measurements and compared with tetrapyrazine cavita $\text{nd}$  (Figure 14 B) and the tetramethylene cavita $\text{nd}$  (Figure 14 C).

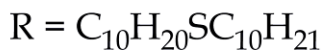
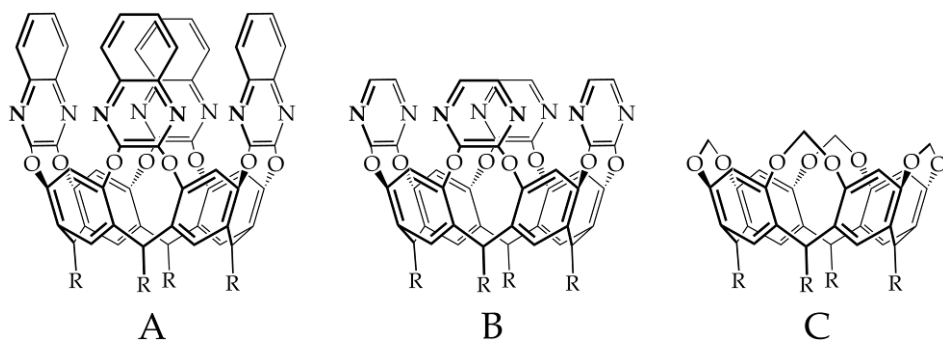


**Figure 14.** Chemical structures of quinoxaline- (QxCav) A, pyrazine- (PzCav) B and methylene- (MeCav) C bridged cavita $\text{nds}$ .

The cavitand monolayers were exposed on the benzene and toluene vapors (110 ppm each) and the complexation event were monitored (Figure 15).

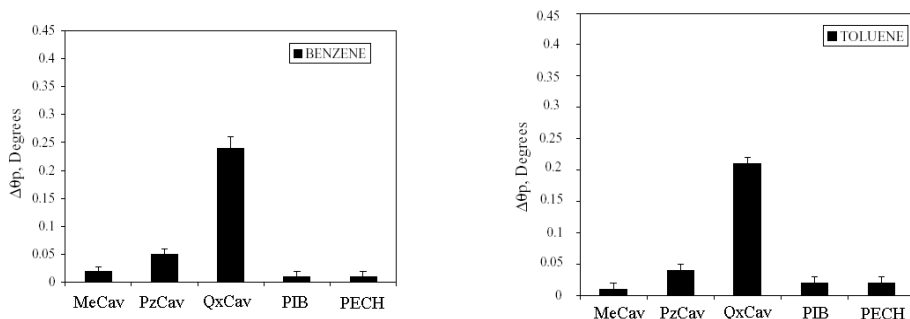


**Figure 15.** Graphs showing relative response of MeCav, PzCav, QxCav, PIB and PECH towards 110 ppm of benzene and toluene.

In the analysis the PIB and PECH polymers were used as referenced materials. It is clear that deep QxCav receptor favours aromatic guest inclusions over tetrapyrazine cavitands, confirming the high ability of quinoxaline cavitands to selective binds the aromatic hydrocarbon guests due to the presence of unique host-guest non covalent interactions.



## 1.7. References

---

- <sup>1</sup> Janata, J. *Principles of Chemical Sensors*, Plenum press, New York, USA, **1989**.
- <sup>2</sup> D'Amico, A.; Di Natale, C. *IEEE Sensors Journal* **2001**, *1*, 183.
- <sup>3</sup> Janata, J.; Josowicz, M. *Anal. Chem.* **1998**, *70*, 179.
- <sup>4</sup> Hierlemann, A.; Ricco, A. J.; Bodenhöfer, K.; Göpel, W. *Anal. Chem.* **1999**, *71*, 3022.
- <sup>5</sup> Fischer, E. *Ber. Dtsch. Chem. Ges.* **1894**, *27*, 2985.
- <sup>6</sup> Elghanian, R.; Storhoff, J. J.; Mucic, R. C.; Letsinger, R. L.; Mirkin, C. A. *Science* **1997**, *277*, 1078.
- <sup>7</sup> Grate J.W.; Frye, G.C.; *Sensors Update*, WILEY-VCH, Weinheim, **1996**, Vol. 2, 37.
- <sup>8</sup> Janata, J.; *Principles of Chemical Sensors*, Plenum press, New York, USA, **1989**.
- <sup>9</sup> Zampolli, S.; Elmi, I; Mancarella, F.; Betti, P.; Dalcanale, E/; Cardinali, G. C.; Severi, M. *Sens. Actuators B* **2009**, *141*, 322.
- <sup>10</sup> Prodi, L. *New J. Chem*, **2005**, *29*, 20.
- <sup>11</sup> Lakowicz, J. R.; *Principles of Fluorescent Spectroscopy*, 2<sup>nd</sup> Eds, Kluwer Academic/Plenum Publisher, New York, **1999**.
- <sup>12</sup> Kim, J. S.; Quang, D. T. *Chem. Rev.* **2007**, *107*, 3780.
- <sup>13</sup> Prasanna de Silva, A.; Moody, T. S.; Wright, G. D. *Analyst* **2009**, *134*, 2385.

<sup>14</sup> The Picture reprinted from :

[Http://www.equipcoservices.com/images/tutorials/intropid.png](http://www.equipcoservices.com/images/tutorials/intropid.png)

<sup>15</sup> Lehn, J. M. *Angew. Chem. Int.* **1988**, 27, 90.

<sup>16</sup> Rebek, J. *Angew. Chem. Int.* **1990**, 29, 245.

<sup>17</sup> Hunter, C. H.; Lawson, K. R.; Perkins, J.; Urch C. J. *J. Chem. Soc., Perkin Trans.* **2001**, 2, 651.

<sup>18</sup> Nishio, M.; Hirota, M.; Umezawa, Y. *The CH- $\pi$  Interactions*, Wiley-VCH, New York, **1998**.

<sup>19</sup> Cram, D. J.; Cram, J. M.; *Container Molecules and Their Guests*, The Royal Society of Chemistry, Cambridge, **1994**, Chapter 5.

<sup>20</sup> Moran, J. R.; Karbach, S.; Carm D. J. *J. Am. Chem. Soc.* **1982**, 104, 5826.

<sup>21</sup> Cram, D. J.; Karbach, S.; Kim, H. E.; Knobler, C. B.; Maverick, E. F.; Ericson, J. L.; Helgeson, R. C. *J. Am. Chem. Soc.* **1988**, 110, 2229.

<sup>22</sup> a) Tucker, J. A.; Knobler, C. B.; Trueblood, K. N.; Cram D. J. *J. Am. Chem. Soc.* **1989**, 111, 3688.; b) Soncini, P.; Bonsignore, S.; Dalcanale, E.; Ugozzoli, F. *J. Org. Chem.* **1992**, 57, 4608.; c) Haino, T.; Rudkevich, D. M.; Shivanyuk, A.; Rissanen, K., Rebek Jr., J. *Chem. Eur. J.* **2000**, 6, 3797.; d) Paek, K.; Cho, J. *Tetrahedron Lett.* **2001**, 42, 1927.

<sup>23</sup> a) Vincenti, M.; Dalcanale, E.; Soncini, P.; Guglielmetti, G. *J. Am. Chem. Soc.* **1990**, 112, 445.; b) Vincenti, M.; Pelizzetti, E.; Dalcanale, E.; Soncini, P. *Pure Appl. Chem.* **1993**, 65, 1507.

- 
- <sup>24</sup> a) Timmerman, P.; Verboom, W.; Reinhoudt, D. N. *Tetrahedron* **1996**, *52*, 2663.;  
b) Rudkevich, D. M.; Rebek Jr., J. *Eur. J. Org. Chem.* **1999**, 1991.
- <sup>25</sup> Yebeutchou, R. M.; Tancini, F.; Demitri N.; Geremia, S.; Mendichi, R.;  
Dalcanale, E. *Angew. Chem. Int.* **2008**, *47*, 4504.
- <sup>26</sup> a) Moran, J. R.; Karbach, S.; Cram, D.J. *J. Am. Chem. Soc.* **1982**, *104*, 5826.; b)  
Bryant, J. A.; Ericson, J. L.; Cram, D. J. *J. Am. Chem. Soc.* **1990**, *112*, 1255.; c)  
Cram, D. J.; Choi, H. J.; Bryant, J. A.; Knobler, C. B. *J. Am. Chem. Soc.* **1992**, *114*,  
7748.
- <sup>27</sup> Roncucci, P.; Pirondini, L.; Paderni, G.; Massera, C.; Dalcanale, E.; Azov, V.  
A.; Diederich, F. *Chem. Eur. J.* **2006**, *12*, 4775.
- <sup>28</sup> Cram, D. J.; Cram, J. M. *Container Molecules and Their Guests* (Ed. J. F.  
Stoddart), **1994**, Royal Society of Chemistry, Cambridge, Chap. 6.
- <sup>29</sup> Moran, J. R.; Ericson, J. L.; Dalcanale, E.; Bryant, J. A.; Knobler, C. B.; Cram, D.  
J. *J. Am. Chem. Soc.* **1991**, *113*, 5707.
- <sup>30</sup> Skinner, P. J.; Cheetham, A. G.; Beeby, A.; Gramlich, V.; Diederich, F. *Helv.*  
*Chim. Acta.* **2001**, *84*, 2146.
- <sup>31</sup> Dalcanale, E.; Soncini, P.; Bacchilega, G.; Ugozzoli, F. *J. Chem. Soc., Chem.*  
*Commun.* **1989**, 500.
- <sup>32</sup> Pirondini, L.; Dalcanale, E. *Chem. Soc. Rev.* **2007**, *36*, 695.



**Design and synthesis of novel  
QxBox receptors for Benzene  
detection in air**

2

## 2.1. Introduction.

The air pollution increase in vast urban and industrial areas entails design of new air quality control systems capable to monitor the most dangerous pollutants at very low concentration. Nowadays, the real-time air quality control measurements are done by bulky, expensive, high-end systems based on advanced laboratory equipment. Recently, our group reported a low-cost system based on selective detection of harmful Volatile Organic Compounds (VOCs), employing molecular host-guest recognition.<sup>1</sup> We rationally designed a molecular receptor where multiple host-guest interactions are involved in the sensing event. The receptor cavity is able to discriminate aromatic from aliphatic hydrocarbons due to the formation of specific interactions like CH- $\pi$ ,  $\pi$ - $\pi$  interactions and H-bonds. The selective hosting properties of tetraquinoxaline cavitands (QxCav) towards aromatic hydrocarbons have been proven in gas phase<sup>2</sup> as well as in the solid state.<sup>3</sup> This multifunctional receptor was also used in water quality control, exploiting its hydrophobic effect.<sup>4</sup> The gas-solid interface was widely studied in air monitoring, using both mass<sup>5</sup> and surface plasmon resonance transducers.<sup>6</sup> However, using these approaches the discrimination between similar aromatic VOC is impossible to achieve, in particular, selectively release benzene before the other aromatics. This step required a GC system after the pre-concentrating cartridge for VOCs separation (see Chapter 1). Therefore, we decided to design and synthesize a new rigid molecular receptor targeted only toward benzene molecule. The novel structural arrangement of the receptor was achieved by rigidification and tightening the cavity mouth with aliphatic linkers (Figure 1). In this chapter, the synthesis of new rigid tetraquinoxaline cavitands (QxBox) and their use for air quality control systems for selective aromatic hydrocarbon detections will be depicted.

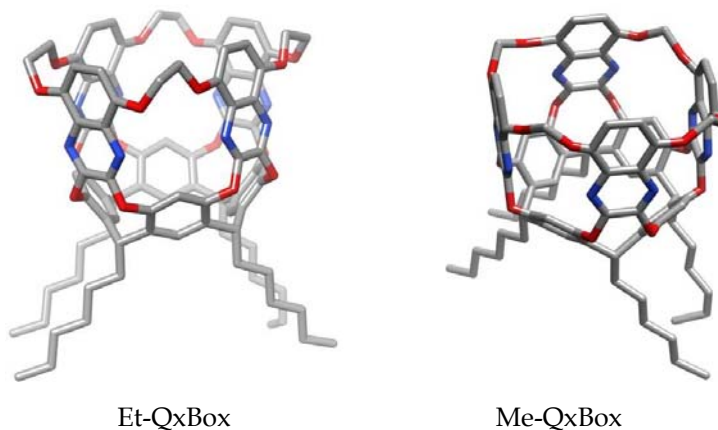


**Figure 1.** The new type of conformationally blocked QxBox receptors reported in this work.

## 2. 2. Selective recognition event within tetraquinoxaline cavitands.

The resorcinarene unit is a versatile scaffold for the development of molecular receptors. The nature of the bridging groups strongly affects shape, dimension and complexation properties of the cavity through the presence of specific non-covalent host-guest interactions (Chapter 1). In a previous work, the influence on the complexation ability of resorcinarene-based molecular receptors based on cavity depth and shape was studied via theoretical calculations using PM3 model.<sup>7</sup> It has been found that weak interactions, mostly  $\pi$ - $\pi$ , CH- $\pi$ , and hydrogen bonds between the guest and the tetraquinoxaline receptor are involved in the complexation phenomena (Figure 2).<sup>8</sup>

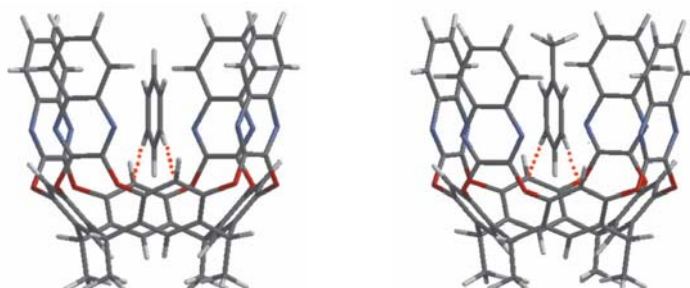


**Figure 2.** Model of the QxCav@benzene and QxCav@toluene complexes.

Figure 2 shows the geometry-optimized structures of the QxCav receptor with two interesting targets, namely benzene and toluene. The complexes are stabilized by weak non-covalent interactions involving the  $\pi$  electrons of the quinoxaline host and by hydrogen bonding of the two guest hydrogens aligned along the  $\pi$  orbital of resorcinarene atoms. The calculated complexation energy for benzene ( $-6.85 \text{ kJ mol}^{-1}$ ) and toluene ( $-6.88 \text{ kJ mol}^{-1}$ ) are very similar, therefore its discrimination is impossible with QxCav. This behaviour is indicated by the cavity size changes related to the free flapping of the quinoxaline walls between *vase* ( $C_{4v}$ ) and *kite* ( $C_{2v}$ ) conformation dictated and controlled by the environment changes (Figure 3).<sup>9</sup>

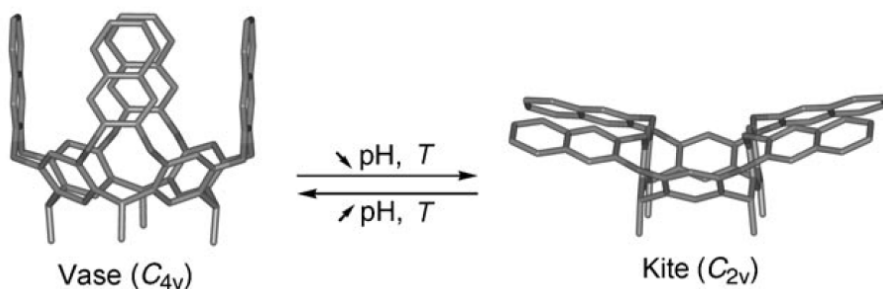
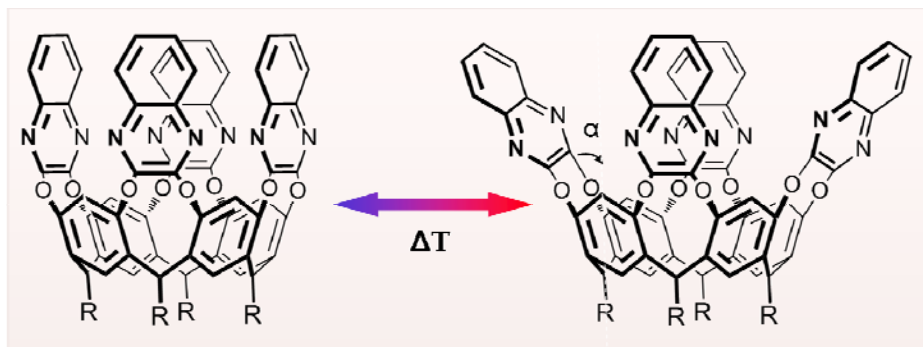


**Figure 3.** *Vase to kite conformational equilibrium of QxCav in the solution.*

In solution *vase*  $\leftrightarrow$  *kite* equilibrium is controlled by two factors: (i) solvation: at low temperatures, solvation of the larger surface favours the *kite* conformer, whereas, at higher temperature, the entropic term  $T\Delta S_{\text{solv}}$  for the solvation of the larger *kite* surface becomes unfavourable and the *vase* conformation predominates; (ii) pH changes of surrounding environment: at low pH the quinoxaline nitrogens becomes protonated promoting its repulsive interactions leading to the cavity opening to *kite* conformation. Diederich extensive studies, on quinoxaline cavitands, confirm the high flexibility of these systems in the solution as well in the solid state.<sup>10</sup> In the solid state, the equilibrium is strongly moved toward *vase* form, and *vase* to *kite* conformation changes are limited and are only temperature depended (Figure 4).





**$\alpha$  = The medium opening angle  $16^\circ$**

Figure 4. The QxCav conformation changes in the solid state.

The temperature increase promotes free movement of four quinoxaline walls with a medium angle  $\alpha$  close to  $16^\circ$  (Figure 4).<sup>11</sup> The vase opening weakens the interaction between the cavity walls and aromatic guests making the receptor less sensitive and selective. In the figure 5 below, the computer simulation presenting 1000 overlaid structures of the tetraquinoxaline cavitands in the vase conformation are shown.<sup>10</sup>

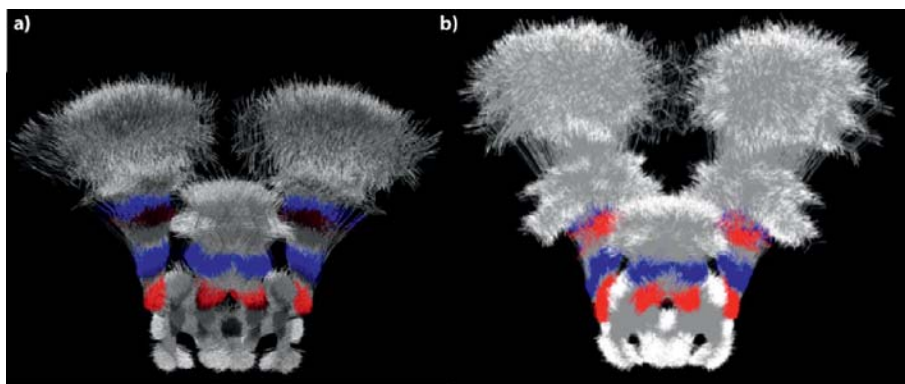


Figure 5. Overlay of 1000 structures of the QxCav vase forms sampled from molecular dynamics simulations.<sup>10</sup>

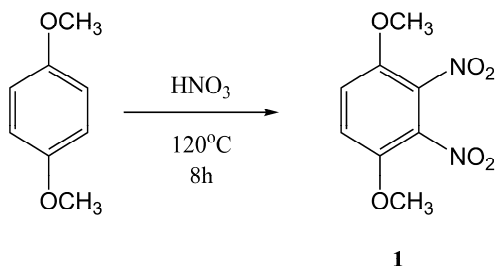
The walls vibration in the solid state confine QxCav to be used as selective stand-alone receptor. Therefore, we designed new systems involving rigid tetraquinoxaline cavitands (QxBox) as receptors for harmful volatile organic compounds, especially the BTEX family, applying a supramolecular approach to analytical chemistry.

### 2.3. Design and synthesis of new rigid QxBox receptors.

Lack of selectivity ascribable to QxCav *vase* functionality in solid state can be overcome by blocking the cavity in a *vase* form rigidification, making new cavitand insensitive to the temperature variations. The cavity blocking is expected to restrain the possible guests number only to the BTEX family. Moreover, the cavity rigidification in stable *vase* form should influence on the complexation forces by its increase. The receptor synthesis is divided in two main parts: 1) the synthesis of the quinoxaline bridging unit; 2) the synthesis of the QxBox cavitand.

#### 2.3.1. Synthesis of the 2,3-dichloro-5,8-dimethoxy quinoxaline bridging unit.

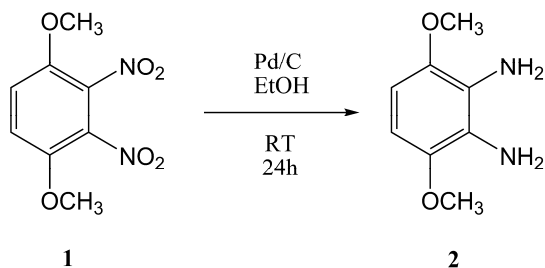
The 2,3-dichloro-5,8-dimethoxy quinoxaline bridging unit was synthesized in four steps starting from the nitration of 1,4-dimethoxy benzene following an electrophilic aromatic substitution reaction (Scheme 1).



**Scheme 1.** Nitration of 1,4-dimethoxy benzene.

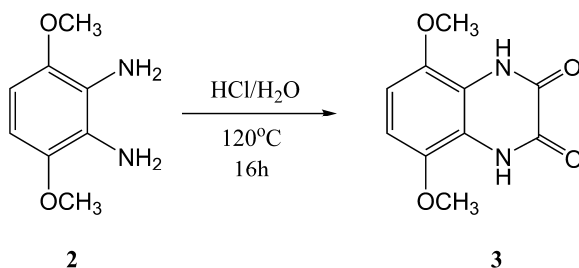
1,4-dimethoxy benzene was reacted with HNO<sub>3</sub> under reflux. The yellow precipitate of 1,4-dimethoxy-2,3-dinitro benzene (1) was filtered, washed with

water, dried and purified by flash chromatography. The nitro groups of product **1** were successively reduced using catalytic amounts of metallic Pd on activated carbon in H<sub>2</sub> atmosphere, giving 1,4-dimethoxy-2,3-diamino benzene (**2**).



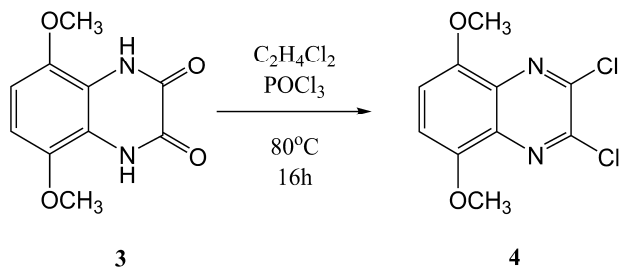
**Scheme 2.** Synthesis of compound **2** by catalytic reduction.

Due to the high reactivity of amino groups, compound **2** was used without further purification for a condensation reaction with oxalic acid under acidic conditions to give **3** in 96% yield.



**Scheme 3.** Condensation of 1,4-dimethoxy-2,3-diamino benzene (**2**) with oxalic acid.

The 2,3-dichloro-5,8-dimethoxy quinoxaline **4** was prepared by chlorination of intermediate **3** by POCl<sub>3</sub> in refluxing dichloroethane.

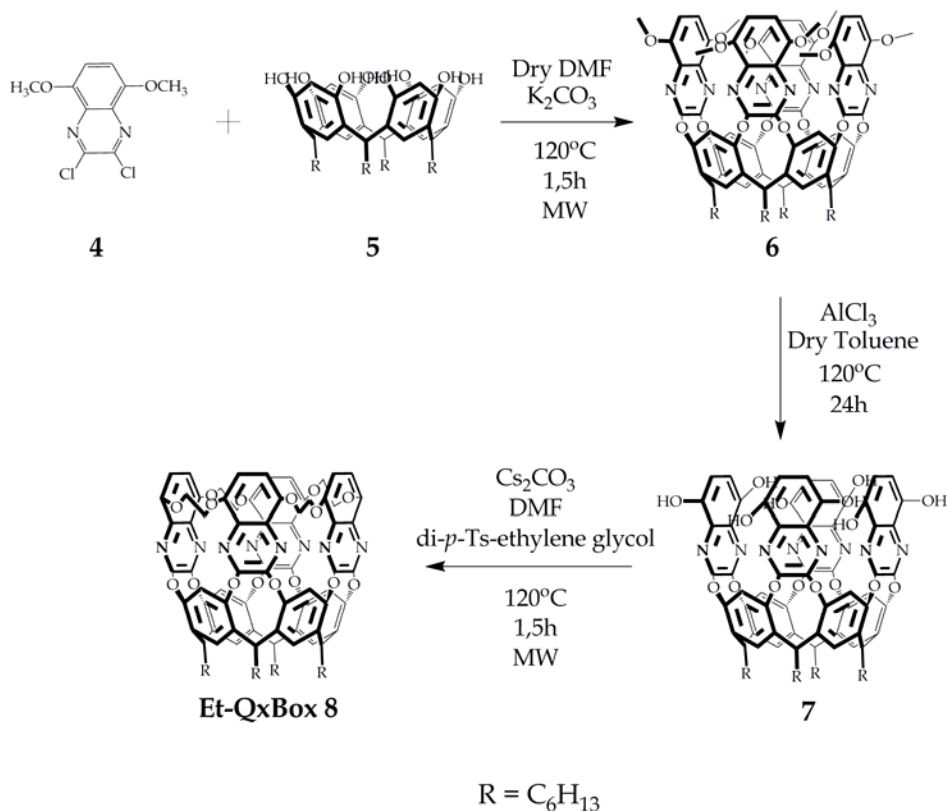


**Scheme 4.** Synthesis of 2,3-dichloro-5,8-dimethoxy quinoxaline (**4**).

The crude was purified by flash chromatography technique giving pure compound **4** in 90% yield.

### 2.3.2. Synthesis of conformationally blocked QxBox cavitands.

As resorcinarene scaffold for QxBox receptor, is the one with hexyl feet was chosen as compromise between solubility and easy of crystallization. Solubility helps in purification of intermediates and final products.



**Scheme 5.** Synthesis of the conformationally blocked Et-QxBox receptor (8).

The synthesis consists of three steps: the first bridging reaction of resorcinarene **5** under basic conditions with the 2,3-dichloro-5,8-dimethoxy quinoxaline (**4**) by Williamson reaction under microwave irradiation, leading to octamethoxy-quinoxaline cavitand (**6**) in 70% yield. The  $^1\text{H}$  NMR studies confirmed the *kite* conformation of the cavitand **6**, due to the presence of  $-\text{OCH}_3$  groups in the 5,8 positions relative to the quinoxaline moiety. The purified cavitand **6** was successively reacted with a Lewis acid ( $\text{AlCl}_3$ ), in dry toluene, to cleave the methyl protecting groups of the quinoxaline walls. The deprotection of eight  $-\text{OCH}_3$  groups influences the cavitand conformation, which was observed by the  $^1\text{H}$  NMR analysis. The cavity changes its shape from  $\text{C}_{2v}$  symmetry observed in the case of cavitand **6**, to the fluctuational *vase* confirmation in the octahydroxy-

quinoxaline cavitand **7** case. Those changes can be easily monitored by the downfield shift of the diagnostic methine triplet of the resorcinarene bridges (Chapter 1). The octahydroxy-quinoxaline cavitand **7** was successively reacted with di-*p*-tosylate-ethylene-glycol employing caesium ion as templating agent and microwave irradiation, leading to the final product - the Et-QxBOX **8** in 70% yield.

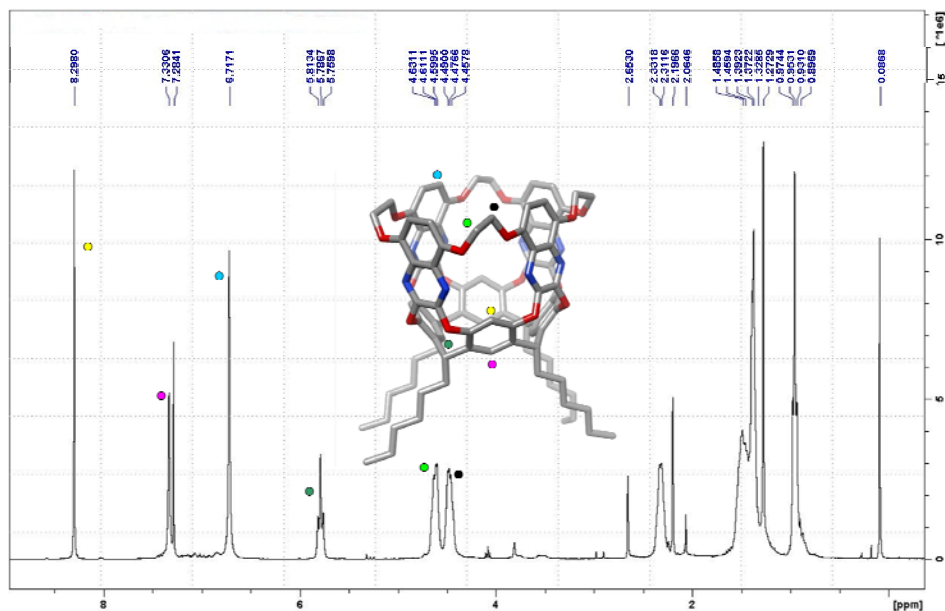
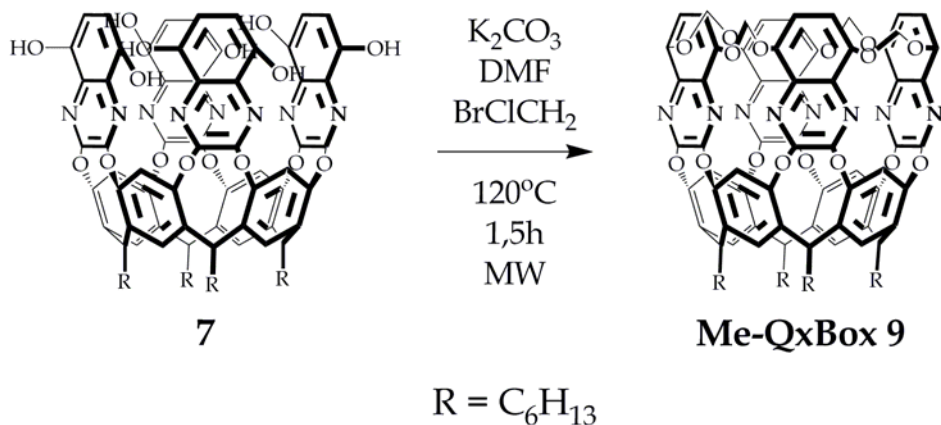


**Figure 5.**  $^1\text{H}$  NMR of Et-QxBox **8** in  $\text{CDCl}_3$ .

The  $^1\text{H}$  NMR above shows the resonances of synthesized Et-QxBox cavitand **8**, where we can distinguish all characteristic peaks: in the low ppm region are present all signals belonging to the hexyl feet. The high ppm region, from 6,7 to 8,3 ppm, is relative to aromatic the signals; (i) resorcinarene scaffold, two singlets, at 7,33 ppm and 8,29ppm respectively, (ii) singlet at 6,71 relative to the quinoxaline bridges. In the middle of the spectrum are present two multiplets, at 4,47 and 4,61 ppm respectively, which correspond to the ethene protons. Its multiplicity and broadening is caused by their slow motion on the NMR time

scale. The diagnostic triplet of the CH resorcinarene signal at 5.76 ppm confirms the rigid *vase* conformation.

The smaller cavitand, Me-QxBox, was prepared by bridging bromochloromethane on cavitand **7** (Scheme 6).



**Scheme 6.** Synthesis of the Me-QxBox cavitand **9**.

In order to create smaller Me-QxBox cavitand, intermediate **7** was bridged by the  $\text{BrClCH}_2$  under basic conditions employing microwave irradiation (Scheme 6). After purification step, the Me-QxBox cavitand **9** was obtained in 5% yield. In Figure 6 below the  $^1\text{H}$  NMR spectrum of the Me-QxBox cavitand is shown. Like in the case of larger, Et-QxBox cavitand **8**, all diagnostic peaks can be clearly defined. The methine signal at 5.61 ppm clearly demonstrate the formation of blocked *vase* cavitand form. The downfield shift of methylene signals, together with their sharpening, compared to the Et-QxBox, suggest that the methylene bridges are oriented outward with respect to the cavity (see crystal structure of Figure 12 for confirmation).

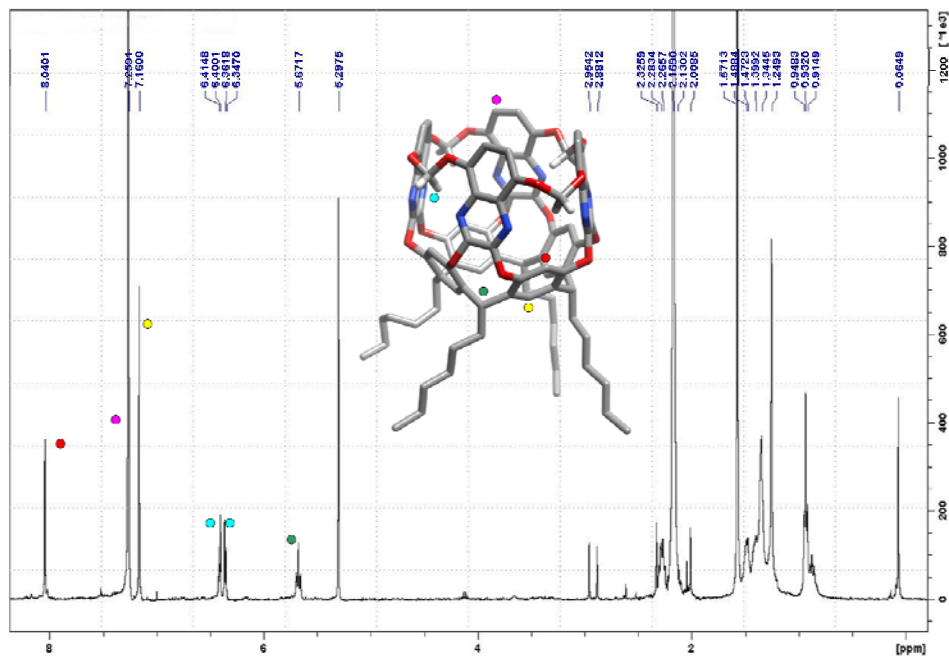


**Figure 6.**  $^1\text{H}$  NMR of Me-QxBox in acetone- $d_6$ .

$^1\text{H}$  NMR studies together with MALDI TOF-TOF analysis confirm the cavitand formation. In both **8** and **9**, the downfield shift of the CH signal of the resorcinarene (Figures 5 and 6, dark green point) ( $\sim 5.70$  ppm in both cases) is indicative of the rigid *vase* configuration.<sup>9</sup>

## 2.4. X-ray crystallographic studies.

The affinity of **Et-QxBox** (**8**) and **Me-QxBox** (**9**) toward aromatic hydrocarbons (benzene, toluene, xylenes, *p*-nitrotoluene) were studied by single-crystal X-ray diffraction analysis. Different crystallization experiments were performed dissolving cavitand **8** in DMSO and adding benzene, toluene, *o*-xylene, *m*-xylene, *p*-xylene and *p*-nitrotoluene respectively. Crystals with benzene, toluene *o*-xylene and *p*-nitrotoluene could be studied through X-ray diffraction analysis, while crystals with *m*-xylene and *p*-xylene were too fragile and thin to be measured. Crystals of cavitand **9** with benzene were obtained from a chloroform solution. The molecular structures of complexes



**Et-QxBox@benzene** (Figure 7), **Et-QxBox@toluene** (Figure 9), **Et-QxBox@o-xylene** (Figure 10), **Et-QxBox@p-nitrotoluene** (Figure 11) and **Me-QxBox@benzene** (Figure 12) were determined; crystallographic and experimental details for the structures are summarized in Tables Z1 and Z2 (Appendix A).

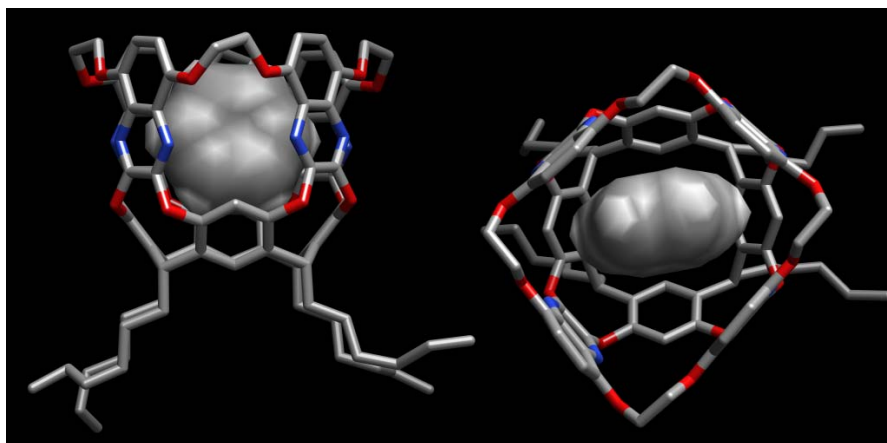


**Figure 7.** Molecular structure of the *Et-QxBox@benzene* complex crystallized from DMSO. The receptor hydrogens have been omitted for clarity.

The position of benzene inside the host is due to the presence of  $\pi$ - $\pi$  and CH- $\pi$  interactions. Two independent cavitands are present in the asymmetric unit (Figure 8), but only one forms a complex with benzene, which also fills the empty spaces of the crystal lattice.

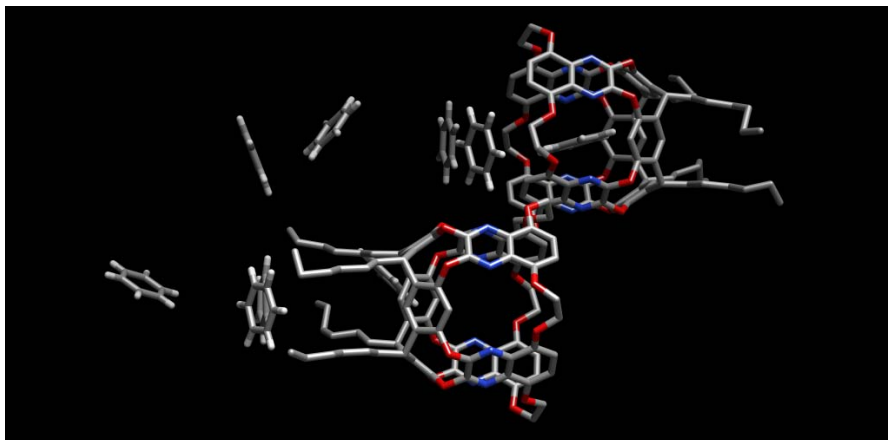


**Figure 8.** *The asymmetric unit of the Et-QxBox@benzene complex.*

The molecular structure of **QxBox@toluene** (Figure 9) shows that also in this case the guest is trapped inside the receptor, even if with a different orientation compared to the benzene complex. The encapsulation is driven by the presence of  $\pi$ - $\pi$  stacking interactions between the aromatic ring and the quinoxaline walls, and by the CH- $\pi$  interactions involving the  $\text{CH}_3$  group, which is disordered over two geometrically equivalent positions.

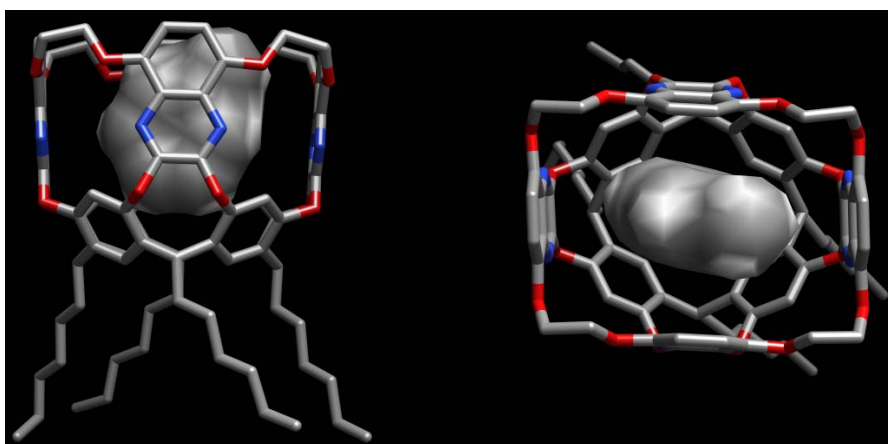


**Figure 9.** *Molecular structure of the Et-QxBox@toluene complex crystallized from DMSO. The receptor hydrogens have been omitted for clarity.*

As could be expected, *o*-xylene behaves essentially like toluene, and the two complexes formed are perfectly comparable in geometry and host-guest interactions (see Figure 10).

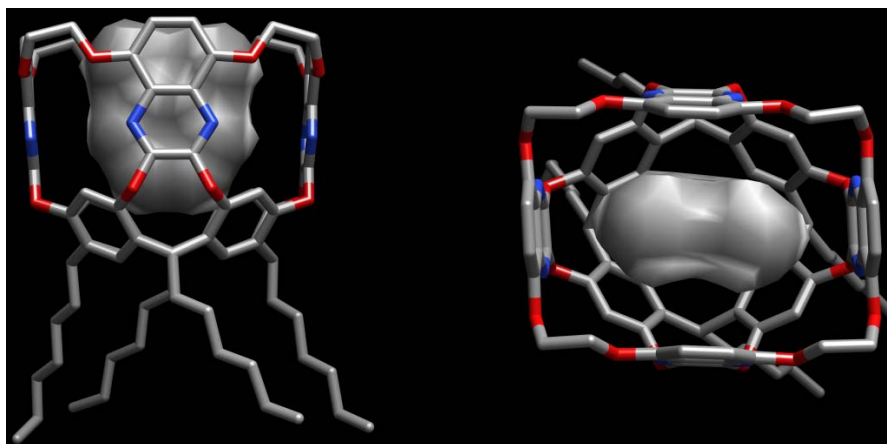


**Figure 10.** Molecular structure of the *Et-QxBox@o-xylene* complex crystallized from DMSO. The receptor hydrogens have been omitted for clarity.

All the attempts to obtain measurable crystals with *meta*- and *para*-xylene were unsuccessful. However, a crystallization competitive experiment was performed, exposing a solution of Et-QxBox to a mixture containing all the three isomers of the xylene family. Only the complex with *o*-xylene crystallized, confirming the preferential affinity of the receptor for this isomer. The relative position of the two methyl substituents has a remarkable influence on the inclusion property of the Et-QxBox. In the case of *m*-xylene the poor affinity can be rationalized assuming that one methyl does not fit nicely in the lower part of the cavity. The situation for *p*-xylene is different however: both methyl substituents can fit in the cavity one toward the outside and one pointing toward the resorcinarene bowl. This last inclusion mode seems to be disfavoured in the QxBox family. None of the crystal structures reported so far with simple aromatics shows the methyl in the lower part. The same behaviour has been assessed in solution via NMR.<sup>12</sup>

The Et-QxBox receptor was also tested in presence of *p*-nitrotoluene, a TNT explosive targant. From a DMSO solution containing Et-QxBox and *p*-nitrotoluene, needle-like monocrystals formed very rapidly over a period of 1-2h. The molecular structure of **QxBox@*p*-nitrotoluene** obtained through X-ray analysis is shown below.

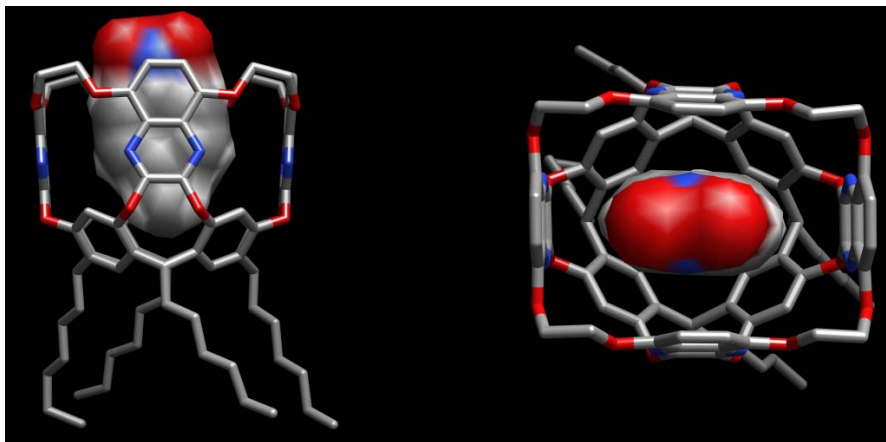


**Figure 11.** Molecular structure of the **Et-QxBox@*p*-nitrotoluene** complex crystallized from DMSO. The receptor hydrogens have been omitted for clarity.

The guest is stabilized inside the cavitand by  $\pi$ - $\pi$  stacking interactions and by CH- $\pi$  interactions involving its hydrogen atoms and the aromatic rings of the cavity. The presence of the NO<sub>2</sub> substituent increases the CH “acidity” of the methyl group, making it attractive to be positioned on the “ $\pi$ -basic” bottom end of the cavity. This behaviour is opposite to that of toluene.

The molecular structure of the **Me-QxBox@benzene** complex is shown in Figure 12. Due to the presence of shorter bridging groups at the upper rim, the available space for the guest is reduced and benzene molecule perfectly fits the inner volume, stabilized by CH- $\pi$  interactions with the aromatic walls of the receptor.

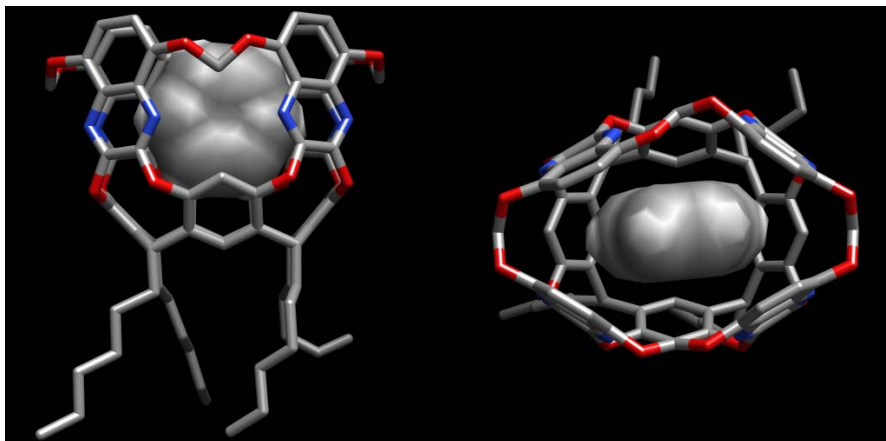


**Figure 12.** Molecular structure of the *Me-QxBox@benzene* complex crystallized from chloroform. The receptor hydrogens have been omitted for clarity.

In order to better understand the complexation properties of the hosts, some geometric calculations were performed with the PARST97 program<sup>13</sup> on Et-QxBox **8** and Me-QxBox **9**. The distances relevant to the cavitand dimensions are summarized in Table 1 and Table 2, respectively.

In the case of Et-QxBox **8**, the depth of the cavity (8.105(6) Å) can be inferred by the distance between the least-squares plane passing through the groups of atoms C7 (A, B, C and D) and C19-C20 (A, B, C and D). The cavity presents a rectangular opening, the dimensions of which are roughly 10 and 7 Å, respectively. The least-squares planes passing through the quinoxaline moieties are inclined with respect to the plane passing through the O1-O2 atoms of 87.09(3), 80.17(3), 86.37(3) and 81.16(3) for groups A, B, C and D, respectively (Figure 13).

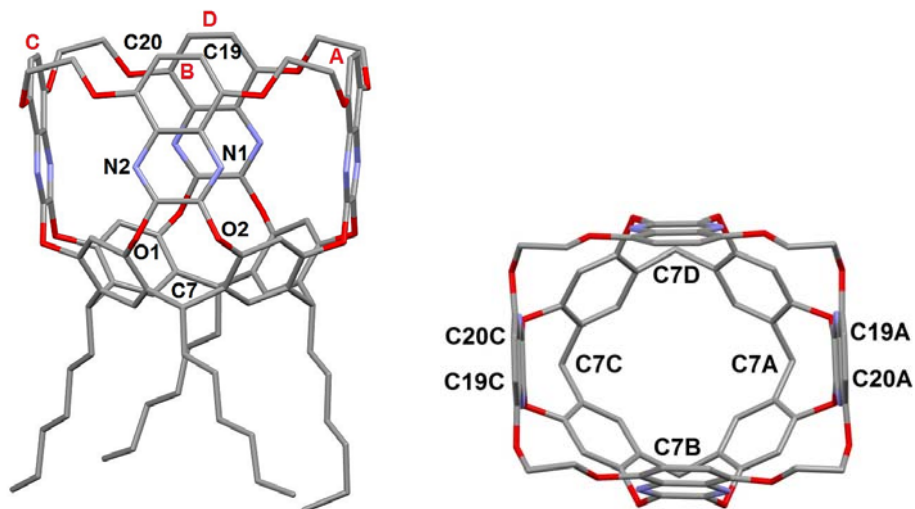


**Figure 13.** Left. Schematic view of the molecular structure of Et-QxBox with the general labelling scheme. Each quinoxaline group is tagged by the letters A, B, C and D, respectively. Hydrogen atoms and solvent molecules have been removed for clarity. Colour code: oxygen, red; nitrogen, blue; carbon, grey. Right: top view. The alkylic chains have been removed for clarity.

C7A-C7C	7.342(6)	C20A-C19C	10.485(6)
C7B-C7D	7.131(6)	C19B-C20D	7.155(6)
C19A-C20C	10.477(6)	C20B-C19D	7.109(6)

**Table 1.** Selected distances ( $\text{\AA}$ ) relative to the dimensions of Et-QxBox cavitand.

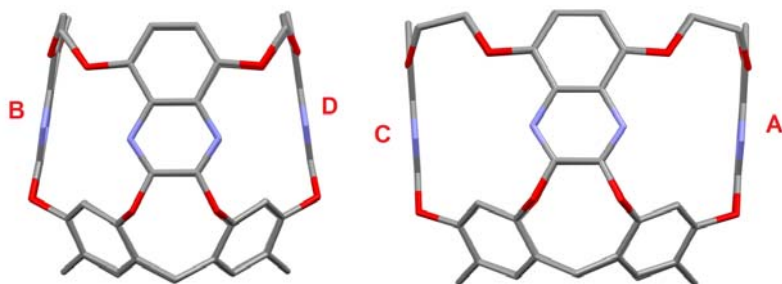


**Figure 14.** Side view of cavitand Et-QxBox showing the different inclination of the quinoxaline moieties. Hydrogen atoms and alkyl chains have been omitted for clarity.

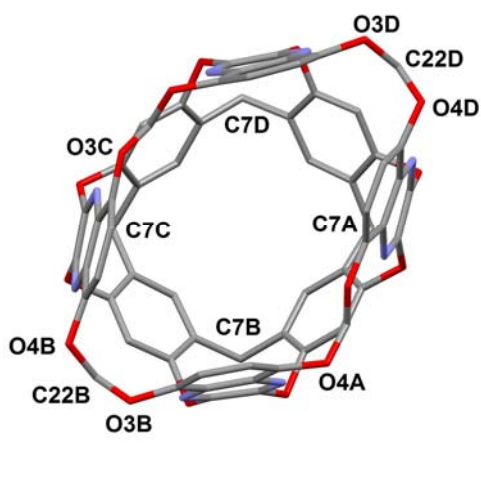


**Figure 15.** Left. Schematic view of the molecular structure of Me-QxBox with the general labelling scheme. Each quinoxaline group is tagged by the letters A, B, C and D, respectively. Hydrogen atoms and solvent molecules have been removed for clarity. Colour code: oxygen, red; nitrogen, blue; carbon, grey. Right: top view. The alkylic chains have been removed for clarity.

C7A-C7C	7.194(4)	AB	63.52(7)
C7B-C7D	7.288(4)	BC	70.19(6)
C22A-C22C	7.789(5)	CD	64.18(5)
C22B-C22D	12.043(4)	DA	63.20(7)

**Table 2.** Selected distances ( $\text{\AA}$ ) and angles ( $^\circ$ ) relative to the dimensions of Me-QxBox cavitand.

The height of the cavity for Me-QxBox (8.063(2)) has been calculated as for Et-QxBox; the biggest difference between the two receptors is in the shape and dimensions of the cavity opening, which in this case is rhombohedral in form (see Table 2 for selected distances). The least-squares planes passing through the quinoxaline moieties (tagged A, B, C and D) are inclined with respect to the plane passing through the O1-O2 atoms of 77.21(3), 81.94(4), 81.27(3) and 84.30(4) for groups A, B, C and D, respectively (Figure 16).

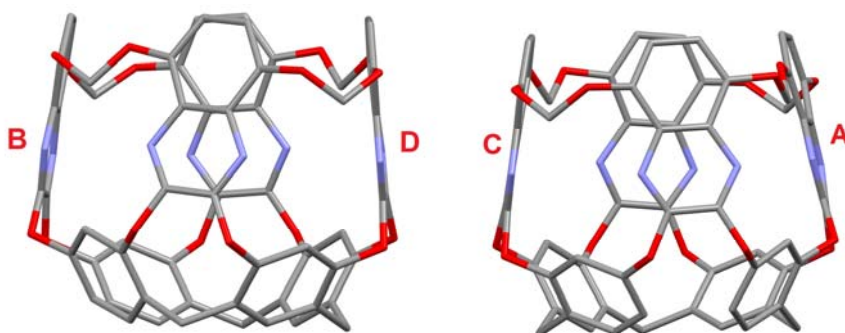


**Figure 16** Side view of Me-QxBox cavitand showing the different inclination of the quinoxaline moieties. Hydrogen atoms and alkyl chains have been omitted for clarity.

Summarising, the smaller entrance of the Me-QxBox cavity (Figure 17 A) favours the entrance of smaller aromatic guests like benzene over the larger



TEX. Et-QxBox cavity (Figure 17 B), having a larger mouth due to the presence of ethylene bridges accommodates all BTEX in a similar fashion.

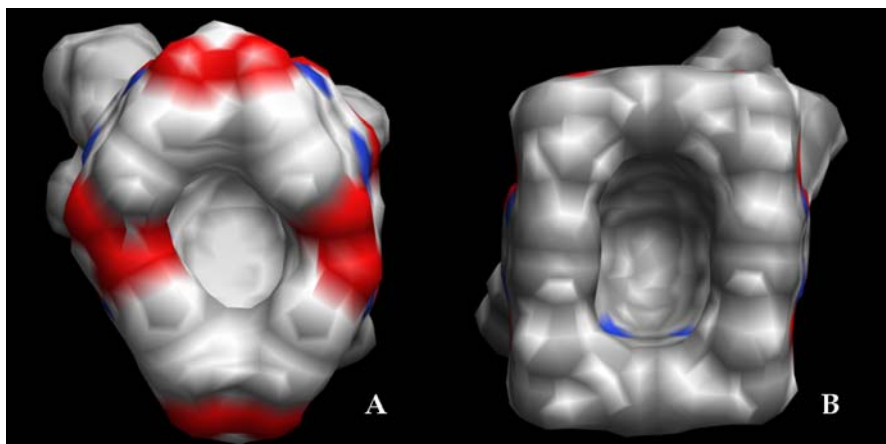


**Figure 17.** The 3D structure models comparison between the Me-QxBox (A) and Et-QxBox (B) cavities.

The trend obtained by the X-Ray studies will be tested in the gas/solid quantitative measurements.

## 2. 5. Analytical measurements.

### 2.5.1. The thermo gravimetric analysis of the QxBox receptors.

The thermal stability of the QxBox receptors was measured by thermo gravimetric analysis. The thermal decomposition of the QxBox receptors was measured in air atmosphere using temperature cycles spanning range from 20°C to 500°C in the case of Me-QxBox (Figure 18) and from 30°C to 700°C in the case of Et-QxBox (Figure 19) respectively.

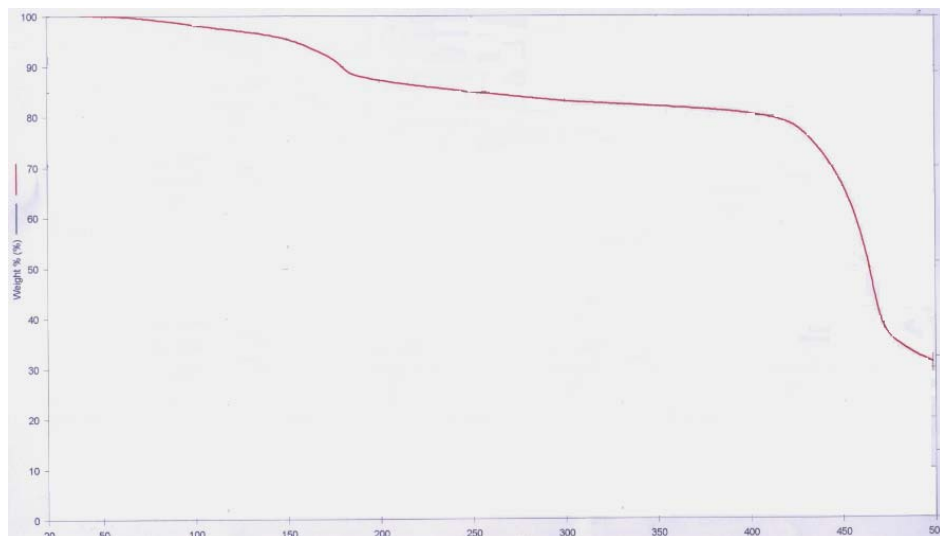


**Figure 18.** TGA analysis of the Me-QxBox receptor in air.

The TGA curve reported above shows the thermal decomposition of Me-QxBox. The first slope that starts at 60°C and finishes at 180°C can be considered as the thermal decomplexation of the entrapped guest inside the cavity. The thermal degradation of the complex starts around 420°C, which is shown by the second slope.

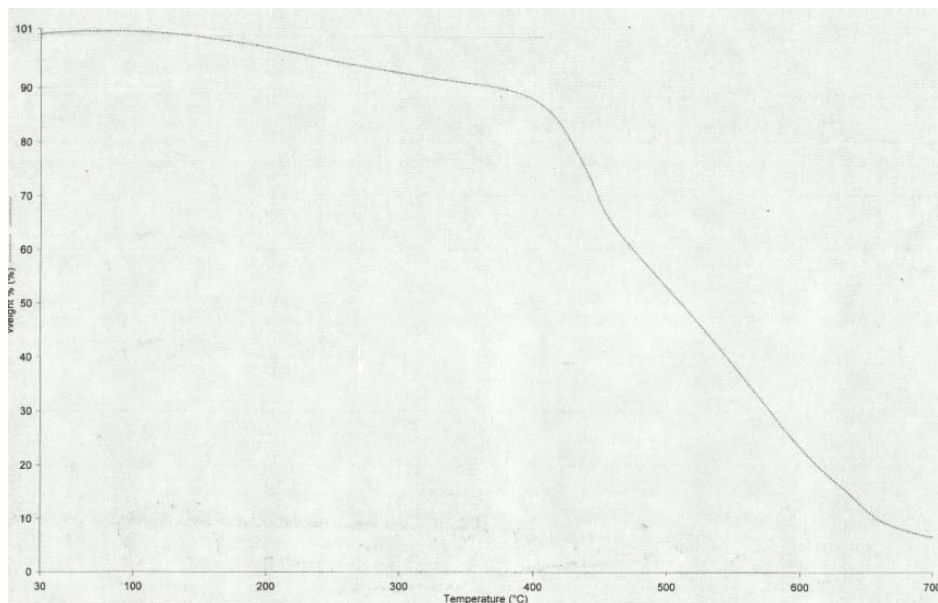


**Figure 19.** TGA analysis of the Et-QxBox receptor in air.

The TGA curve of Et-QxBox is similar to the Me-QxBox one. The initial 7% weight loss is due to the thermal desorption of the aromatic guests complexed in the receptor's cavity. The thermal degradation of Et-QxBox starts at 410°C.

Both TGA analyses show high thermal stability of the new QxBox cavitands, which permits to use them in the stand-alone on-line systems for air monitoring. The observed thermal decomplexation of the entrapped guest is a significant proof of the high complexation forces inside the host molecule.

### 2.5.2. The SPME measurements.

The aim of this part was to perform analytical measurements of new receptors for the entrapment of aromatic hydrocarbons. Solid Phase Micro Extraction (SPME) was used following the general procedure showed below.

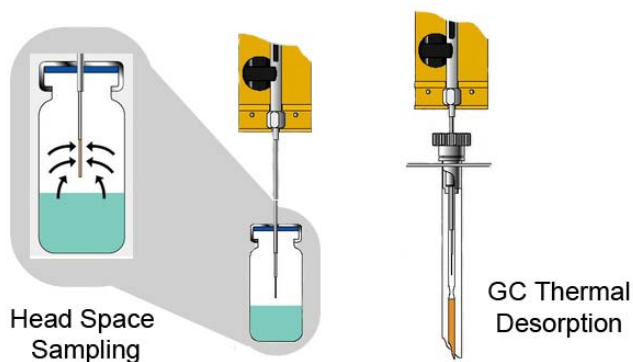


**Figure 20.** SPME setup and procedure.

The sample to be analyzed is closed in a sealed vial and the fibre is introduced in the headspace of the vial without immersing it into the liquid. Then, the incubation is performed for different times and at various temperatures, and the thermal desorption is performed in the GC inlet. The fibre for the analysis was prepared coating the commercial silicon fibre with the fine powdered QxBox receptor with the help of epoxy glue. In this way, the cavitand is only physisorbed on the polymeric surface and not covalently linked to the resin.

The fibres were controlled by SEM imaging using LEICA CAMBRIDGE 430i with EDX OXFORD ISIS working at 25 kV at distance of 18mm.

### The QxBox SPME analysis.

Figure 21 shows the SEM image of the SPME fibre coated with crystalline Et-QxBox receptor. The dispersion of the cavitand on the surface is homogeneous and the calculated average thickness of the film is  $48 \pm 3 \mu\text{m}$ .

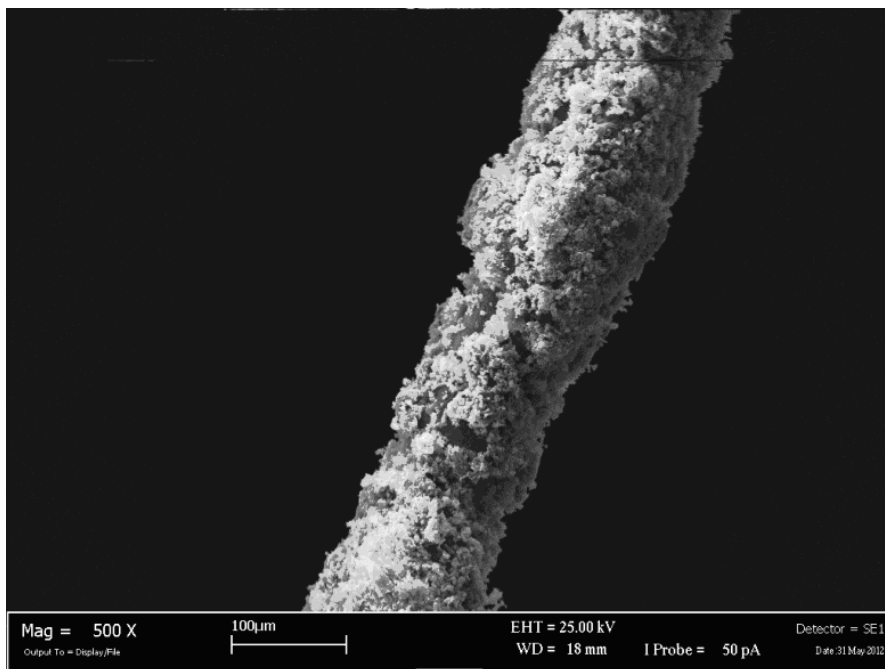


**Figure 21.** SEM image of Et-QxBox coated silicon fibre for SPME analysis.

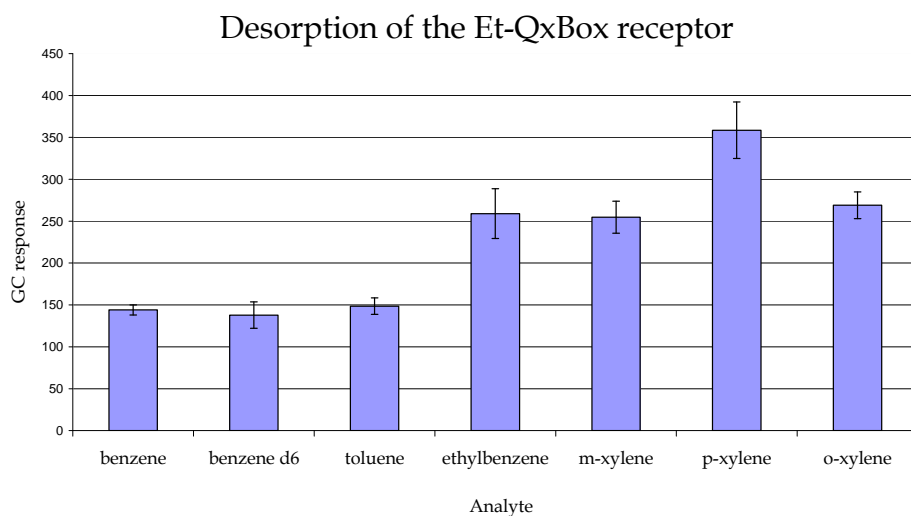
### The analytical selectivity tests.

Selectivity analyses were performed as follows: the fibre was incubated in the headspace of the vial containing the BTEX mixture in methanol, with ratio reported in Table 3, at 40°C for 15 min. Concentrations and composition of the BTEX mixture reproduce exactly the ones observed in the urban environment.

Complex	Concentration [ng/m <sup>3</sup> ]
Benzene	70
Toluene	411
Ethylbenzene	95
<i>m-, p</i> -Xylene	190
<i>o</i> -Xylene	95

**Table 3.** The BTEX concentration used for the selectivity tests.

The fibre was introduced into the inlet of the GC-MS system and thermal desorption was performed. The response factors of the individual analytes were calculated with respect to the actual amount of the substance that reaches the detector. Using the response factors, it was possible to correct the data, obtaining the exact selectivity of the materials. Due to the strong complexation, BTEX desorption was performed at 250°C. The normalized response are reported in Graph 1 Et-QxBox (8)



**Graph 1.** Normalised desorption profile of the Et-QxBox SPME fibre performed at 250°C (benzene- $d_6$  is used as a reference).

These studies evidence that the solid Et-QxBox binds all BTEX compounds from the gas phase. There is a slight preference for xylene and ethylbenzene over benzene and toluene. The gas/solid behaviour is different from the one observed in the crystallization, since in this case also *o*- and *p*-xylene can be detected. This discrepancy infers an important role to cavity desolvation on the liquid phase. Toluene and benzene are less taken, and present almost the same response, showing that a single  $\text{CH}_3$  group does not influence so much the complexation.

The same protocol was used in order to determine Me-QxBox selectivity toward BETX. The Me-QxBox cavitand was fixed on SMPE fibre, and its surface homogeneity was controlled by the SEM microscopy analysis, confirming good homogeneity of the fibre coating (Figure 22).

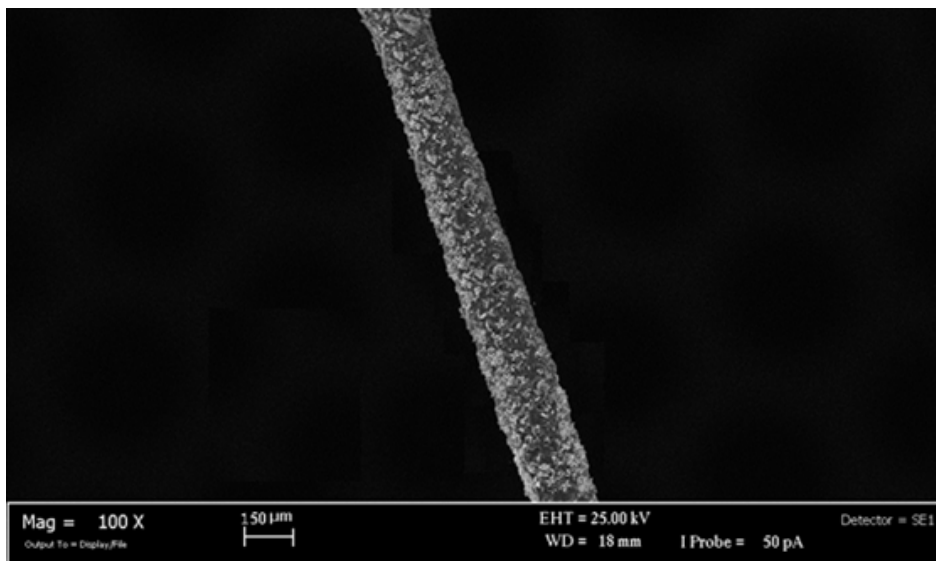
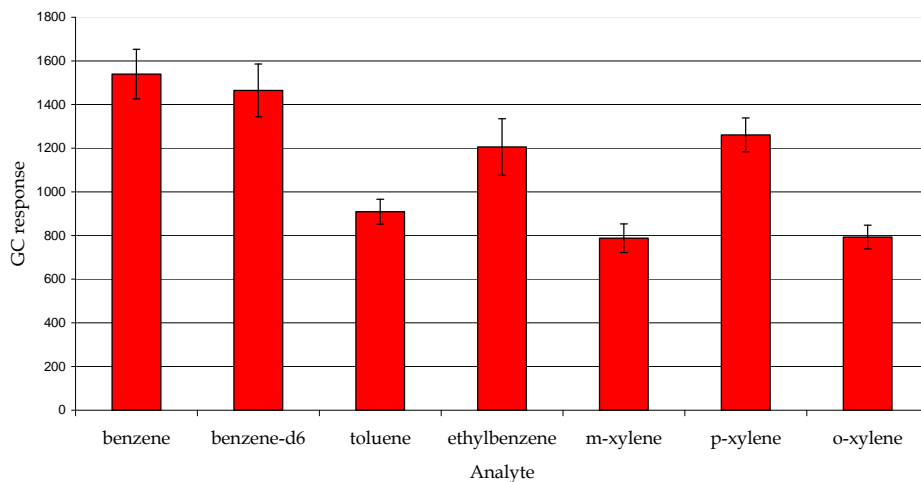


**Figure 22.** SEM image of Me-QxBox coated silicon fibre for SPME analysis.

The same conditions used for the Et-QxBox selectivity measurements were used as well in this part and Graph 2 shows the desorption profile of Me-QxBox (9).

## Desorption of the Me-QxBox receptor

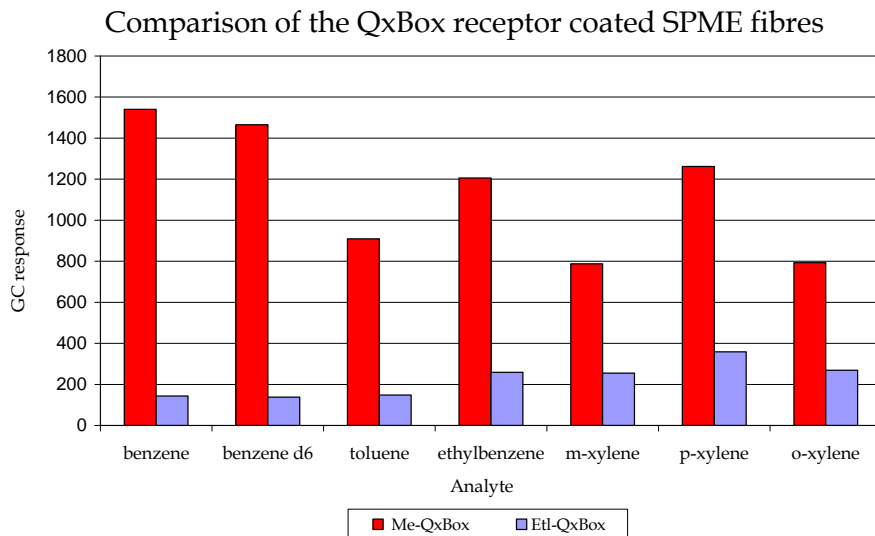


**Graph 2.** Normalised desorption profile of the Me-QxBox SPME fibre performed at 250°C (benzene- $d_6$  is used as a reference).

The use of methylene bridges for the receptor rigidification provides a better match between the shape of the cavity and the shape of the guest, which eventually leads to an improved selectivity pattern. The extremely rigid Me-QxBox cavity pushes the selectivity toward benzene. The benzene uptake predominates over methyl-decorated toluene and xylenes due to tight cavity mouth.



Graph 3 shows the comparison between Me-QxBox and Et-QxBox SPME fibres uptake.



**Graph 3.** Comparison of the selectivity between QxBox receptors.

As it can be inferred from graph 3, the tightening of the cavity mouth has a strong influence both on selectivity and uptake ability. Me-QxBox outperforms Et-QxBox in both. As for selectivity the cavity entrance reduction favours benzene uptake over TEX as planned. Now benzene is the best adsorbed analyte, as desired. The sensitivity boost rationalization is more complicated: a kinetically stronger inclusion driven by tightening could possibly shift the partition coefficient between solid and gas phase toward the solid one. Indeed, the cavity tightening strongly influences the receptor binding forces. While the larger Et-QxBox receptor prefers bigger molecules like xylenes, due to the interactions described previously, the tight Me-QxBox receptor presents better affinity toward the smaller benzene ring (with an increase of the binding forces of eleven times)

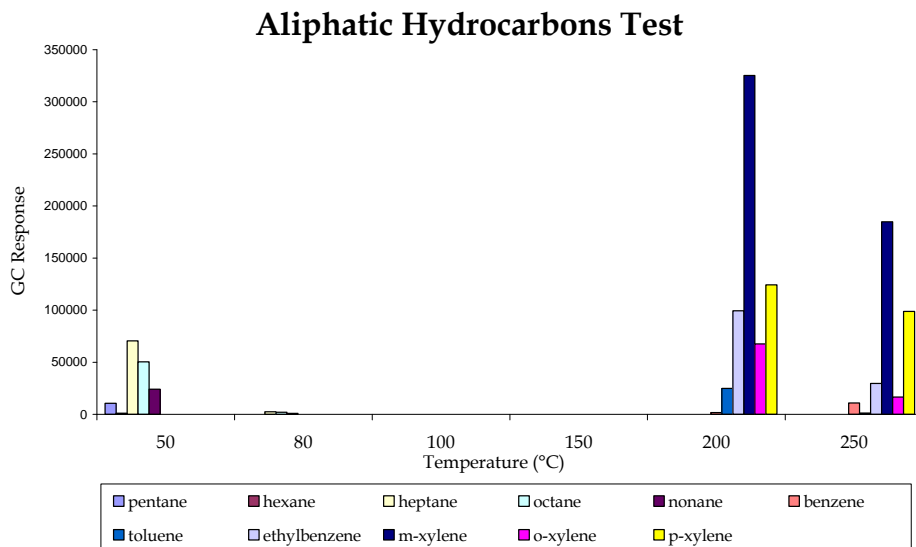
**Aliphatic hydrocarbon test.**

In order to mimic the real environment the test using aliphatic hydrocarbons in superior concentration, in compare to the BTEX, has been performed. The aliphatic hydrocarbon composition (Table 4) was used in large access in order to examine the QxBox performance in environment containing large access of the not interesting ingredients.

Analyte	Concentration [ng/m <sup>3</sup> ]
pentane	32100
hexane	38400
heptane	44600
octane	50900
nonane	57100

**Table 4.** *The aliphatic hydrocarbons, with their concentration, used for the desorption tests.*

The fibre was incubated in the head-space of the vial containing BTEX mixture (see Table 3) together with aliphatic hydrocarbons (see Table 4) dissolved in methanol for 15 minutes. The analysis were performed in various desorption temperatures in order to obtain full desorption profile of the system (see Graph 4 below).



**Graph 4.** *The desorption profile of the Et-QxBox cavitand upon aliphatic and aromatic hydrocarbons exposure.*

The aliphatic hydrocarbons were release only at low temperature, mostly at 50°C. Some traces of heptane, octane and nonane were detectec as well at 80°C. No release above 80°C were observed, which confirm that aliphatic hydrocarbons does not perform any specific interaction with the QxBox receptor and can not influences on the BTEX uptake and its further release from the cavity. The BTEX analytes were desorbed only at high temperatures as expected.

Measured limits of detection (LOD) for BTEX uptake by the Me-QxBox and Et-QxBox were compared with the LOD values of commercially used systems for air quality control toward aromatic hydrocarbons (Table 5).

LOD [ng/m <sup>3</sup> ]						
	EtQxBOX (15 min)	MeQxBOX (15 min)	DVB -CAR- PDMS (15 min)	CAR- PDMS (15 min)	RADIE- LLO® (24 h)	OPTIC FIBRE <sup>14</sup> (25 min)
benzene	2,8	0,40	17,1	16,4	290	1,6
toluene	0,08	0,34	2,1	4,4	90	1,5
etilbenzene	0,01	0,51	4,8	14,2	40	1,2
m-xilene	0,002	1,17	6,1	18,4	70	1,3
p-xilene	0,001	0,56	6,1	18,4	80	1,7
o-xilene	0,1	1,02	14,3	24,6	10	2,0

**Table 5.** LOD comparison between the QxBox receptors and commercial available systems.

The Me-QxBox and Et-QxBox receptors present better performances compared to the systems using Radiello® as well as high-ended apparatus based on the optical fibres. Tested commercially used fibres, CAR-PDMS and DVB-CAR-PDMS, offer lower sensitivity and poor selectivity with respect to QxBox receptors. The shorter time of analysis together with higher sensitivity toward BTEX mixture and higher selectivity makes our system the most promising material for air quality control toward harmful aromatic hydrocarbons.

## 2.6. The stand-alone mini-GC system for VOCs monitoring.

To preliminarily understand the Et-QxBox behaviour, the final device (see Chapter 1) modified by removing the GC separation column (replaced by a by-pass), to tests cavitands performance (Figure 23).

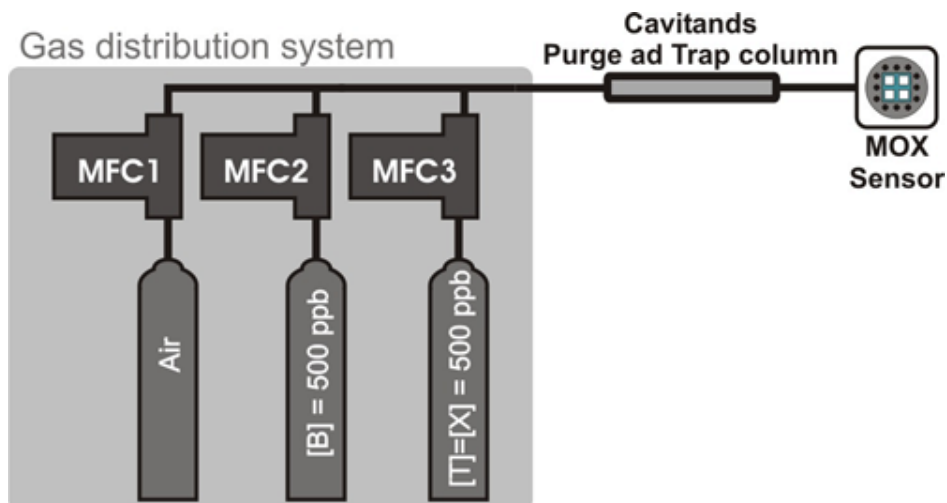


**Figure 23.** The Purge and Trap setup used in Et-QxBox desorption kinetics measurements.

The apparatus setup used for QxBox receptors testing toward BETX is composed by a gas distribution system comprising several mass flow controllers connected to certified cylinders provides a calibrated mixture of aromatic VOCs, which is then sampled by the Et-QxBox cavitand in a glass “trap” in a powder form (Figure 24). At the end of the by-pass “trap”, the sensor (Metal Oxide (MOX) or Photo Ionization Detector (PID)) is placed in a low-volume chamber and connected to the PC.



**Figure 24.** The “trap” filled with crystalline for of the Et-QxBox receptor with 2€ coin for size indication.

The sampling process was performed at room temperature with 11 sccm flux of nitrogen mixture of benzene and toluene-xylene. The temperature was increased by ramping with approximately 50°C per 1 minute, and obtained signal was transduced using PID sensor. The desorption kinetics of Et-QxBox cavitated is shown on the figure 25.

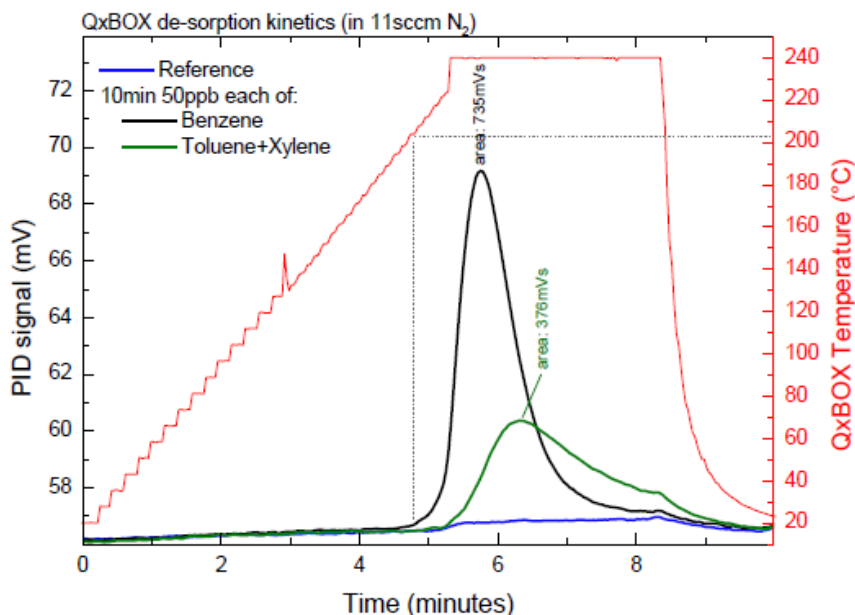


**Figure 25.** The desorption kinetics of the Et-QxBox cavitated using purge and trap system.

As shown on the figure above, the Et-QxBox start to release benzene around 205°C (after 4,5 minutes), with the desorption maximum around 240°C. In the case of Toluene-Xylene mixture its release from the receptor cavity was found around 240°C. The desorption kinetics between Benzene and mixture of Toluene-Xylene is evident, and due to the different complexation forces described previously.

The control experiment employing the QxCav cavitand was performed in order to compare those two similar tetraquinoxaline cavitands. For the tests the same setup was used, except of the sensor type (PID was replaced by the MOX sensor). The sampling process was performed at room temperature with 30 sccm flux of nitrogen mixture of benzene and toluene-xylene. The temperature was increased by ramping with approximately 30°C for 5 minutes, and the results are reported in the figure 26 below.

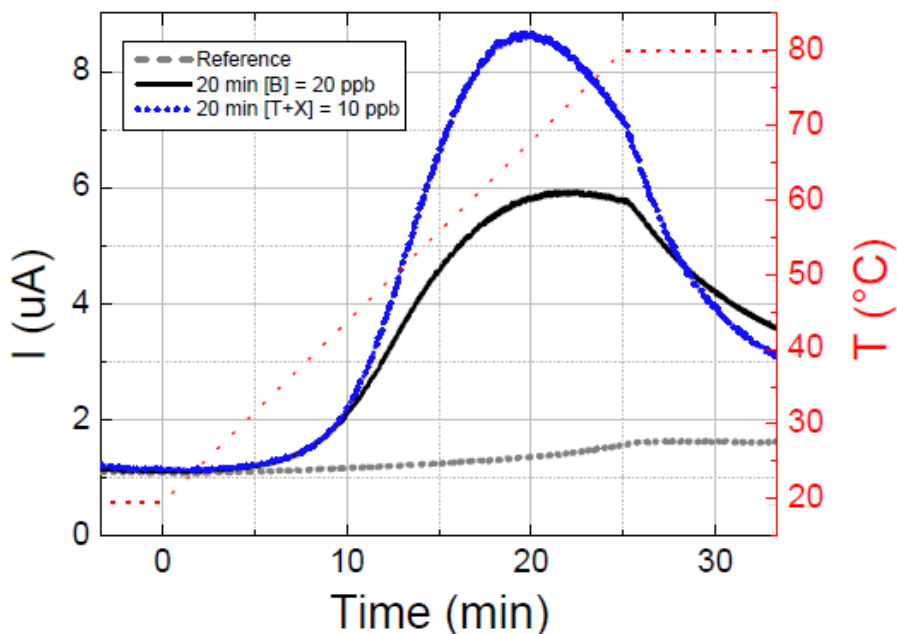


**Figure 26.** *The desorption kinetics of the QxCav cavitand using purge and trap system.*

As shows the figure above, the desorption kinetics of the QxCav is different from the Et-QxBox. The response toward Benzene is minor than in the case of Toluene-Xylene mixture and no differences, neither in the desorption temperature, nor in the release time were observed. The Et-QxBox cavitand overrides QxCav in sensitivity and selectivity. Another advantage is better efficiency: in the case of Et-QxBox cavitand the benzene release starts above 200°C, while in the case of QxCav receptor the analyte release began at room

temperature. Another advantage of the rigid QxBox receptor is linearity of the response with sampling time (Figure 27).

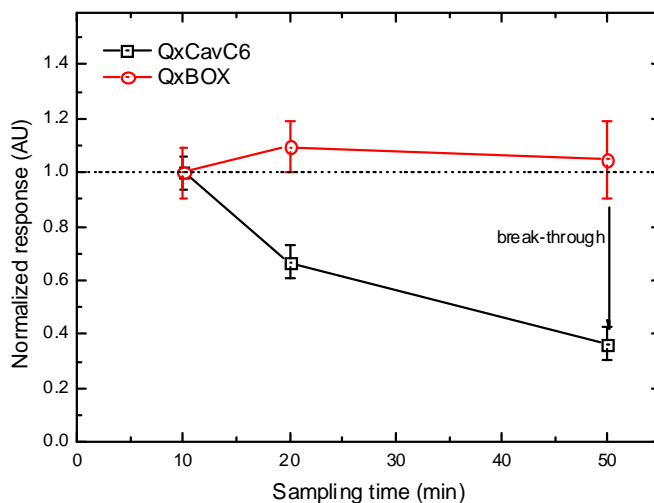


**Figure 27.** Normalized response of the mini-GC system towards benzene, at increasing sampling times.

The “mini-GC response” is defined as the response towards 1 ppb of benzene sampled for 1 min, and the “normalized response” as the response normalized to the first point, which is corresponding to 10 min sampling. In the case of Et-QxBox, when benzene is sampling for 10 min, the system have normalized response = 1 (1 mA /ppb /min). The Et-QxBox cavitand keeps the same normalized response even, if we increase the sampling time to 50 min. In the case of QxCav receptor the linearity is not kept (Figure 27). If the sampling time is increased to the 50 min, the normalized response of QxCav is much lower, lower than 0.4, this means that it is losing part (>60%) of the sampled during the first part of the 50 min, due to a analyte breakthrough caused by the cavity movements in the solid state.



## 2.7. Fluorescent measurements.

One of the main issues in the development of chemical sensors is the effective transduction of the host-guest interactions to the analytically useful data. The use of fluorescence, which is one of the most sensitive analytical techniques (Chapter 1), as high sensitivity transducer of specific host-guest recognition event has been recently implemented in our group thanks to the cooperation with the group of Prof. Luca Prodi from the University of Bologna.<sup>15</sup> The presence of a cavity frozen in the *vase* conformation by four bridges (methylene and ethylene), promotes changes in the Et-QxBox receptor properties. Indeed, upon UV light excitation, the Et-QxBox cavitant becomes fluorescent, while this behaviour was not observed in the case of the QxCav cavitant. In Figure 28 the emission spectra of Et-QxBox and QxCav are compared.

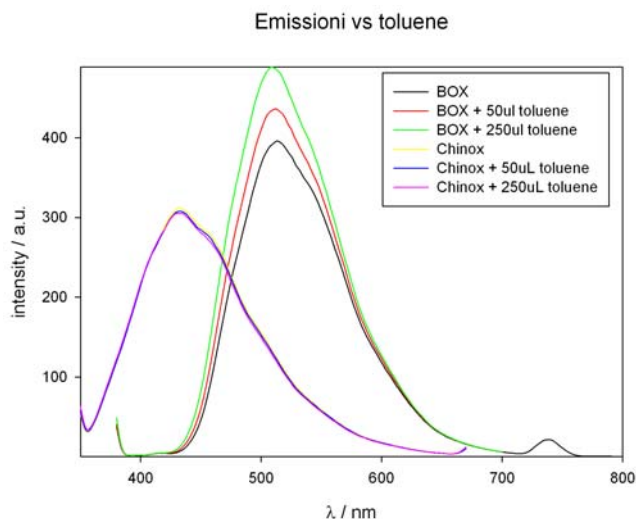


**Figure 28.** Luminescent titration of Et-QxBox (right) and QxCav (left) with toluene.

Upon addition of the guest molecules the luminescence intensity increases in the Et-QxBox case, while QxCav is insensitive upon titration with toluene. Possibly, the presence of the complexed toluene molecule performs the energy transfer, which affects the luminescent properties of the host molecule. In order to explore the luminescent properties of the system, fluorescent titration was

performed. The Et-QxBox cavitand was dissolved in the DMSO and titrated with *o*-, *p*-, and *m*-xylene and the results are summarised below.

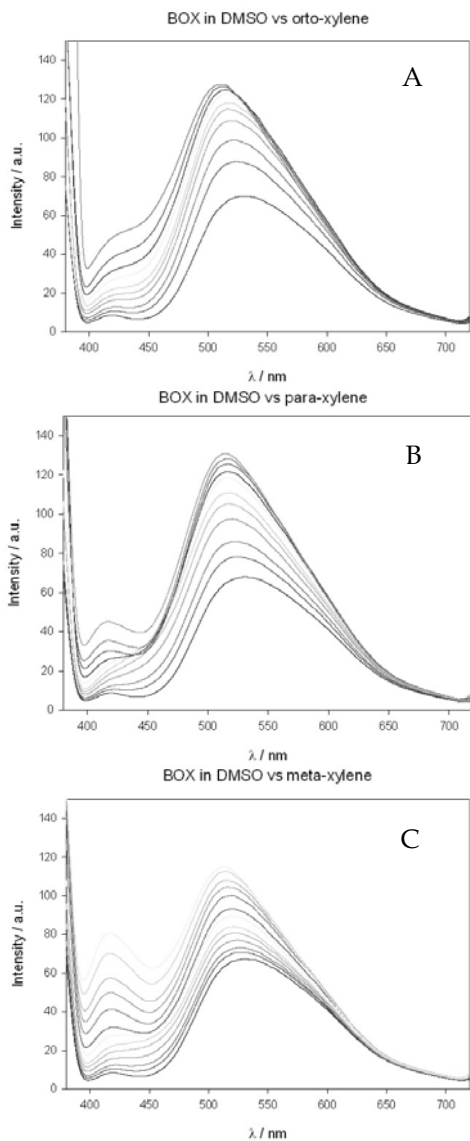


**Figure 29.** The fluorescence titration of the Et-QxBox with *o*-xylene (A), *p*-xylene (B) and *m*-xylene (C) in DMSO.

The maximum of the intensity of uncomplexed Et-QxBox cavitand was found to be at  $\lambda = 520$  nm. The xylene addition caused luminescence intensity increase in all three cases. A small shift in emission maximum was also observed and after system saturation by the analyte was found to be at  $\lambda = 510$  nm in all cases. So, the emission wavelength change is directly caused by the analyte concentration changes.

The luminescence measurement of the Et-QxBox receptor were performed in solution, confirming its high sensitivity toward aromatic guests (Toluene, Xylenes). The solid state measurements are ongoing. If this increase in fluorescence emission will be maintained in the solid state, the receptor will be extremely appealing for stand-alone device for selective benzene detection in the urban areas.

## 2.8. Conclusions and perspectives.

The design and the synthesis of novel rigid QxBox receptors has been accomplished. The cavity blocking by the use of four aliphatic linkers, which hold the four quinoxaline walls in the rigid *vase* form, strongly affects the cavitands selectivity and sensitivity. The tightening strategy implemented in the case of Me-QxBox by the aliphatic linkers shortening boosted the receptor performances. For selectivity the cavity boosted preference toward the benzene molecule over TEX. For sensitivity, Me-QxBox turned out to be by far more efficient than commercial fibres in trapping BTEX. The X-Ray studies of the Qx-Box@analyte complexes provided a clear view of the type and number of interactions present. The gas/solid measurements performed by the SPME analysis gave the information about the system behaviour upon exposure to the analytes from the gas phase. The benzene discrimination from the other TEX hydrocarbons has been achieved in the case of Me-QxBox cavitand. The Et-QxBox cavitand has been tested in the final device. The benzene separation from xylenes has been confirmed by the ramp thermal desorption. The cavity blocking by the aliphatic bridges induced the appearance of fluorescent properties in the QxBox receptors. The analyte uptake was found to be a promoter of luminescence intensity increase. In the future, the final device will be tested in the urban areas in order to understand the system properties in

real-time measurements. The device modification are planned, the removal of the mini-GC column together with electronic transducer. The future operating mode will be based on the fluorescence measurements.

## **2.9. Acknowledgements.**

Special thanks to Dr. Chiara Massera from Parma University for the crystal structures determination, to Nicolò Riboni and Dr. Federica Bianchi from Parma University for SPME analysis, to Dr. Stefano Zampolli from CNR-IMM Bologna for the final device fabrication and tests, to Dr. Damiano Genovese and Prof. Luca Prodi from Bologna University for luminescence measurements.

## 2.10. Experimental part

**General Methods.** All commercial reagents were ACS reagent grade and used as received. Solvents were dried and distilled using standard procedures.  $^1\text{H}$  NMR spectra were recorded on Bruker Avance 300 (300 MHz) and on Bruker Avance 400 (400 MHz) spectrometers. All chemical shifts ( $\delta$ ) were reported in parts per million (ppm) relative to proton resonances resulting from incomplete deuteration of NMR solvents. Electrospray ionization mass spectrometry (ESI-MS) experiments were performed on a Waters ACQUILITY UPLC SQ Detector. The Matrix-assisted laser desorption/ionization analysis (M@LDI TOF-TOF) were performed on AB SCIEX MALDI TOF-TOF 4800 Plus using *o*-Cyano-4-hydroxycinnamic acid as a matrix. The GC-Mass analysis were performed on Hewlett-Packard 6890 series plus equipped in Supelco® SLB™ 5ms column and Hewlett-Packard 5973 MS Selective Mass Detector. The TGA analysis were performed on TGA 7 (Perkin Elmer, Waltham, MA, USA) apparatus in air.

### 2.10.1. Synthesis of the QxBox receptors.

#### 1,4-dimethoxy-2,3-dinitro benzene (1)

1,4-dimethoxy benzene (180 mmol) was added into ice-cooled  $\text{HNO}_3$  100% (200 mL) in small portions and stirred for 1h at  $0^\circ\text{C}$ . The ice-bath was removed a yellow precipitate was formed, and the reaction was stirred at  $120^\circ\text{C}$  for 8h. After cooling to RT, the yellow emulsion was poured into a beaker containing ice-cooled water and filtered. The product was recrystallized three times from glacial acetic acid and purified by flash chromatography. Yield: 70%.

$^1\text{H-NMR}$  (400 MHz,  $\text{CDCl}_3$ ):  $\delta$  = 3.98 (s, 6H,  $\text{CH}_3\text{OAr}$ ), 7.20 (s, 2H, ArH)

**GC-MS:** m/z 229  $[\text{M}]^+$

#### 1,4-dimethoxy-2,3-diamino benzene (2)

1,4-dimethoxy-2,3-dinitro benzene **1** (90 mmol), Pd/C in catalytic amount and absolute ethanol (200 mL) were placed inside a reactor under  $\text{H}_2$  atmosphere.

The reactor was mounted in PARR Hydrogenation apparatus under H<sub>2</sub> at 3 bar and was stirred at RT for 24h. The product was filtered through celite, washed with ethanol and the solvent was removed under reduced pressure. The final product was obtained in quantitative yield.

<sup>1</sup>H-NMR (400 MHz, CDCl<sub>3</sub>): δ = 3.08 (bs, 4H, H<sub>2</sub>NAr), 3.77 (s, 6H, CH<sub>3</sub>OAr), 6.25 (s, 2H, ArH)

GC-MS: m/z 169 [M]<sup>+</sup>

### 5,8-dimethoxyquinoxaline-2,3-dione (3)

1,4-dimethoxy-2,3-diamino benzene (7.7 mmol, 1 eq.) dissolved in 4N HCl (10 mL) and a 4N HCl solution of oxalic acid (10 mmol, 1.3 eq.) were added to a flask and refluxed for 16h. After cooling to RT the formed precipitate was filtered through paper filter. The collected solid was dried under vacuum. Compound **3** was obtained pure in 95% yield.

<sup>1</sup>H-NMR (400 MHz, DMSO-*d*<sub>6</sub>): δ = 3.77 (s, 6H, CH<sub>3</sub>OAr), 6.68 (s, 2H, ArH), 11.20 (s, 2H, CNHC)

GC-MS: m/z 223 [M]<sup>+</sup>

### 2,3-dicloro-5,8-dimethoxyquinoxaline (4)

Compound **3** (11.4 mmol, 1 eq.), POCl<sub>3</sub> (228 mmol, 20 eq.) and three drops of dry DMF were added into dry C<sub>2</sub>H<sub>4</sub>Cl<sub>2</sub> (100 mL) under Ar and stirred at 80°C for 16h. After cooling to RT the solvent was removed under vacuum and the obtained solid was dissolved in DCM and filtered through celite. The crude was purified by flash chromatography. The final product was obtained as a yellow solid in 98% yield.

<sup>1</sup>H-NMR (400 MHz, CDCl<sub>3</sub>): δ = 4.05 (s, 6H, CH<sub>3</sub>OAr), 7.07 (s, 2H, ArH)

GC-MS: m/z 260 [M]<sup>+</sup>

### Resorcinarene [C<sub>6</sub>H<sub>13</sub>, H] (5)

Resorcinol (109 mmol, 1 eq.) and heptaldehyde (109 mmol, 1 eq.) were added to a ice-cooled round-bottomed flask containing MeOH (60 mL), a 37% solution of

HCl (200 mmol, 2 eq.) was added dropwise over 30 min. After the addition, the reaction was stirred at 50°C for 5 days. The reaction was quenched with water, filtered, dried under vacuum and recrystallized three times from MeOH. The final product **5** was obtained as a fine beige powder in 60% yield.

<sup>1</sup>H-NMR (400 MHz, Acetone-*d*<sub>6</sub>): δ = 0.90 (t, 12H, *J* = 6.6 Hz, CH<sub>3</sub>CH<sub>2</sub>CH<sub>2</sub>), 1.27-1.45 (m, 32H, -CH<sub>2</sub>-), 2.31 (q, 8H, *J* = 7.8 Hz, CHCH<sub>2</sub>CH<sub>2</sub>), 4.31 (t, 4H, *J* = 7.8 Hz, CHCH<sub>2</sub>CH<sub>2</sub>), 6.25 (s, 4H, ArH<sub>down</sub>) 7.56 (s, 4H, ArH<sub>up</sub>), 8.45 (s, 8H, ArOH)

ESI-MS: *m/z*: 847 [M+Na]<sup>+</sup>

### Octamethoxy-Quinoxaline cavitand (**6**)

Resorcinarene **5** (0.15 mmol, 1 eq.), 2,3-dichloro-5,8-dimethoxyquinoxaline **4** (0.62 mmol, 4 eq.) and dry K<sub>2</sub>CO<sub>3</sub> (1.88 mmol, 12 eq.) were dissolved in dry DMF into an oven-dried microwave vessel under Ar atmosphere and stirred under microwave irradiation at 120°C for 1.5 h. Afterwards, the mixture was extracted with DCM/H<sub>2</sub>O, the organic fractions were dried over Na<sub>2</sub>SO<sub>4</sub> and the solvent was removed under reduced pressure. The crude was purified by flash chromatography and the final product was obtained as yellow powder in 70% yield.

<sup>1</sup>H-NMR (300 MHz, CDCl<sub>3</sub>) - *kite* conformation: δ = 0.77 (t, 12H, *J* = 6.2 Hz, CH<sub>3</sub>CH<sub>2</sub>CH<sub>2</sub>), 1.10-1.25 (m, 32H, -CH<sub>2</sub>-), 1.97 (q, 8H, *J* = 6.8 Hz, CHCH<sub>2</sub>CH<sub>2</sub>), 3.92 (t, 4H, *J* = 7.4 Hz, CHCH<sub>2</sub>CH<sub>2</sub>), 3.98 (s, 24H, CH<sub>3</sub>OAr), 6.8 (s, 4H, ArH<sub>down</sub>), 6.90 (s, 8H, CH<sub>3</sub>OArH<sub>2</sub>) 7.37 (s, 4H, ArH<sub>up</sub>)

MALDI TOF-TOF: *m/z*: 1569 [M]<sup>+</sup>

### Octahydroxy-quinoxaline cavitand (**7**)

Cavitand **6** (0.12 mmol, 1 eq.) was dissolved in toluene (10 mL) under Ar atmosphere and AlCl<sub>3</sub> (1.32 mmol, 10.5 eq.) was added and stirred at 130°C for 24h. 30 mL of H<sub>2</sub>O were then added into the boiling toluene and a yellow precipitate was formed. After cooling down to room temperature, the solvent was removed and the yellow solid was sonicated with 1N HCl, filtered and dried under vacuum. The final product was obtained pure as a brown solid in 90% yield.

<sup>1</sup>H-NMR (400 MHz, DMSO-*d*<sub>6</sub>) - fluxional *vase* conformation:  $\delta$  = 0.79 (t, 12H,  $J$  = 6.6 Hz, CH<sub>3</sub>CH<sub>2</sub>CH<sub>2</sub>), 1.14-1.35 (m, 32H, -CH<sub>2</sub>-), 2.33 (bq, 8H CHCH<sub>2</sub>CH<sub>2</sub>), 4.62 (bt, 4H, CHCH<sub>2</sub>CH<sub>2</sub>), 6.94 (s, 8H, CH<sub>3</sub>OArH<sub>2</sub>), 7.51 (s, 4H, ArH<sub>down</sub>), 7.77 (s, 4H, ArH<sub>up</sub>), 9.21 (s, 8H, ArOH)

**MALDI TOF-TOF:** m/z: 1457 [M]<sup>+</sup>

### Et-QxBox cavitand (8)

The octahydroxy-quinoxaline cavitand **7** (0.13 mmol, 1 eq.), di-*p*-tosylate-ethyleneglycol (0.76 mmol, 5.5 eq.), and Cs<sub>2</sub>CO<sub>3</sub> (2.6 mmol, 20 eq.) were dissolved in dry DMF (5 mL) under Ar into an oven-dried microwave vessel and stirred under microwave irradiation at 120°C for 1,5 h. Afterwards, the reaction was extracted with DCM/H<sub>2</sub>O, the organic fractions were dried over Na<sub>2</sub>SO<sub>4</sub> and the solvent was removed under reduced pressure. The crude was purified by flash chromatography yielding the final product as a yellow solid in 70% yield.

<sup>1</sup>H-NMR (300 MHz, CDCl<sub>3</sub>) - *vase* conformation:  $\delta$  = 0.95 (t, 12H,  $J$  = 6.4 Hz, CH<sub>3</sub>CH<sub>2</sub>CH<sub>2</sub>), 1.20-1.62 (m, 32H, -CH<sub>2</sub>-), 2.33 (bq, 8H CHCH<sub>2</sub>CH<sub>2</sub>), 4.45-4.65 (m, 16H, ArOCH<sub>2</sub>CH<sub>2</sub>O), 5.78 (t, 4H,  $J$  = 7.9 Hz, CHCH<sub>2</sub>CH<sub>2</sub>), 6.70 (s, 8H, ArH<sub>2</sub>), 7.4 (s, 4H, ArH<sub>down</sub>), 8.30 (s, 4H, ArH<sub>up</sub>)

**MALDI TOF-TOF:** calculated for C<sub>92</sub>H<sub>88</sub>N<sub>8</sub>O<sub>16</sub> [M] m/z: 1560.6318, found m/z= 1560.6299

### Me-QxBox cavitand (9)

The octahydroxy-quinoxaline cavitand **7** (0.066 mmol, 1 eq.), Bromo-chloro-methane (2 mmol, 30 eq.) and dry K<sub>2</sub>CO<sub>3</sub> (0.1 mmol, 14 eq.) were dissolved in dry DMF (5 mL) under Ar, placed into an oven-dried microwave vessel and stirred under microwave irradiation at 120°C for 1,5 h. Afterwards, the mixture was extracted with DCM/H<sub>2</sub>O, the organic fractions were dried over Na<sub>2</sub>SO<sub>4</sub> and the solvent was removed under reduced pressure. The crude was purified by flash chromatography and the final product was obtained as a yellow solid in 5% yield.



**<sup>1</sup>H-NMR** (300 MHz, Acetone-*d*<sub>6</sub>) - *vase* conformation:  $\delta$  = 0.88 (t, 12H,  $J$  = 6.7 Hz, CH<sub>3</sub>CH<sub>2</sub>CH<sub>2</sub>), 1.21-1.47 (m, 32H, -CH<sub>2</sub>-), 2.52 (bq, 8H CHCH<sub>2</sub>CH<sub>2</sub>), 5.76 (t, 4H,  $J$  = 7.5 Hz, CHCH<sub>2</sub>CH<sub>2</sub>), 6.20 (d, 4H,  $J$  = 6.1 Hz, ArOCH<sub>2</sub>O), 6.60 (d, 4H,  $J$  = 6.1 Hz, ArOCH<sub>2</sub>O), 7.32 (s, 8H, ArH<sub>2</sub>), 7.94 (s, 4H, ArH<sub>down</sub>), 8.13 (s, 4H, ArH<sub>up</sub>)

**MALDI TOF-TOF:** calculated for C<sub>88</sub>H<sub>80</sub>N<sub>8</sub>O<sub>16</sub> [M] m/z: 1504.5692, found m/z= 1504.2636

### 2.10.2. X-Ray analysis.

Intensity data and cell parameters were recorded at 190K on a Bruker APEX II equipped with a CCD area detector and a graphite monochromator (MoK $\alpha$  radiation  $\lambda$  = 0.71073 Å). The structures were solved by direct methods using the SIR97 program<sup>16</sup> and refined on  $F_o^2$  by full-matrix least-squares procedures, using the SHELXL-97 program.<sup>17</sup> Both programs were used in the WinGX suite.<sup>18</sup> The data reductions were performed using the SAINT<sup>19</sup> and SADABS<sup>20</sup> programs. The PLATON SQUEEZE procedure<sup>21</sup> was used for compounds **Et-QxBox@benzene**, **Et-QxBox@toluene**, **Et-QxBox@o-xylene** and **Me-QxBox@benzene** to treat regions of diffuse solvent which could not be sensibly modelled in terms of atomic sites. Their contribution to the diffraction pattern was removed and modified  $F_o^2$  written to a new HKL file. In all cases the number of electrons located were included in the formula, formula weight, calculated density,  $\mu$  and F(000). In the case of **Et-QxBox@benzene** the residual electron density of 682 electrons per unit cell was assigned to 16 benzene molecules. In the case of **Et-QxBox@toluene** and **Et-QxBox@o-xylene** the residual electron density of 82 and 88 electrons per unit cell respectively, was assigned to 2 DMSO molecules. In the case of **Me-QxBox@benzene** the residual electron density of 122 electrons per unit cell was assigned to two chloroform molecules. All the non-hydrogen atoms were refined with anisotropic atomic displacements, with the exclusion of i) some carbon atoms of the alkyl chains and some benzene molecules in **Et-QxBox@benzene**; ii) some atoms of the DMSO solvent and the two disordered methyl carbon atoms of the toluene guest; iii) the methyl atoms of the disordered DMSO molecule in **Et-QxBox@o-xylene**; iv) some atoms of the alkyl chains and of the DMSO solvent and the oxygen atoms of the *p*-nitrotoluene guest in **Et-QxBox@p-nitrotoluene**, v) some

atoms of the disordered alkyl chains in **Me-QxBx**. The hydrogen atoms were included in the refinement at idealized geometries (C-H 0.95 Å) and refined “riding” on the corresponding parent atoms. The weighting schemes used in the last cycle of refinement were  $w = 1/[\sigma^2 F_o^2 + (0.200P)^2]$ ,  $w = 1/[\sigma^2 F_o^2 + (0.1724P)^2 + 0.6729P]$ ,  $w = 1/[\sigma^2 F_o^2 + (0.1522P)^2 + 0.4653P]$ ,  $w = 1/[\sigma^2 F_o^2 + (0.1310P)^2 + 5.8484P]$  and  $w = 1/[\sigma^2 F_o^2 + (0.0911P)^2]$  where  $P = (F_o^2 + 2F_c^2)/3$  for **Et-QxBx@benzene**, **Et-QxBx@toluene**, **Et-QxBx@o-xylene**, **Et-QxBx@p-nitrotoluene** and **Me-QxBx@benzene** respectively.

### 2.10.3. Solution preparation.

Solutions of benzene, toluene, ethylbenzene and xylene at the concentration of 1000 mg/L were obtained from pure compounds in 1 mL vials using methanol as solvent. Solutions of pentane, hexane, heptanes, octane, nonane and decane at the concentration of 1000 mg/L were obtained from pure compounds in 1 mL vials using n-pentane as solvent. Working solutions at the concentration of 10 mg/L were obtained by dilution from the stock solutions.

A BTEX mixture corresponding to the effective air composition was prepared

### 2.10.4. SPME Sampling

Preparation of the fiber: The cavitand, in the form of fine powder, is placed on a silicon support with the help of an epoxy resin resistant at high temperature. A SEM image of the coating is recorded with a LEICA CAMBRIDGE 430i with EDX OXFORD ISIS working at 25 kV at distance of 18mm.

Extraction in Headspace: A solution containing each analyte at 100 ng/l is placed in a 12 mL vial at 40°C for 15 minutes in the presence of the Fiber.

Commercial Fibers used for comparison experiment: StableFlex™, 65µm PDMS-DVB, Supelco (Milano, Italia).

### 2.10.5. GC-MS analysis.

Gas-chromatograph HP 6890 Series Plus, Agilent Technologies (Milano, Italia):

- Column: HP5-MS (l=30 m, i.d.=0.25 mm, d.f.=0.25 µm) (Agilent Technologies);
- Carrier gas: helium
- Carrier gas flux: 1 mL/min
- Carrier gas pressure: 70 KPa.
- Injector Temp: 200°C
- Injection mode: splitless
- Temperature program : 40°C for 8 minutes (20°C/min until 200°C are reached) and then 200°C for 5 minutes (10°C/min until 260°C are reached)

Mass Spectrometer **MSD 5973, Agilent Technologies:**

- Source Temperature: 200°C;
- Transfer Line temperature: 200°C;
- Ionization: E.I. (70 eV);
- Voltage: 2200 V;
- Acquisition modality: Time scheduled monitoring;
- Solvent delay: 0.5 minutes;
- Dwell time: 30 ms;
- Monitored ions: Range from 40 to 150  $m/z$
- Monitored ions BTEX (SIM):
  - from 0.5 to 2 min: 78, 84  $m/z$  for benzene and benzene- $d_6$
  - from 2 to 4 min: 91  $m/z$  for toluene
  - from 4 to 16 min: 91, 106  $m/z$  for ethylbenzene and xylenes
- Monitored aliphatic hydrocarbons ions (SIM):
  - from 0 to 2,00 min 43, 57, 72  $m/z$  for pentane
  - from 0 to 2,00 min 43, 57, 72, 86  $m/z$  for hexane
  - from 2,00 to 3,50 min 43, 57, 71, 100  $m/z$  for heptane
  - from 3,50 to 5,00 min 43, 57, 85, 114  $m/z$  for octane
  - from 5,00 to 16,00 min 43, 57, 85, 128  $m/z$  for nonane

The Mass Spectrometer was tuned using perfluorotributylamine and the analytes were identified by comparison with the retention time of standard solution and with the MS spectra reported in NIST Library (National Institute of Standards and Technology).

## 2.11. References.

- 
- <sup>1</sup> a) Zampolli, S.; Betti, P.; Elmi, I.; Dalcanale, E. *ChemComm.* **2007**, 2790.; b) Zampolli, S.; Elmi, I.; Mancarella, F.; Betti, P.; Dalcanale, E.; Cardinali, G. C.; Severi, M. *Sens. Actuators B* **2009**, 141, 322.
- <sup>2</sup> Vincenti, M.; Dalcanale, E.; Soncini, P.; Guglielmetti, G. *J. Am. Chem. Soc.* **1990**, 112, 445.
- <sup>3</sup> Soncini, P.; Bonsignore, S.; Dalcanale, E.; Ugozzoli, F. *J. Org. Chem.* **1992**, 57, 4608.
- <sup>4</sup> a) Dalcanale, E.; Costantini, G.; Soncini, P. *J. Inclusion Phenom. Mol. Recognit. Chem.* **1992**, 13, 87; b) Ferrari, M.; Ferrari, V.; Marioli, D.; Taroni, A.; Suman, M.; Dalcanale, E. *IEEE Trans. Instrum. Meas.* **2006**, 55, 828.
- <sup>5</sup> Hartmann, J.; Hauptmann, P.; Levi, S.; Dalcanale, E. *Sens. Actuators, B*, **1996**, 35, 154.
- <sup>6</sup> Feresenbet, E. B.; Busi, M.; Ugozzoli, F.; Dalcanale, E.; Shenoy, D. K. *Sens. Lett.* **2004**, 2, 186.
- <sup>7</sup> Bianchi, F.; Pinalli, R.; Ugozzoli, F.; Spera, S.; Careri, M.; Dalcanale, E. *New. J. Chem.*; **2003**, 27, 502.
- <sup>8</sup> Vincenti, M.; Dalcanale, E. *J. Chem. Soc.; Perkin Trans. 2* **1995**, 1069.
- <sup>9</sup> Azov, V. A.; Jaun, B.; Diederich, F. *Helv. Chim. Acta.* **2004**, 87, 449.
- <sup>10</sup> Shirtcliff, L.; Xu, H.; Diederich, F. *Eur. J. Org. Chem.* **2010**, 846.
- <sup>11</sup> Pochorovski, I.; Breiten, B.; Schweizer, W. B.; Diederich, F. *Chem. Eur. J.* **2010**, 16, 12590.

- <sup>12</sup> Soncini, P.; Bonsignore, S.; Dalcanale, E.; Ugozzoli, F. *J. Org. Chem.* **1992**, *57*, 4608.
- <sup>13</sup> Nardelli, M. *J. Appl. Crystallogr.* **1996**, *29*, 296.
- <sup>14</sup> Silva, L. I. B.; Santos, T. A. P.; Duarte, A. C. *Talanta* **2009**, *78*, 548.
- <sup>15</sup> Maffei, F.; Betti, P.; Genovese, D.; Montalti, M.; Prodi, L.; De Zorzi, R.; Geremia, S.; Dalcanale, E. *Angew. Chem. Int. Ed.*, **2011**, *50*, 4654.
- <sup>16</sup> Altomare, A.; Burla, M. C.; Camalli, M.; Cascarano, G. L.; Giacovazzo, C.; Guagliardi, A.; Moliterni, A. G. G.; Polidori, G.; Spagna, R. *J. Appl. Crystallogr.* **1999**, *32*, 115.
- <sup>17</sup> Sheldrick, G. M. *SHELXL97. Program for Crystal Structure Refinement*, University of Göttingen: Göttingen, Germany, **1997** and *Acta Cryst. A* **2008**, *64*, 112.
- <sup>18</sup> WinGX, Farrugia, L. J.; *J. Appl. Crystallogr.* **1999**, *32*, 837.
- <sup>19</sup> *SAINTE, Software Users Guide*, 6.0; Bruker Analytical X-ray Systems: 1999.
- <sup>20</sup> Sheldrick, G. M. *SADABS Area-Detector Absorption Correction*, 2.03; University of Göttingen: Göttingen, Germany, **1999** and *SADABS v. 2008-1*, **2008**
- <sup>21</sup> Sluis, P. v.d. and Spek, A. L. *Acta Cryst. Sect A* **1990**, *46*, 194.

**QxCage: The ultimate  
approach for Benzene  
detection in air**

3

### 3.1. Introduction.

The outstanding molecular recognition properties of QxBx receptors prompted us to continue on this approach to find the ultimate receptor for benzene detection in air. The discrimination among aromatic hydrocarbons has been achieved by the Me-QxBx cavitand with high sensitivity on the gas/solid interface, making it the most promising receptor available for air quality control. The lack of selectivity presented by QxCav cavitand has been decreased meaningfully by blocking the cavity in the rigid vase conformation with four aliphatic linkers. Unfortunately, the necessity to use a GC column for the Benzene/Toluene separation step is still a pivotal issue. Therefore, a new fresh approach based on the selective cavity shaping toward benzene has been taken.

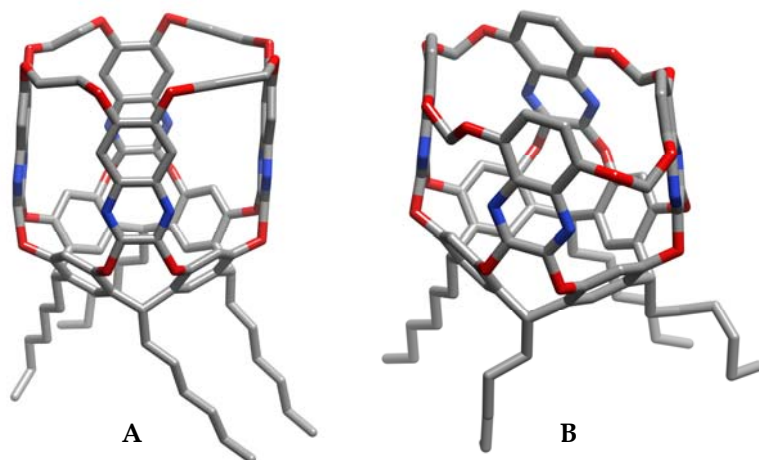


**Figure 1.** *The conceptual 3D model of the QxCage receptor (A) and the molecular structure of the Me-QxBx receptor (B).*

In the case of QxBx receptors, the tightening of the cavity using short aliphatic hydrocarbons as quinoxaline linking units was found to be effective in sensitivity enhancing. Moreover, bridges shortening, from two to one carbon atom, increased the receptor sensitivity increment toward benzene eleven times. Based on those two experimental results a new receptor was implemented, moving the ethylene linkers from the 5,8 positions to 6,7 positions (relative to the quinoxaline moiety, Figure 1A). The computer simulations performed on the 3D model of the new QxCage molecule shows



that new positions of the bridges should tighten the entrance of the cavity making it accessible only for benzene. Figure 2 shows the 3D simulation of the new QxCage receptor compared with Et-QxBox

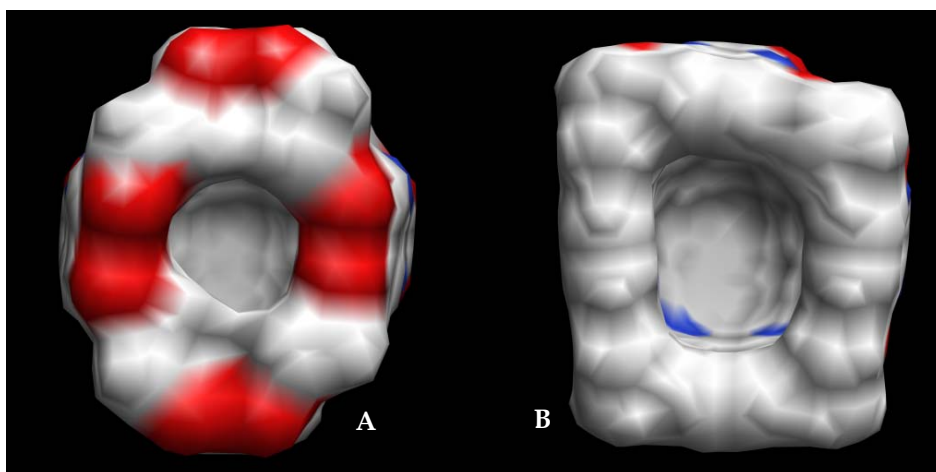


**Figure 2.** Comparison between the 3D structural models of QxCage (A) and Et-QxBox (B).

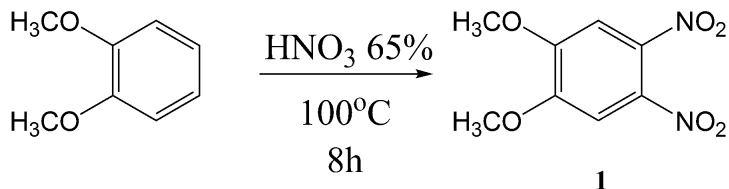
The new 6,7-positions of the bridging units create a narrower cavity entry, with respect to the Et-QxBox receptor, making it less accessible for alkyl substituted molecules like TEX. This change should allow the separation of benzene from other aromatic hydrocarbons directly at the molecular level.

### 3.2. Synthesis of new QxCage receptor.

As in the QxBox case, the multistep synthesis of the new tetraquinoxaline cavitaund (QxCage) is divided in two parts: 1) synthesis of 2,3-dichloro-6,7-dimethoxy quinoxaline bridging unit; 2) synthesis of the QxCage cavitaund

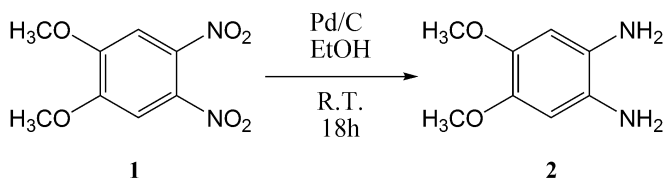
### 3.2.1. Synthesis of 2,3-dichloro-6,7-dimethoxy quinoxaline bridging unit

The synthesis starts with nitration of the veratrole following an electrophilic aromatic substitution reaction in concentrated nitric acid (Scheme 1).



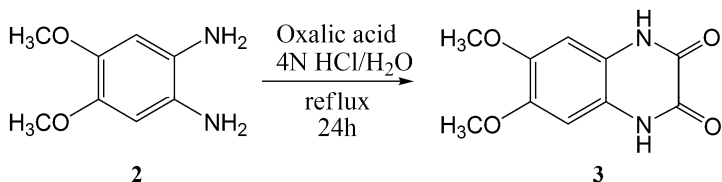
**Scheme 1.** Nitration of the 1,2-dimethoxy benzene.

The 1,2-dimethoxy benzene was reacted with 65% HNO<sub>3</sub> under reflux (Scheme 1). The yellow of 1,2-dimethoxy-4,5-dinitro benzene (1) obtained was successively reduced using catalytic amount of metallic Pd on activated carbon in H<sub>2</sub> atmosphere to give 1,2-dimethoxy-4,5-diamino benzene (2).



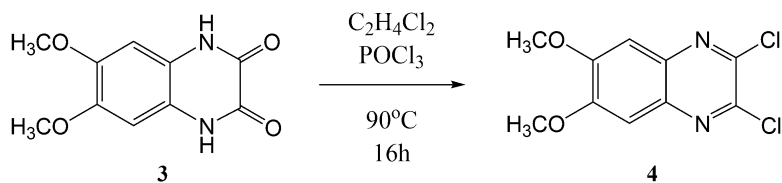
**Scheme 2.** Catalytic reduction of the 1,2-dimethoxy-4,5-dinitro benzene.

The condensation of product 2 with oxalic acid under acidic conditions gave heterocycle 3 in 77% yield (Scheme 3).



**Scheme 3.** Condensation of 1,2-dimethoxy-4,5-diamino benzene (2) with oxalic acid.

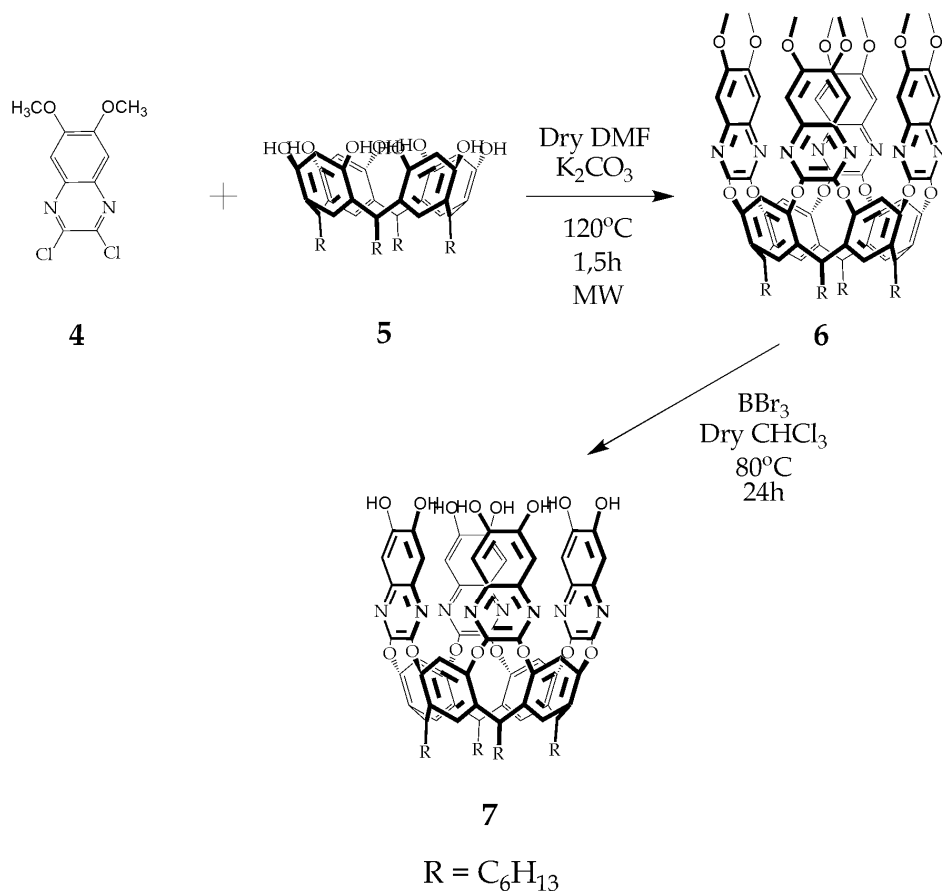
The final step, the chlorination of the 6,7-dimethoxyquinoxaline-2,3-dione (**3**), was performed using POCl<sub>3</sub> in dichloroethane (Scheme 4).



**Scheme 4.** The synthesis of 2,3-dichloro-6,7-dimethoxyquinoxaline (**4**).

### 3.2.2. QxCage cavitand synthesis: the direct approach.

The QxCage synthesis was attempted following the same three step preparation procedure used for the QxBox series. The first two steps worked out as expected leading to the octamethoxy quinoxaline cavitand **6** and the oxtrahydroxy quinoxaline cavitand **7**, respectively (Scheme 5).



**Scheme 5.** Synthesis of the QxCage precursor (7).

Moving the methoxy groups in **6** from the 5,8 positions of the QxBox precursor (figure 3B) to the 6,7 positions influence the cavitand conformation in solution. The downfield shift and broadening of the methine bridges diagnostic triplet indicates that the compound is not any more in the kite conformation but it is fluxional (Figure 3).

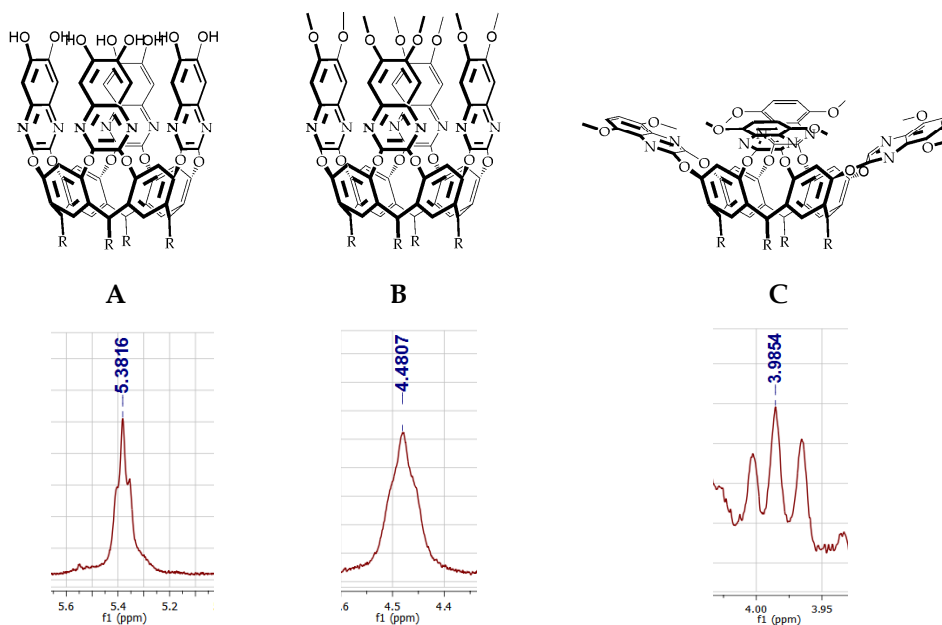
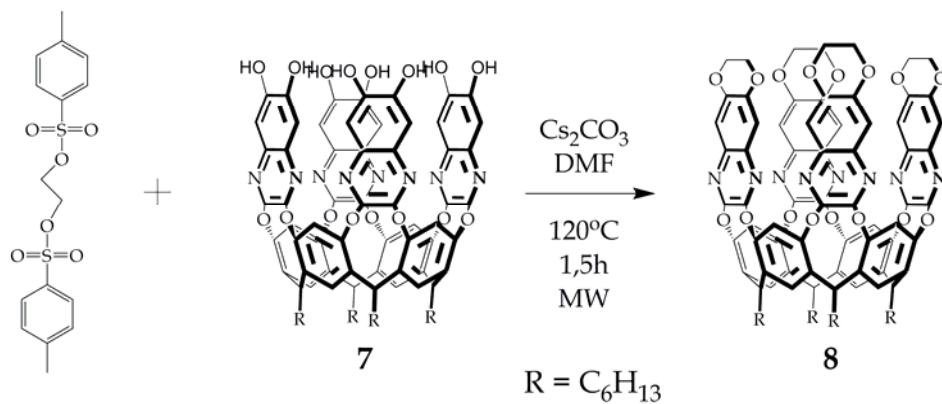


**Figure 3.**  $^1\text{H}$  NMR spectra presenting: the fluctional vase conformation of the QxCage cavitaand precursor **6** (A), the fluctional vase conformation of the cavitaand **6** (B) and the corresponding QxBox (C) precursor.

On the contrary, Octahydroxy cavitaand **7** is in the pure vase form (Figure 3). This change is due to the presence of hydrogen bonding between *para* hydroxyl groups placed on the cavity entrance. This strong interaction tightens the cavity holding it in the vase form.

As a third step, the reaction between octahydroxy cavitaand **7** and di-*p*-tosylate ethylene glycol was performed (Scheme 6).



Scheme 6. The synthesis of Deep-QxCav 8.

$^1\text{H}$  NMR and MALDI TOF-TOF analyses gave the impression that the desired compound 8 was formed. The 1560.8065 mass correspond to the theoretical one calculated and the proton resonances were in line with expectations.

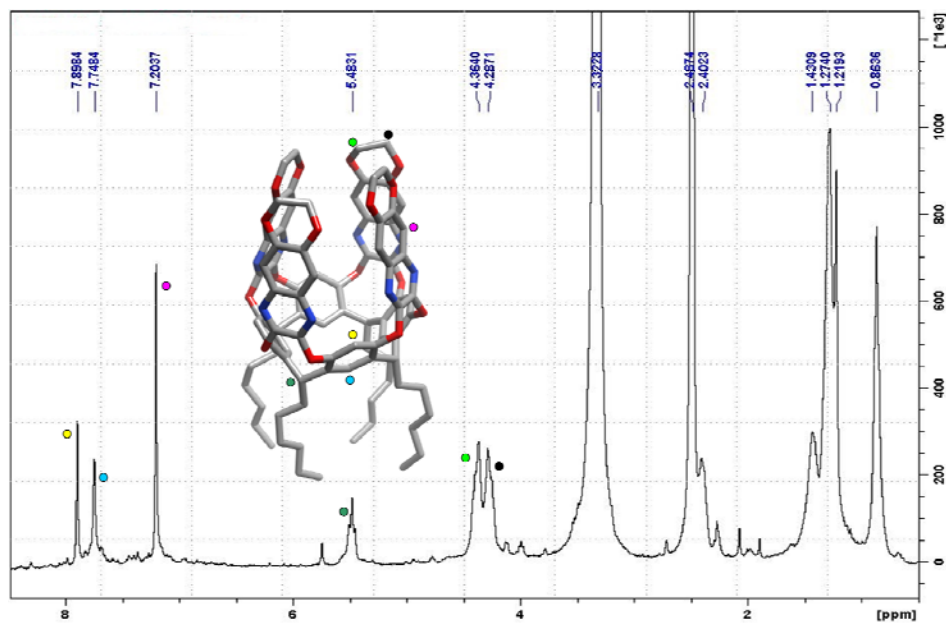
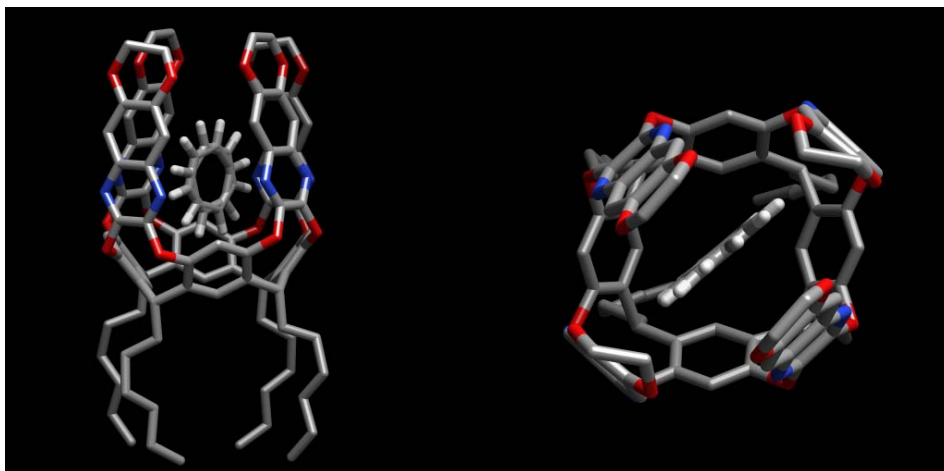


Figure 4.  $^1\text{H}$  NMR of cavitand Deep-QxCav 8 in  $\text{DMSO-d}_6$ .

However, only after complete structure determination (see below) the cavita<sup>nd</sup> was showed to be a non-bridged isomer of the desired molecule.

### 3.3. X-ray crystallographic studies.

The Deep-QxCav affinity toward benzene was also studied in the solid state *via* single crystal X-ray diffraction analysis. Crystals were obtained by slow evaporation of a DMSO solution of the receptor and the guest. Figure 6 shows the side and top views of the molecular structure of the complex. Crystallographic and experimental details for the structures are summarized in Table Z3 (Appendix A).



**Figure 5.** Molecular structure of the *Deep-QxCav@benzene* complex showing the guest disordered over two positions with occupancy factor 0.5 each. Colour code: carbon, grey; nitrogen, blue; oxygen, red; hydrogen, white. Only the hydrogen atoms of benzene are shown for clarity.

The presence of benzene inside the host, disordered over two different positions, is stabilized by  $\pi$ - $\pi$  and CH- $\pi$  interactions with the aromatic cavity walls. Equivalent sets of interactions are formed in both orientations, one rotated of ca.  $30^\circ$  with respect to the other.

The depth of the cavity ( $10.510(3) \text{ \AA}$ ) can be inferred by the distance between the least-squares plane passing through the groups of atoms C7 (A, B, C and D) and C22-C23 (A, B, C and D), see figures 6 and 7. The cavity presents a rectangular opening, the dimensions of which are roughly 5 and  $8.2 \text{ \AA}$ , respectively. The least-squares planes passing through the quinoxaline moieties are inclined with respect to the plane passing through the O1-O2 atoms of  $75.12(3)$ ,  $85.25(2)$ ,  $75.20(3)$  and  $85.24(3)$  for groups A, B, C and D, respectively.

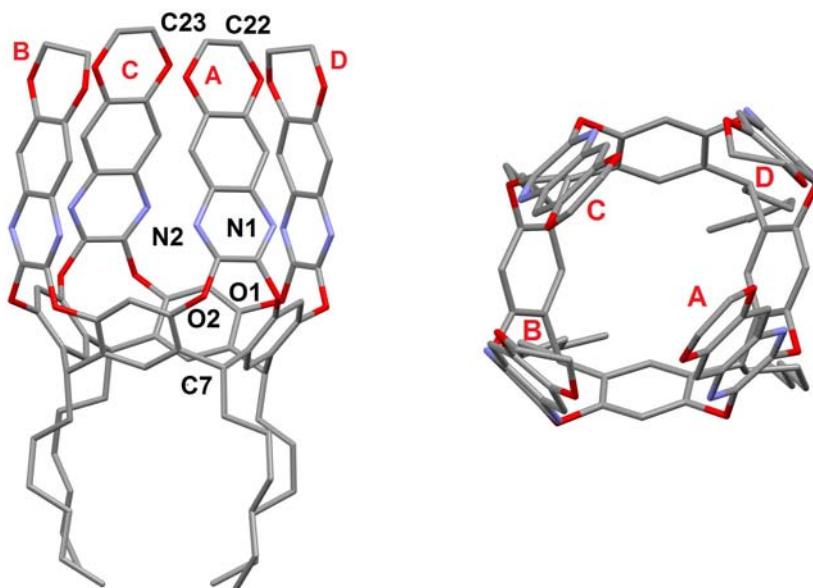


**Figure 6.** *Left. Schematic view of the molecular structure of Deep-QxCav 8 with the general labelling scheme. Each quinoxaline group is tagged by the letters A, B, C and D, respectively. Hydrogen atoms and solvent molecules have been removed for clarity. Colour code: oxygen, red; nitrogen, blue; carbon, grey. Right: top view. The alkylic chains have been removed for clarity.*



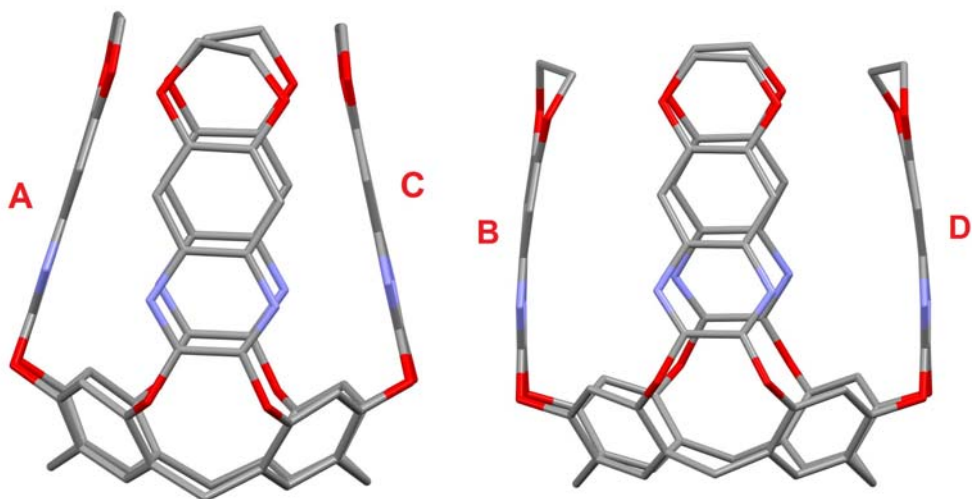


**Figure 7.** Side view of Deep-QxCav showing the different inclination of the quinoxaline moieties. Hydrogen atoms and alkyl chains have been omitted for clarity.

### 3.4. Thermo gravimetric analysis.

Following the successful analysis protocol established in the case of the QxBox receptors (Chapter 2), the TGA analysis was carried out in order to measure the thermal degradation of Deep-QxCav cavitand (Figure 8).

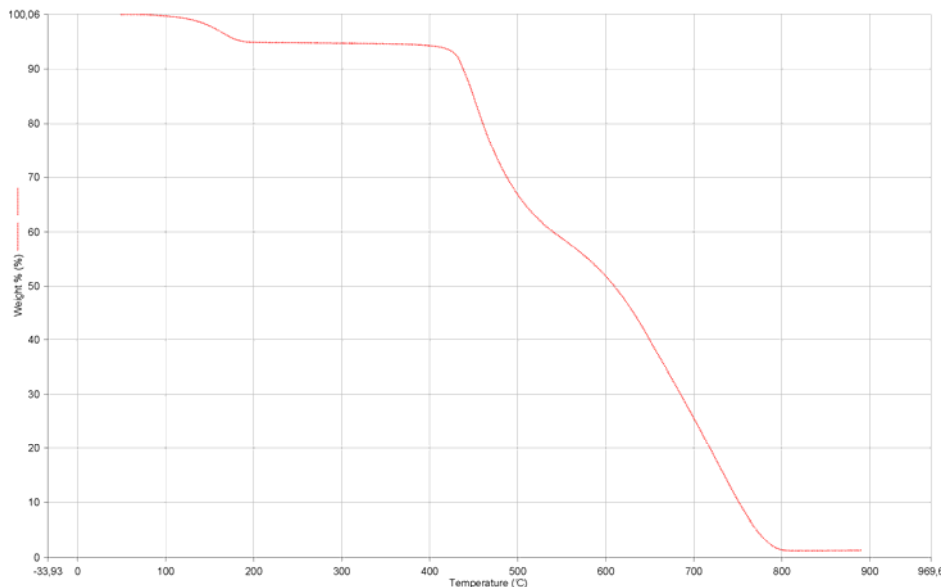


**Figure 8.** The TGA curve of the Deep-QxCav cavitant 8 in air.

The analysis was made in air atmosphere, heating the sample with a gradient of 20°C each minute up to 900°C. In the graph, we can distinguish two slopes of the curve: the first one, at 150°C shows the weight decrease of 4,28% due to the thermal release of the entrapped molecules inside the receptor cavity; the second one at 430°C shows the thermal decomposition of Deep-QxCav. The receptor presents high thermal stability, which allows to use it in analytical measurements.

### 3.5. Conclusions and perspectives.

The goal of the project – the synthesis of novel rigid quinoxaline cavitands for benzene sensing in air, was accomplished with partial success. The synthesis of the new bridging unit 2,3-dichloro-6,7-dimethoxy quinoxaline has been made with high 85% overall yield. Moving the four aliphatic linkers from 5,8 positions on the quinoxaline walls to 6,7 positions resulted in a different cavitant behaviour. The fluctuational vase conformation of the octahydroxy quinoxaline cavitant 7 was a prerequisite to help in blocking the

cavity with the four aliphatic bridges. Regrettably, the expected rigid cavitand was not obtained: the proximity of the two terminal hydroxyl groups caused the formation of a third “ring” on the quinoxaline wall forming Deep-QxCav **8**. Due to high similarity to the Et-QxBox cavitand, <sup>1</sup>H NMR and MALDI TOF-TOF analysis were misleading. The X-Ray diffraction analysis clarified the cavitand structure. The synthesis of a rigid QxCage cavitand with four aliphatic linkers at the 6,7 positions is still ongoing following a new synthetic strategy.

### **3.6. Acknowledgments.**

Special thanks to Dr. Chiara Massera from Parma University for the crystal structure determination

### 3.7. Experimental part

**General Methods.** All commercial reagents were ACS reagent grade and used as received. Solvents were dried and distilled using standard procedures.  $^1\text{H}$  NMR spectra were recorded on Bruker Avance 300 (300 MHz) and on Bruker Avance 400 (400 MHz) spectrometers. All chemical shifts ( $\delta$ ) were reported in parts per million (ppm) relative to proton resonances resulting from incomplete deuteration of NMR solvents. The Matrix-assisted laser desorption/ionization analysis (M@LDI TOF-TOF) were performed on AB SCIEX MALDI TOF-TOF 4800 Plus using *o*-Cyano-4-hydroxycinnamic acid as a matrix. The GC-Mass analysis were performed on Hewlett-Packard Agilent 6890 series equipped in Supelco<sup>®</sup> SLB<sup>™</sup> 5ms column and Hewlett-Packard 5973 MS Selective Mass Detector.

For the synthesis of resorcinarene [ $\text{C}_6\text{H}_{13}$ , H] see Chapter 2.

#### 1,2-dimethoxy-4,5-dinitro benzene (1)

1,2-dimethoxy benzene (40 mmol) was added dropwise into the flask containing an aqueous solution of  $\text{HNO}_3$  65% (25 mL) and stirred for 1h at RT. A yellow precipitate was formed and the reaction was stirred at  $100^\circ\text{C}$  for an additional 8h. The reaction was cooled to RT and the yellow emulsion was poured into a beaker containing ice-cooled water, filtered and dried under vacuum. The pure product **1** was obtained by a three fold recrystallization from glacial acetic acid with a 80% yield.

$^1\text{H}$  NMR (400 MHz,  $\text{CDCl}_3$ ):  $\delta$  = 4.05 (s, 6H,  $\text{CH}_3\text{OAr}$ ), 7.35 (s, 2H, ArH)

GC-MS:  $m/z$  229  $[\text{M}]^+$

#### 1,2-dimethoxy-4,5-diamino benzene (2)

To a suspension of compound **1** (30 mmol) in absolute ethanol (50 mL) a catalytic amount of palladium on charcoal (10%, w/w) was added. The reactor was mounted in a PARR hydrogenation apparatus and air atmosphere was

replaced with H<sub>2</sub> at 3 bar. The reaction was stirred at RT for 24h. The product was filtered through celite, washed with ethanol and the solvent was removed under reduced pressure obtaining the final product **2** with a quantitative yield.

<sup>1</sup>H NMR (400 MHz, CDCl<sub>3</sub>): δ (ppm) = 3.25 (bs, 4H, H<sub>2</sub>NAr), 3.80 (s, 6H, CH<sub>3</sub>OAr), 6.40 (s, 2H, ArH)

GC-MS: m/z 169 [M]<sup>+</sup>

### 6,7-dimethoxyquinoxaline-2,3-dione (**3**)

A solution of compound **2** in 4 N HCl (26 mmol, 1 eq.) was added to a stirring solution of oxalic acid (34 mmol, 1,3 eq.) in a 4N HCl solution (33 mL) and refluxed for 16h. After cooling to RT the formed precipitate was filtered and dried under vacuum, giving the desired product **3** with a 77% yield.

<sup>1</sup>H-NMR (300 MHz, DMSO): δ (ppm) = 3.65 (s, 6H, CH<sub>3</sub>OAr), 6.72 (s, 2H, ArH), 11.70 (s, 2H, CNHC)

GC-MS: m/z 223 [M]<sup>+</sup>

### 2,3-dicloro-6,7-dimethoxyquinoxaline (**4**)

6,7-dimethoxyquinoxaline-2,3-dione **3** (20 mmol, 1 eq.), POCl<sub>3</sub> (400 mmol, 20 eq.) and three drops of dry DMF were added into C<sub>2</sub>H<sub>4</sub>Cl<sub>2</sub> (100 mL) and stirred at 90°C for 16h. Subsequently, the solvent was removed under vacuum and the obtained solid was dissolved in CH<sub>2</sub>Cl<sub>2</sub> and filtered through celite. The crude was purified by flash chromatography giving the pure compound in 80% yield.

<sup>1</sup>H-NMR (400 MHz, CDCl<sub>3</sub>): δ = 4.04 (s, 6H, CH<sub>3</sub>OAr), 7.25 (s, 2H, ArH)

GC-MS: m/z 260 [M]<sup>+</sup>

### Octamethoxy quinoxaline cavitand (**6**)

Resorcinarene **5** (0,35 mmol, 1eq.), 2,3-dichloro-6,7-dimethoxyquinoxaline **4** (0,51 mmol, 4,5 eq.), dry K<sub>2</sub>CO<sub>3</sub> (1.87 mmol, 16 eq.) and dry DMF were added into an oven-dried microwave vessel under Ar atmosphere and reacted under microwave irradiation at 120°C for 2h. Afterwards, the mixture was extracted with DCM/H<sub>2</sub>O and the organic fractions were collected, dried over Na<sub>2</sub>SO<sub>4</sub>

and the solvent was removed under reduced pressure. The crude was purified by flash chromatography affording cavitand **6** in 92% yield.

**<sup>1</sup>H-NMR** (300 MHz, CD<sub>2</sub>Cl<sub>2</sub>) - fluctuational vase conformation:  $\delta$  = 0.88 (t, 12H,  $J$  = 6.5 Hz, CH<sub>3</sub>CH<sub>2</sub>CH<sub>2</sub>), 1.23-1.32 (m, 32H, -CH<sub>2</sub>-), 2.16 (bq, 8H, CHCH<sub>2</sub>CH<sub>2</sub>), 4.04 (s, 24H, CH<sub>3</sub>OAr), 4.48 (bt, 4H, CHCH<sub>2</sub>CH<sub>2</sub>), 7.02 (s, 4H, ArH<sub>down</sub>), 7.24 (s, 8H, CH<sub>3</sub>OArH<sub>2</sub>) 7.48 (s, 4H, ArH<sub>up</sub>)

**MALDI TOF-TOF:** m/z: 1569 [M]<sup>+</sup>

### Octahydroxy quinoxaline cavitand (**7**)

Cavitand **6** (0.03 mmol, 1 eq.) was dissolved in CHCl<sub>3</sub> (10 mL) and BBr<sub>3</sub> (3.80 mmol, 120 eq.) was added dropwise under Ar atmosphere. The mixture was stirred at 80°C for 24h and H<sub>2</sub>O (30 mL) was added into a boiling solution. After cooling down to room temperature, chloroform was removed and the yellow solid was sonicated with 1N HCl, filtrated and dried under vacuum obtaining the final product in quantitative yield.

**<sup>1</sup>H-NMR** (300 MHz, DMSO) - vase conformation:  $\delta$  = 0.85 (t, 12H,  $J$  = 6.3 Hz, CH<sub>3</sub>CH<sub>2</sub>CH<sub>2</sub>), 1.12-1.37 (m, 32H, -CH<sub>2</sub>-), 2.37 (bq, 8H CHCH<sub>2</sub>CH<sub>2</sub>), 5.38 (bt, 4H, CHCH<sub>2</sub>CH<sub>2</sub>), 7.08 (s, 8H, CH<sub>3</sub>OArH<sub>2</sub>), 7.69 (s, 4H, ArH<sub>down</sub>), 7.84 (s, 4H, ArH<sub>up</sub>), 9.94 (s, 8H, ArOH)

**MALDI TOF-TOF:** m/z: 1457 [M]<sup>+</sup>

### Deep-QxCav (**8**)

Cavitand **7** (0.052 mmol, 1 eq.), di-*p*-tosylate-ethylene glycol (0.52 mmol, 10 eq.), dry Cs<sub>2</sub>CO<sub>3</sub> (0.63 mmol, 12 eq.) and dry DMF (5 mL) were added into an oven-dried microwave vessel under Ar atmosphere and reacted under microwave irradiation at 120°C for 1,5h. The reaction was quenched in water and extracted with DCM/H<sub>2</sub>O. The organic fractions were collected and dried over Na<sub>2</sub>SO<sub>4</sub>. After filtration the solvent was removed under reduced pressure and the crude was purified by flash chromatography. The final product was obtained in 90% yield.

**<sup>1</sup>H-NMR** (300 MHz, DMSO) - vase conformation:  $\delta$  = 0.86 (s, 12H, CH<sub>3</sub>CH<sub>2</sub>CH<sub>2</sub>), 1.20-1.48 (m, 32H, -CH<sub>2</sub>-), 2.40 (bq, 8H CHCH<sub>2</sub>CH<sub>2</sub>), 4.28-4.42 (m,

16H, ArOCH<sub>2</sub>CH<sub>2</sub>O), 5.48 (t, 4H,  $J = 7.6$  Hz, CHCH<sub>2</sub>CH<sub>2</sub>), 7.20 (s, 8H, ArH<sub>2</sub>), 7.74 (s, 4H, ArH<sub>down</sub>), 7.89 (s, 4H, ArH<sub>up</sub>)

**MALDI TOF-TOF:** m/z: calculated for C<sub>92</sub>H<sub>88</sub>N<sub>8</sub>O<sub>16</sub> [M] m/z: 1560.6318, found m/z= 1560.8065

### **X-Ray analysis data.**

Data collection and structure resolution for **Deep-QxCav@benzene** were carried out as described in Chapter 2. All the non-hydrogen atoms were refined with anisotropic atomic displacements, with the exclusion of the disordered benzene guest. The hydrogen atoms were included in the refinement at idealized geometries (C-H 0.95 Å) and refined "riding" on the corresponding parent atoms. The weighting scheme used in the last cycle of refinement was  $w = 1/[\sigma^2 F_o^2 + (0.0507P)^2 + 1.2866P]$ , where  $P = (F_o^2 + 2F_c^2)/3$ .





**Water soluble**

**Phosphonate cavitands**

4

## 4.1. Introduction.

The molecular recognition processes which undergo in aqueous media are challenging. While organic-soluble systems have offered insight into the forces involved in this binding events they do not account for the strong desolvation and entropic benefits experienced in water. As many research groups have discovered, working in water presents many problems that are either not an issue in organic solvents or simply easier to manage. A common problem is solubility, defined as "An analytical composition of a saturated solution expressed as a proportion of a designated solute in a designated solvent".<sup>1</sup> Often each piece of a multicomponent system is water-soluble, while the resulting complex is not. Obtaining the desired protonation state of each functional group can also be troublesome. Buffers are required to maintain the appropriate pH, but depending on the buffer's identity, they can lead to more solubility problems and often change the binding properties of the host.

Examples of supramolecular structures like cyclodextrins,<sup>2</sup> cyclophanes,<sup>3</sup> calyx[*n*]arenes,<sup>4</sup> cavitands etc. that can be solubilized in water without losing their recognition properties are known.<sup>5</sup> In particular, cavitands are interesting molecular receptors thanks to their outstanding complexation abilities.<sup>6</sup> In fact, the hemispherical skeleton forms a rigid and preorganized cavity that is a universal scaffold, accessible for modification by versatile functional groups, for specific guest recognition through weak non-covalent interactions.

Theoretically the water solubility in cavitands can be obtained through proper upper and lower rim functionalization by neutral, positively charged or negative charged groups. In reality charged groups are more effective and their positioning is also very important, as well as the dimension of the cavitand.

In this chapter the synthesis of resorcinarene-based tetraphosphonate cavitand functionalized by neutral and cationic groups for water-solubility will be described.

### 4.1.1. Water-soluble cavitands.

Many approaches were taken to functionalize both the upper and lower rim of the resorcinarene-based receptors, with proper water solubilizing functional groups. The water solubilizing group could be inserted into the resorcinarene scaffold in three different positions (Figure 1): as feet at the lower rim (R), as bridging groups (R'), and as apical groups (R'').

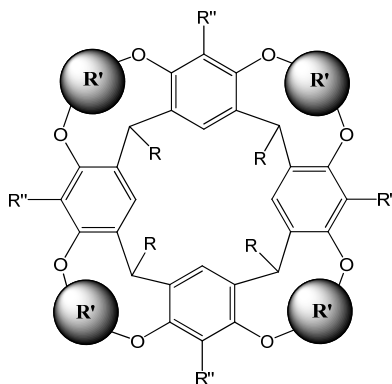


**Figure 1.** Resorcinarene-based scaffold sites suitable for the insertion of solubilizing groups.

In particular, the choice of the bridging groups R' is pivotal to determine shape, dimensions and complexation properties of the final cavitand receptor. The choice of proper lower rim pendants functionalization R affects the cavitand solubility and are suitable meanings for possible surface grafting

In terms of cavity size, the smaller cavitand available is the methylene bridged one.<sup>7</sup> As such they have been used as molecular receptors for binding small neutral molecules,<sup>8</sup> in the field of wastewater treatment, for their ability to complex organic molecules in water.<sup>9</sup> Besides neutral methylene bridged cavitands, nice examples of charged cavitands have been reported by different research groups and their ability to complex anions fully investigated.

As an example in 1995, Sherman and co-workers reported the synthesis of a negatively charged methylene bridged cavitand, functionalized at the apical position with four phenolates, as sodium salts (Figure 2A).<sup>10</sup>

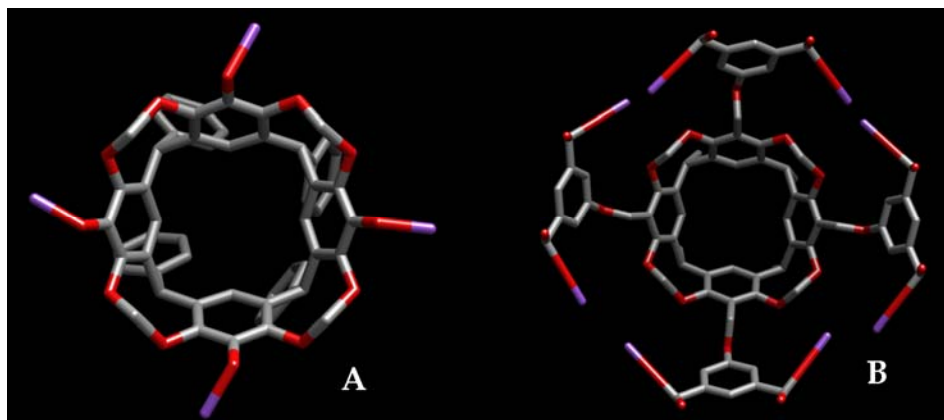


**Figure 2.** *The water-soluble methylene-resorcinarene cavitands.*

This cavitand is water soluble and shows good binding properties towards the caesium cation. Interestingly, the insertion of a  $\text{CH}_2$  spacer between the aromatic rings of the resorcinarene scaffold and the ONa groups, completely suppress the water solubility of the cavitand, even at pH greater than 12.<sup>10</sup> In 2000 Hong and co-workers reported the formation of a methylene-bridged cavitand functionalized at the apical position with four isophthalates (Figure 2B).<sup>11</sup> Under basic conditions, this octa-anionic cavitand binds cationic guests such as N-methylpyridinium, acetylcholine and *N,N,N*,-4-tetramethylbenzenaminium with association constants ranging from  $10^1$  to  $10^3 \text{ M}^{-1}$ . Due to unfavourable electrostatic interactions, the anionic guests are not complexed by this cavitand.

Alternatively, water solubility can be obtained functionalizing the lower rim of the cavitands with suitable “feet”. It is important to highlight that while these hydrophilic feet improve the water solubility of the cavitand, they strongly affect its behaviour in the organic solvents, making the cavitand synthesis challenging.

In 2000, Diederich and co-workers reported the synthesis of a water soluble ethylene bridged cavitand. The driving force for water solubility is the presence at the lower rim of four neutral polyethylene chains. In fact the merely presence of 4 amidinium groups at the upper rim was found to be not sufficient to provide hydrophilicity to the receptor (Figure 3).<sup>12</sup>

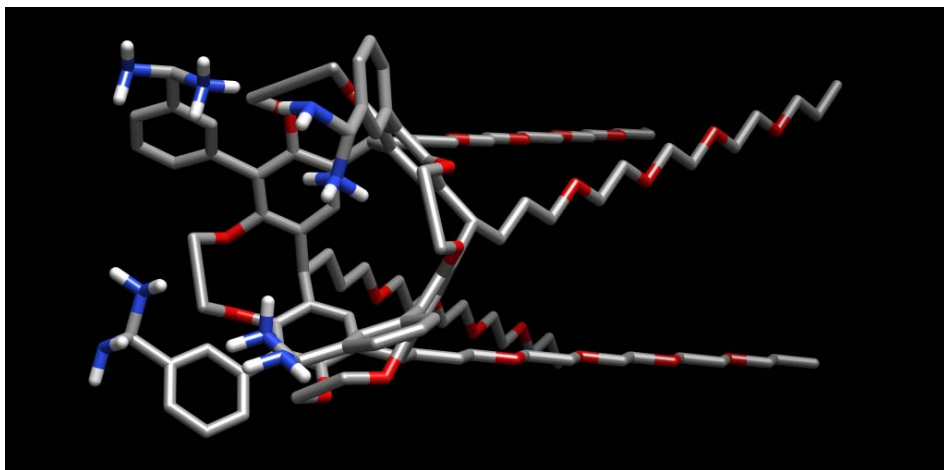


**Figure 3.** *The 3D model of water-soluble cavitand functionalized by four ethylene glycol pendants and four amidinium groups at the apical position.*

This cavitand, thanks to the presence of an ethylene bridging units, exhibits a larger cavity compared to the methylene-bridged one, and it is able to complex bigger guests (Figure 4).

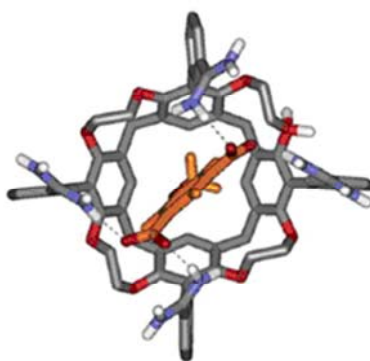


**Figure 4.** *The structure of Diederich's ethylene bridged cavitand complexed with one methoxyisophthalate moiety with marked hydrogen bonds between host and guest. The glycol pendants have been omitted for clarity.*

In particular, the Authors reported that complexes with guests like 5-methoxy- and 5-nitroisophthalate of 1:2 host-guest stoichiometry, with binding constants of  $10^4 \text{ M}^{-1}$  and  $10^3 \text{ M}^{-1}$  respectively. In  $\text{D}_2\text{O}$ , the 1 : 2 host-guest complex is likely composed of one isophthalate guest occupying the hydrophobic cavity of the cavitand while the second guest is present outside—perhaps associated by electrostatic and/or non-specific hydrophobic contacts. This binding mode allows both guest molecules to make favourable electrostatic contacts with the amidinium groups on the upper rim of the host.

In order to create hosts with larger cavities, resorcinarene was condensed with electron-poor aromatic rings to give “deep cavitands as reported by -Rebek and Co-workers.<sup>13</sup> The authors reported the synthesis of a cavitand where the resorcinarene skeleton was functionalized with four aromatic bridging units bearing 8 amide groups with the four ammonium centres placed on the pendant alkyl chains of the cavitand were used to reach water-solubility (Figure 5). Upon dissolution in water, these structures exist in the *kite* conformation as  $\text{D}_{2v}$  velcra-plex dimers—most likely to maximize burial of lipophilic surfaces from aqueous solvent. The cavitand resulted to be able to sense molecules presenting an hydrophobic centre formed by a polar group (ammonium or hydroxyl) like isopropyl ammonium chloride, via solvophobic effect. In particular, Rebek and co-workers, demonstrated that upon exposure to guests of suitable size and shape, the cavitand rearrange to the  $\text{C}_{4v}$  vase conformation.

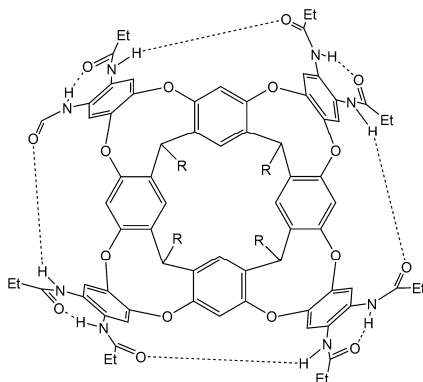


**Figure 5.** The vessel-cavity formation through intramolecular hydrogen bonds.

Interestingly, in the presence of polar protic solvents, the *kite-vase* equilibrium is shifted toward the *vase* conformation by the intramolecular hydrogen bonds of the upper rim. This change leads to the well defined cavity creation and to the guest entrapping force enhancement.

Another type of the water-soluble deep cavitand has been reported by Gibb's group. The presence of eight aromatic bridging units gives depth to the cavitand, while its hydrophilic character is due to the presence at the lower rim of external carboxyl acids coat formed from four carboxylic groups placed on the upper rim of the cavity, and four groups at the lower rim (Figure 6a). These cavitands dimerize in solution in the presence of a suitable guest as templating agent.<sup>14</sup> The capsule is held together by  $\pi$ - $\pi$  weak interactions between the aromatic walls of the two cavitands, by additive host-guest interactions and by hydrophobic effect (Figure 6b).

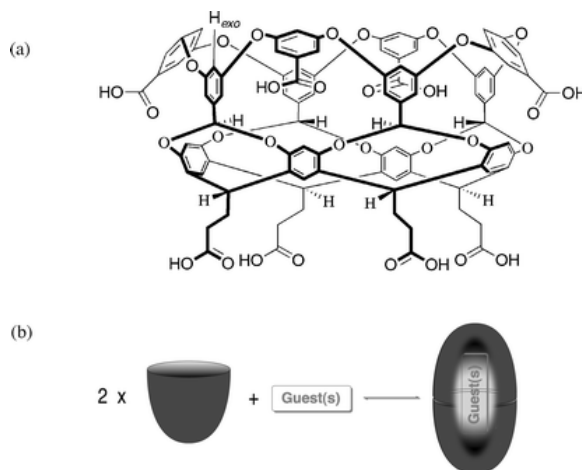


**Figure 6.** The Gibb's deep octaacid cavitand (a), and its capsule formation upon guest encapsulation (b).<sup>14</sup>

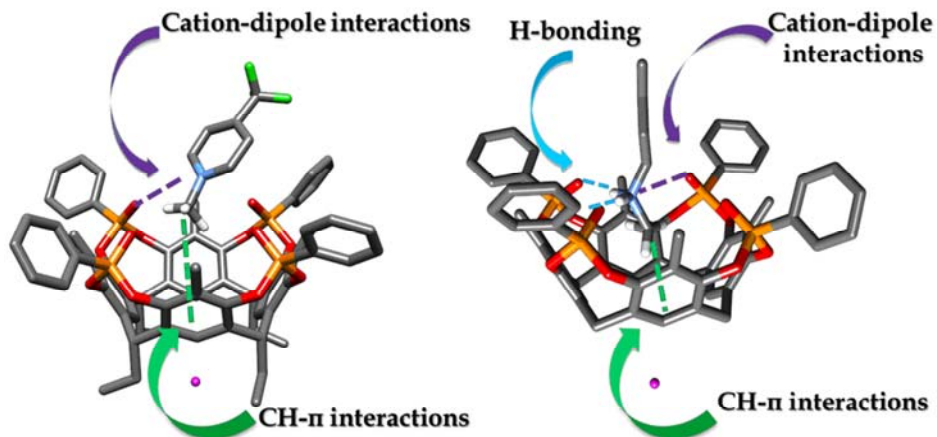
The homodimerization of the two cavitands into a capsule spectrum was observed through  $^1\text{H}$  NMR upon encapsulation of appropriate suitable, in terms of shape and size, steroidal guest. A remarkable binding constant of  $10^8$

$M^{-1}$  for (+)-dehydroisoandrosterone was reported, indicating the strong influence of the hydrophobic effect, which is the main driving force for complex formation. This is supported by the observation that addition of 20% methanol to an aqueous solution of the capsule led to its breakdown. In fact, being the methanol a good solvent for the guest, it is able to take it away from the capsule, suppressing the solvophobic effect and leading to the capsule disassembly.

## 4.2. The complexation properties of tetraphosphonate cavitands.

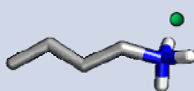
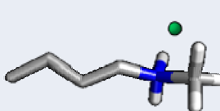
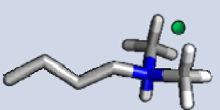
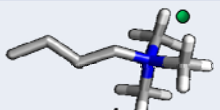
In the design of cavitands, the choice of the bridging groups connecting the phenolic hydroxyls of the resorcinarene scaffold is pivotal, since it determines shape, dimensions and complexation properties of the resulting cavity. The possibility to design a cavitand selective toward specific classes of guests is very appealing. The introduction of phosphonate groups into the resorcinarene scaffold as bridging units, leads to the formation of multifunctional cavitand receptors. The **P=O** group highly influences the enhancement of the molecular recognition properties of the cavitand and plays an important role in the guest complexation, providing abilities to bind neutral likewise charged species toward reversible non-covalent interactions like H-bonding and cation-dipole (Figure 7).<sup>6</sup> In recent years our group demonstrated that the cavitand functionalized at the upper rim with four **P=O** groups orientated inward the rigid cavity, named **Tiiii**, presents remarkable molecular recognition properties toward N-methyl ammonium salts.<sup>6a</sup> The molecular recognition process is due to the presence of three interaction modes: (1)  $N^+ \cdots O=P$  cation-dipole interactions, (2)  $CH_3-\pi$  interactions of the acidic  $^+NH_2-CH_3$  group with the  $\pi$  basic cavity and (3) two simultaneous hydrogen bonds between two adjacent **P=O** bridges and the two nitrogen protons (Figure 7).





**Figure 7.** Interaction between tetraphosphonate host and *N*-methylpyridinium salts (left), *N*-alkylammonium salts (right).

Within the ammonium salt series, it was demonstrated by ITC measurements<sup>15</sup> that the mono-methylated ammonium ions presented the highest  $K_a$ , while the non-methylated ammonium ions presented the lower  $K_a$  (Table 1). The  $K_a$  for trimethylated ammonium salts is too low to be measured.

Guest	$K \pm \delta K$ ( $M^{-1}$ )	$\Delta H \pm \delta H$ ( $KJ \cdot mol^{-1}$ )	$\Delta G \pm \delta G$ ( $KJ \cdot mol^{-1}$ )	$T\Delta S \pm T\delta S$ ( $KJ \cdot mol^{-1}$ )
 1	$1.5 \pm 0.8 \cdot 10^3$	$-8.7 \pm 0.2$	$-18.5 \pm 1.0$	$9.8 \pm 1.7$
 2	$3.9 \pm 0.8 \cdot 10^5$	$-16.1 \pm 0.6$	$-31.9 \pm 0.5$	$15.8 \pm 1.0$
 3	$6.1 \pm 0.7 \cdot 10^3$	$-8.7 \pm 0.1$	$-22.0 \pm 0.3$	$13.3 \pm 0.5$
 4	INTERACTION TOO LOW TO BE MEASURED			

**Figure 8.** ITC measurements of the titrations of the guests 1–4 into the solution of **Tiiii**[ $C_3H_7$ ,  $CH_3$ , Ph] in methanol at 303 K.

The **Tiiii** preference toward the monomethylated moiety over di- and trimethylated ones is determined by the number of H-bonds formed between the **P=O** groups and the NH of the guest, while non-methylated ammonium ions are disfavoured by the lack of  $CH_3-\pi$  interactions.

This peculiar affinity of **Tiiii** cavitands toward the  $H_2N^+-CH_3$  group is potential valuable for the detection of a broad range biologically active compound containing this residue like synthetic drugs<sup>16</sup> cancer biomarkers<sup>17</sup> and neurotransmitters.<sup>18</sup> In particular, the possibility to monitor processes taking place into living cells in the diagnostic field is very appealing. The most recent effort in the direction of exploring diagnostic field application with synthetic receptors is detecting histone proteins methylation. Histone methylation is involved in heterochromatin formation and maintenance, X-chromosome inactivation, transcriptional regulation, DNA repair, and genomic

imprinting. Histones are methylated on lysine or arginine residues by histone methyltransferases (HMTs). Nature has evolved a special motif for recognizing the methylation state of lysine, called the “aromatic cage”. It is a preorganized collection of aromatic amino acids residues that coordinate to create a desolvated  $\pi$ -electronic rich pocket, occasionally containing an adjacent anionic residue. Taking inspiration from Nature, researchers have explored the possibility to use chemical approaches to recognize methylated lysine using a synthetic pocket. In 2012, three nice examples of this chemical approach has been reported in literature by Hof<sup>19</sup>, Nau<sup>20</sup> and Crowley<sup>21</sup>. The three authors reported studies in which a water soluble p-sulfonatocalix[4]arene macrocycle resulted to bind lysine residues in proteins, particularly trimethylated lysine. The data collected by Crowley also indicate that the calix[4]arene is a mediator of protein-protein interactions and potentially could be employed in generating assembly and promoting crystallization.

Lysine methylation has been associated to different human diseases like prostate cancer<sup>22</sup> and Alzheimer.<sup>23</sup> Moreover, sarcosine, the mono N-methylated derivative of glycine, has been recently singled out as a possible early marker of the aggressive forms of prostate cancer.<sup>17</sup>

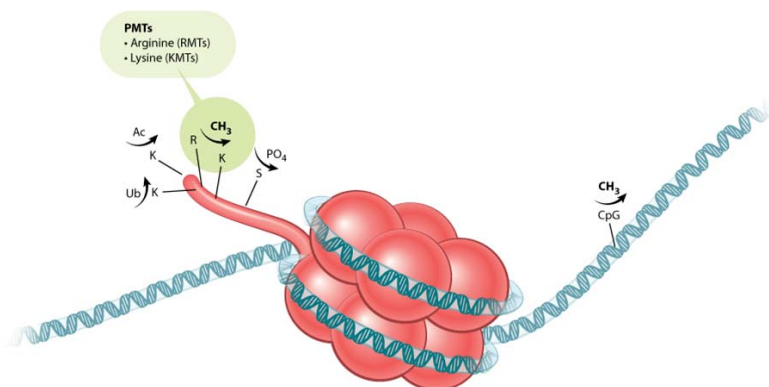


**Figure 9.** *The enzymatic modification of lysine group placed on histone tail.*<sup>24</sup>

The **Tiiii** complexation properties toward sarcosine detection has been extensively studied by our research group.<sup>25</sup> X-Ray structure presented in Figure 10 confirms the ability of **Tiiii** cavitand to bind the sarcosine. As

highlighted in the figure, the non-covalent interactions involved in this process resulted to be, as already mentioned, hydrogen bonds, cation-dipole interaction and  $\text{CH}_3\text{-}\pi$  interactions. The association constant calculated by ICT measurements resulted to be  $K_{\text{ass}} = 2.64 \cdot 10^4 \text{ M}^{-1}$  in MeOH.

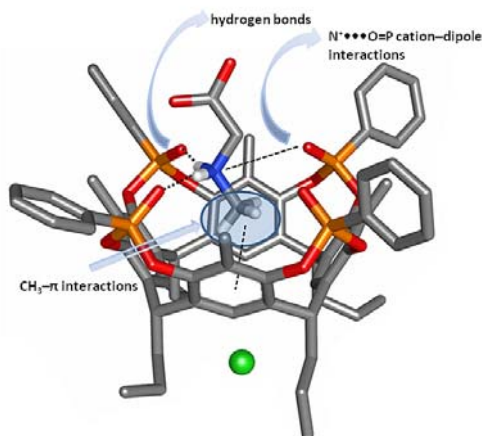


**Figure 10.** Crystal structure of the complex of *Tiii@sarcosine hydrochloride* with interaction modes.

The ability of the tetraphosphonate cavitand to selectively detect sarcosine in urine in presence of possible interferents like glycine and inorganic salt at the solid-liquid interface was fully demonstrated by our research group.<sup>25</sup>

To address the diagnostic field application of **Tiii** receptor directly in a biological environmental the water solubility issue of **Tiii** cavitand must be faced and solved.

### 4.3. Design and synthesis of water-soluble **Tiii** cavitand.

The aim of the project was based on the design and synthesis of a new type of water-soluble cavitand. Two synthetic approaches were explored synthesise such receptor: (i) direct functionalization of the  $\text{P=O}$  bridging group by the neutral glycol units and (ii) modification of the lower rim pendants with four charged amino groups.

### 4.3.1. The glycolated tetraphosphonate cavitand.

The neutral glycol chains are known to favour the solubility in water of organic species.<sup>11</sup> Therefore, we thought to functionalize the cavitand with four triethylene glycol (TEG) chains, inserting them directly into the four phosphonate bridging units. In Figure 11 the target cavitand is reported: the receptor is functionalized at the upper rim with four triethylene glycol units, and at the lower rim with 4 short C<sub>3</sub> chains (not shown in the figure), in order to reduce its hydrophobicity.

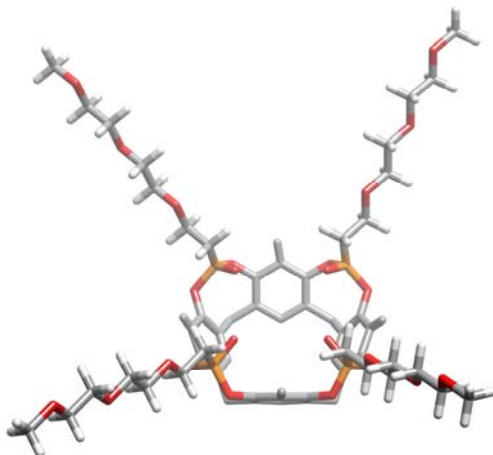
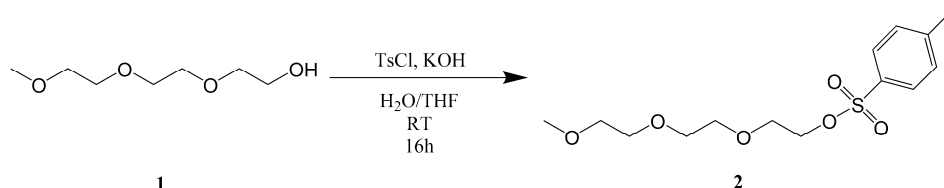


**Figure 11.** Modelling of the target *Tiiii* cavitand, presenting 4 TEG units directly attached onto the  $P=O$  bridges. The H atoms of the resorcinarene have been omitted for clarity as well as the C<sub>3</sub> chains at the lower rim.

For the synthesis of the desired cavitand, it was necessary to synthesise both the resorcinarene both the TEG-phosphonyl dichloride bridging unit. In this chapter, only the synthesis of the bridging agent will be presented, since the synthesis of the resorcinarene has been already fully discussed in the previous chapter.

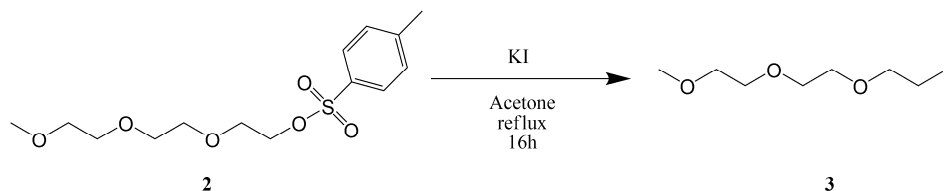
### 4.3.2. Synthesis of triethylene-glycol-phosphonic dichloride.

The first step of the synthesis was the activation of the triethylene-glycol monomethyl ether **1** with tosyl-chloride. The reaction was performed in a mixture of H<sub>2</sub>O/THF under basic condition, at room temperature for 16h. After purification, product **2** was obtained as dense oil in 95% yield (Scheme 1).



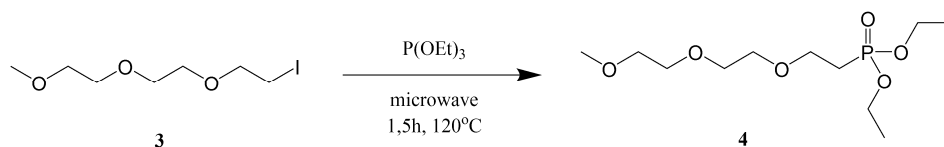
**Scheme 1.** TEG tosylation under basic conditions.

Compound **2** was converted into the iodine derivative one, by reaction with KI in refluxing acetone. After quenching of the reaction and crude purification, **3** was obtained with an excellent yield, as a brown liquid (Scheme 2).



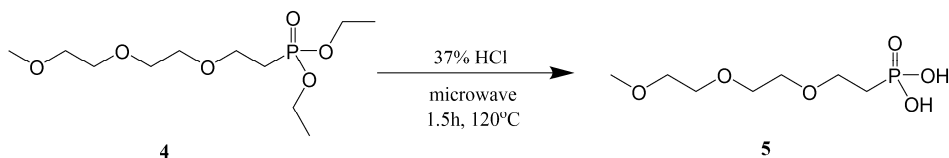
**Scheme 2.** Iodination of compound 2.

The phosphonate derivative was obtained through Arbuzov reaction. Compound **3** was reacted with P(OEt)<sub>3</sub> at 120°C for 1,5 h under microwave irradiation. The reaction was quenched in water, and product **4** was purified through vacuum distillation. **4** was obtained as a colourless liquid in 80% yield (Scheme 3).



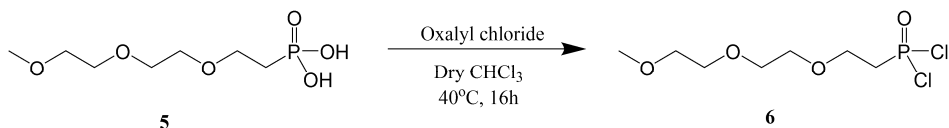
**Scheme 3.** Synthesis of the triethylene-phosphonic-glycol diethyl ester **4**.

The next step was the compound **4** hydrolysis under acidic condition. The reaction was performed in presence of HCl 37% under microwave irradiation. Phosphonic acid **5** was obtained pure as a colourless liquid after vacuum drying (Scheme 4).



**Scheme 4.** *Synthesis of compound 5.*

The final molecule, the dichloride derivative **6**, was synthesized by reacting compound **5** with oxalyl chloride in freshly distilled  $\text{CHCl}_3$  (Scheme 5.). The solvent was removed under vacuum and product **6** was obtained as a yellow solid without further purification.



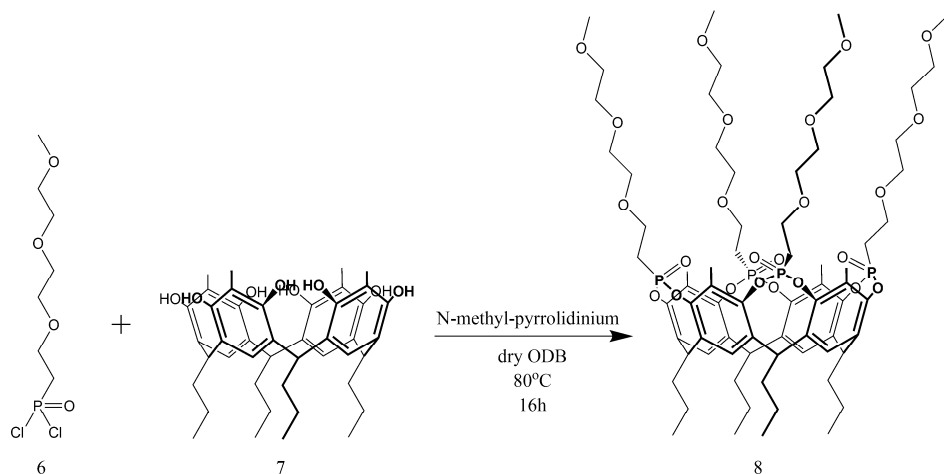
**Scheme 5.** *The synthesis of final TEG-phosphonic dichloride (6).*

Due to its high reactivity, **6** was characterised only by  $^1\text{H}$  and  $^{31}\text{P}$  NMR analyses. The NMR spectra were recorded using vacuum dried NMR tube sealed under Ar atmosphere. ESI-Mass analysis was not performed because the dichloride derivative undergoes to very fast hydrolysis.

### 4.3.3. Bridging reaction between TEG-phosphonic-dichloride and the resorcinarene.

The preparation of tetrakisphosphonate cavitand **8** was performed by reacting TEG-phosphonic-dichloride **6** with resorcinarene **7**. The synthesis of resorcinarene **7** is not reported since the standard procedure already discussed previously (see Chapter 2). The bridging reaction was performed using *o*-dichlorobenzene (ODB) as solvent, in presence of *N*-methyl-pyrrolidine as

templating agent, in order to maximize the formation of the isomer with all four P=O groups oriented inward the cavity (Scheme 6).

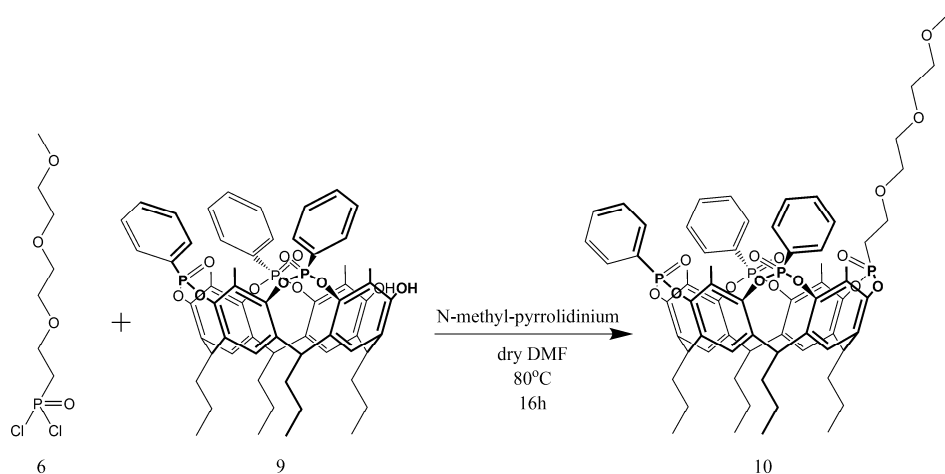


**Scheme 6.** Synthesis of **Ti<sup>iii</sup>** [ $C_3H_7$ ,  $CH_3$ , TEG] **8**.

After quenching of the reaction in water and the purification steps, the obtained product was fully characterized by  $^1H$  and  $^{31}P$  NMR, and by ESI and MALDI TOF-TOF mass spectroscopy. Unfortunately, the analyses demonstrated that the product obtained was not formed. After crude purification by the flash column chromatography, only resorcinarene and the hydrolysed bridging moiety **6** were separated. Other attempts to obtain the desired cavitant were performed, using different reaction conditions. In particular different solvents like DMF, DMA,  $CHCl_3$ , and DMSO were tested as well as different bases, like N-methylpyrrolidine,  $K_2CO_3$ , NaH and  $CS_2CO_3$  at different temperatures (80-150°C). The microwave irradiations were also used without success.

In order to understand if the dichloro- derivative **6** was a suitable bridging agent for our cavitant, we decided to perform a control experiment. We used cavitant **9**,<sup>26</sup> presenting at the upper rim 3 phenyl phosphonate groups pointing inward the cavity and two hydroxyl groups available for the bridging reaction with **6** (Scheme 7).





**Scheme 7.** Bridging reaction between 3P=O cavitand **9** and bridging unit **6**.

The bridging reaction was performed under Ar, using N-methyl-pyrrolidine as templating agent and DMF as solvent. The reaction was quenched in water, and the product purified by column chromatography.

This time the reaction led to the formation of cavitand **10**. The product formation was confirmed by the  $^1\text{H}$ ,  $^{31}\text{P}$  NMR analyses as well as by ESI-MS spectrometry. In figure 12 the  $^{31}\text{P}$  NMR spectrum of cavitand **10** is reported. Three different peaks were observed, in a 1:2:1 stoichiometry ratio, in agreement with the different surrounding experienced by the P=O groups.

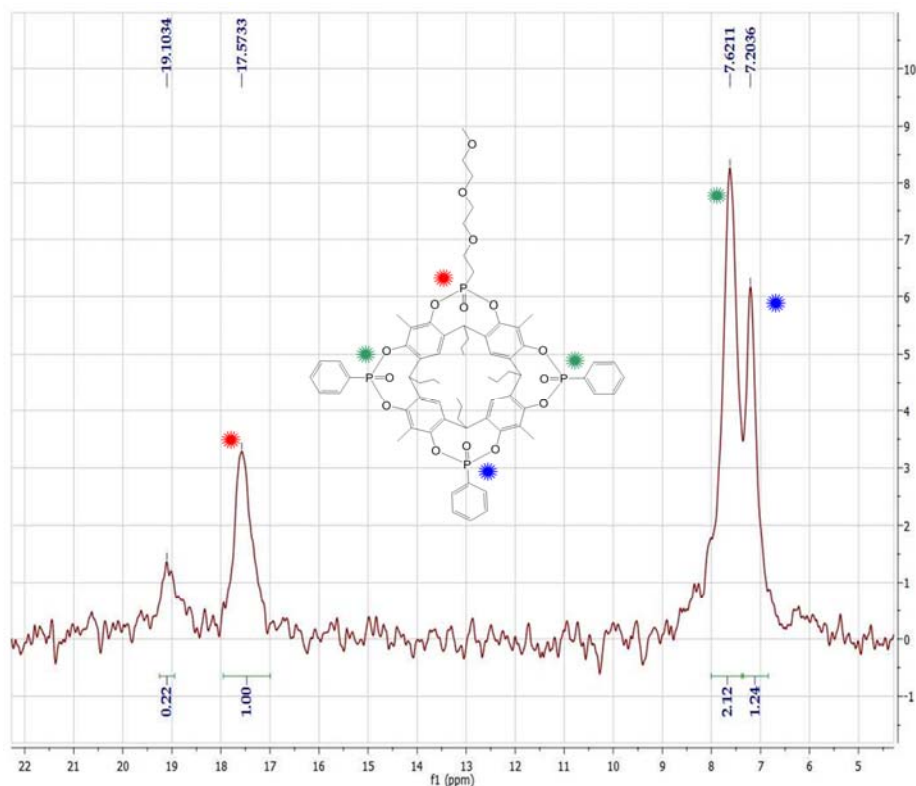
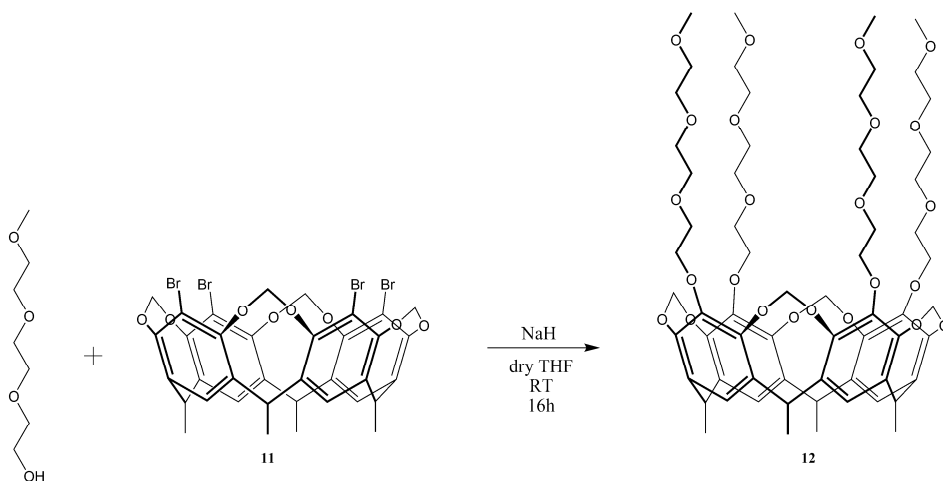


**Figure 12.** The  $^{31}\text{P}$  NMR spectrum of *Tiii* cavitant with one TEG chain directly connected to the one  $\text{P}=\text{O}$  bridge.

The lower field peak at 17,57 ppm corresponds to the phosphorus directly attached to the glycol chain. The two peaks at 7,26 ppm and 7,20 ppm are diagnostic for the  $\text{Ph}-\text{P}=\text{O}$  groups pointing inward the cavity. Unfortunately, attempts to solubilize cavitant **10** in water failed. The presence of just one polyethylene glycol chain was not sufficient to obtain a water soluble cavitant.

In order to insert more than one TEG chains at the upper rim of the cavitant, we decided to functionalize the apical position of the cavitant. To this purpose, model cavitant **12** with for bromide at the apical position was synthesised following literature procedure. We decided to use the model cavitant **12** to see if the selected protocol could be successful, in order to transfer it onto the tetraphosphonate cavitant (Scheme 8).



**Scheme 8.** Preparation of TEG-functionalised MeCav 12.

Triethylene-glycol-monomethyl ether was reacted directly with the cavitand **11** in THF as solvent, under basic conditions, for 16h. The reaction was quenched in water and the crude product was purified by flash column chromatography. Product **12** was fully characterized by  $^1\text{H}$  NMR spectroscopy and ESI-MS spectrometry. Once again attempts to solubilise cavitand **12** in water failed. The cavitand resulted soluble only in common organic solvents like: DCM, Acetone, DMSO,  $\text{CHCl}_3$  or MeOH. The  $\text{H}_2\text{O}/\text{MeOH}$  mixture (1:9) causes the cavitand precipitation. The obtained results demonstrated that the functionalization of the cavitand with four TEG chains is not sufficient to obtain a water soluble receptor.

#### 4.4. The tetraamino-tetraphosphonate cavitand.

After the failure of inducing water solubility with a TEG derivatization, we decided to functionalize the lower rim of the receptor with four amino groups. The use of amino groups in order to provide water-solubility to cavitands is known.<sup>13</sup> To foster the hydrophilicity of our receptor we decided to use a different phosphonate group: not the phenyl phosphonate but the ethyl phosphonate. The idea behind the choice was that reducing the number of

carbon atoms, the system will gain a more hydrophilic character. In Figure 13 the 3D structure model of the target cavitand is shown.

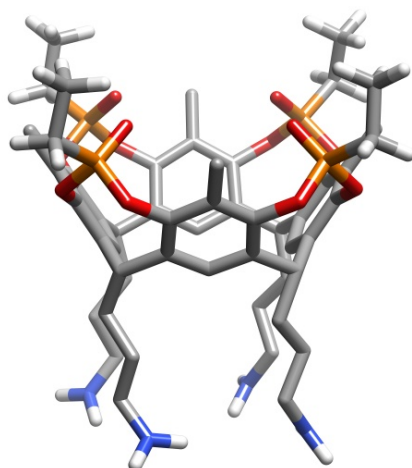
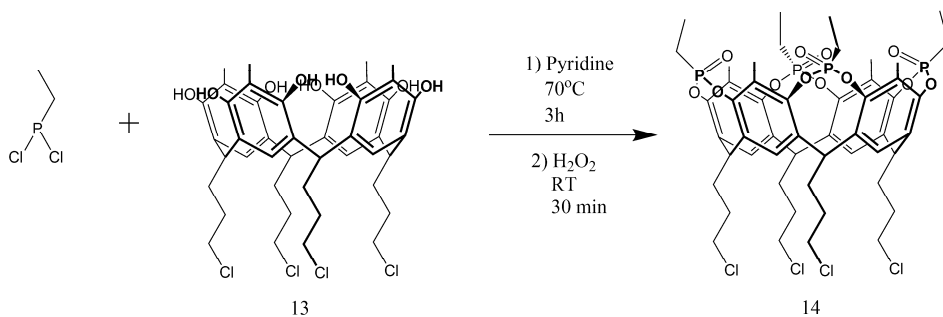


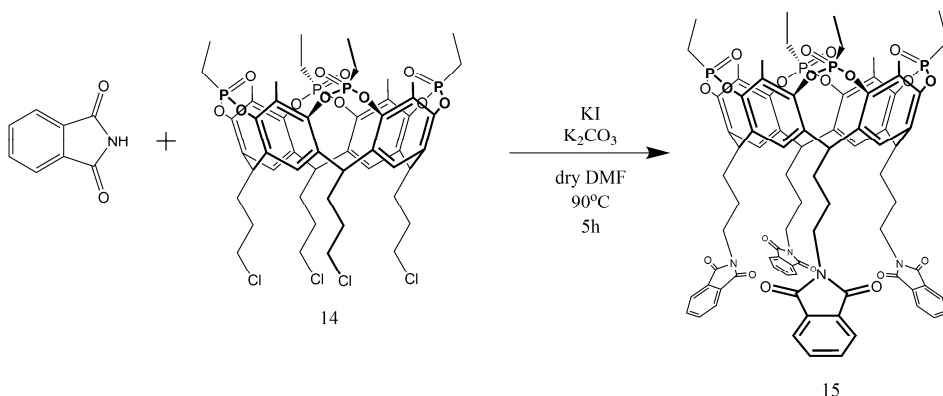
**Figure 13.** 3D structure model of **Ti<sub>iii</sub>** cavitand functionalised at the upper rim with four ethylphosphonate bridging units and at the lower rim by four amino groups.

The target molecule was synthesized in three steps starting from the tetrachloro-footed resorcinarene **13** (Scheme 9). The bridging reaction was performed using standard conditions: the resorcinarene was dissolved under Ar atmosphere in dry pyridine, which operates both as solvent and as base, then dichloroethyl-phosphine was added and the reaction was stirred at 70°C. After 3 hours, H<sub>2</sub>O<sub>2</sub> was added directly to the mixture reaction in order to oxidize *in-situ* the phosphine to phosphonate group. As for the case of phenylphosphonate, this procedure gives only the desired **Ti<sub>iii</sub>** cavitand **14**, and no traces of other isomers, in particular the **Ti<sub>iiio</sub>**, were detected.



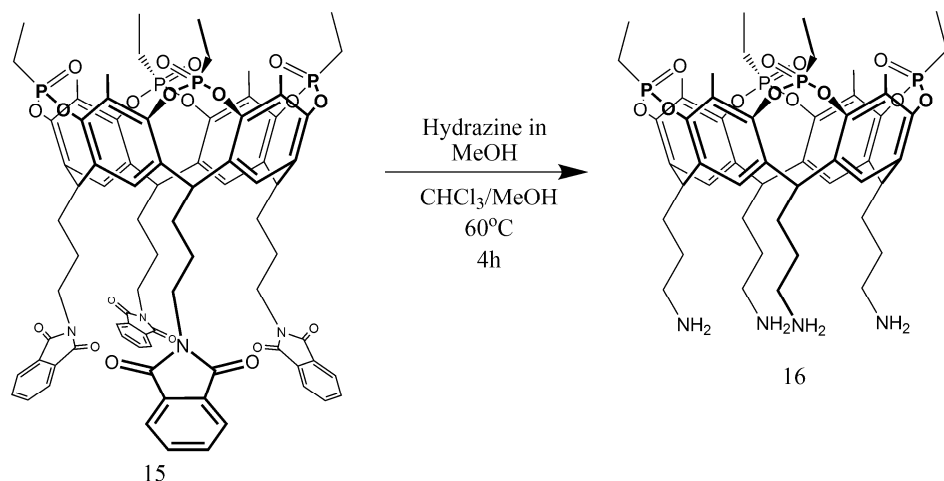
**Scheme 9.** Synthesis of **Tiii** [C<sub>3</sub>H<sub>6</sub>Cl, CH<sub>3</sub>, C<sub>2</sub>H<sub>5</sub>] cavitand **14**.

To convert the four Cl atoms at the lower rim of the cavitand into four amino groups, we used the synthesis of Gabriel. The first step of the synthesis was the reaction between cavitand **14**, and phthalimide, in presence of KI as catalyst, K<sub>2</sub>CO<sub>3</sub> as base and DMF as solvent. The reaction was performed at room temperature for 5 hours. After purification through flash chromatography, the desired product **15** was obtained as white solid in 50% yield (Scheme 10).



**Scheme 10.** Synthesis of tetraphthalimide **Tiii** cavitand (**15**).

The last step was the cleavage of the phthalimides in presence of hydrazine, to obtain the amino groups (Scheme 11). Cavitand **16** was obtained as solid in good yield.



**Scheme 11.** Synthesis of the *Ti<sup>III</sup>* [ $C_3H_8N$ ,  $CH_3$ ,  $C_2H_5$ ] cavitand **16**.

The protonated form of cavitand **16** resulted highly soluble in water. It was fully characterized by  $^1H$ -NMR,  $^{31}P$ -NMR and ESI-MS. From the  $^1H$ -NMR, performed in  $D_2O$ , it resulted that one of the four amino group is a salt of the Hydrazine-phthalimide complex. We found in literature that this salt can be formed using this procedure.<sup>27</sup> In figure 14 the  $^1H$  NMR spectrum of desired cavitand **16** is shown and the diagnostic peaks highlighted. Therefore, the presence of four  $N^+H_3$  groups at the lower rim is sufficient to make cavitand soluble in water, provided that the  $P=O$  bridges at the upper rim bear small substituents.

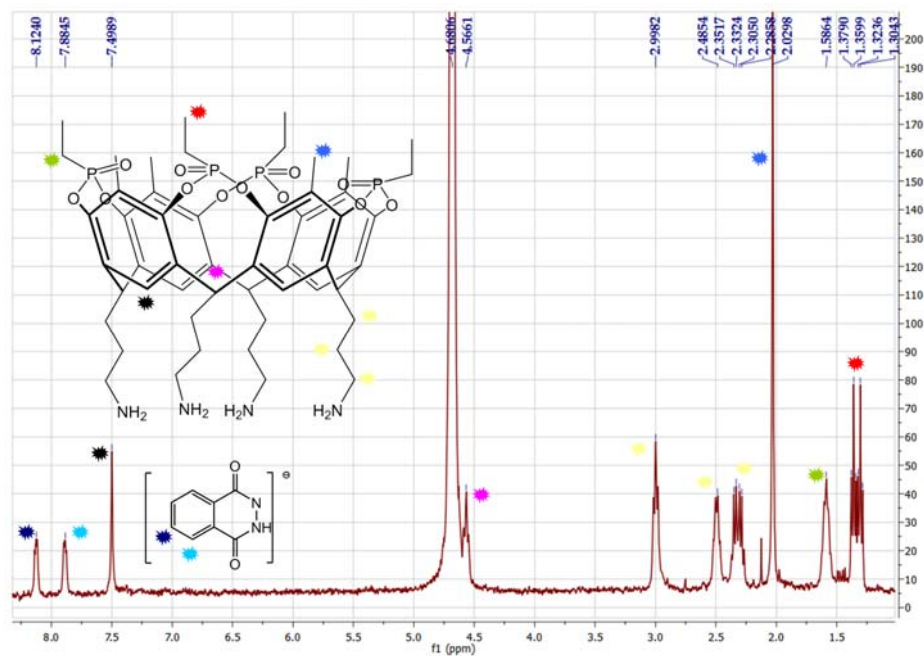


**Figure 14.**  $^1\text{H}$  NMR spectrum of **16** with phthalimide salt in  $\text{D}_2\text{O}$ .

The two multiplets at 7.88 ppm and 8.12 ppm belong to the aromatic ring of the salt. Figure 15 below shows the  $^{31}\text{P}$  NMR spectrum of **16**. The presence of only one peak confirms that the cavitand obtained is the isomer with all the four  $\text{P}=\text{O}$  groups oriented inward the cavity.

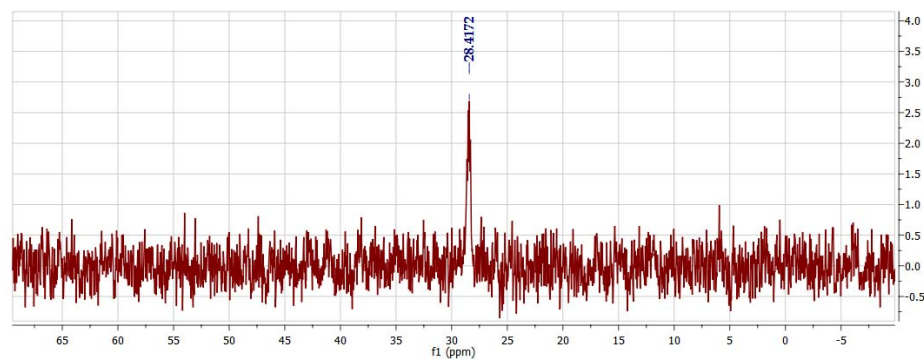


**Figure 15.**  $^{31}\text{P}$  NMR spectrum of cavitand **16** in  $\text{D}_2\text{O}$ .

## 4.5. Conclusions and perspectives.

Different synthetic approaches have been tested to synthesise a water soluble tetraphosphonate cavitand. The first attempt of inserting four triethylen glycol chains onto the bridging  $\text{P}=\text{O}$  group failed. We were able to synthesise with success the new dichloride sintone **6**, but the bridging reaction did not lead to the achievement of the desired cavitand. Different reaction conditions were tested, changing solvent, base and temperature, unfortunately without successes. Cavitand **8**, functionalized with just one  $\text{P}=\text{O}$  bridging group bearing a triethylene glycol chain was synthesised with success, but it turned to be not water soluble.

The model cavitand **12** presenting four methylene groups as bridging units and for triethylene glycol chains at the apical position was successfully synthesised. Unfortunately the cavitand resulted not soluble in water, and for this reason any attempt to synthesise the tetraphosphonate analog was not performed.

The synthesis of a tetraphosphonate cavitand functionalised at the upper rim with four ethylphosphonate groups and at the lower rim with four amino groups was successfully performed. Cavitand **16** resulted soluble in acidic water.

The receptor has been sent to prof. Peter Crowley at the National University of Ireland to be tested in the binding of biologically interesting ammonium species.

## 4.6. Acknowledgments.

Special thanks to Dr. Roberta Pinalli and Dr. Daniela Menozzi from University of Parma for support and fruitful discussions on this topic.



## 4.7. Experimental part.

**General Methods.** All commercial reagents were ACS reagent grade and used as received. Solvents were dried and distilled using standard procedures.  $^1\text{H}$  NMR spectra were recorded on Bruker Avance 300 (300 MHz), the  $^1\text{H}$  NMR and  $^{31}\text{P}$  NMR spectra were recorded on Bruker Avance 400 (400 MHz) spectrometers. All chemical shifts ( $\delta$ ) were reported in parts per million (ppm) relative to proton resonances resulting from incomplete deuteration of NMR solvents.  $^{31}\text{P}$  NMR spectra were recorded on Avance 400 (162 MHz) and all chemical shifts were reported to external standard 85%  $\text{H}_3\text{PO}_3$  at 0 ppm. Electrospray ionization mass spectrometry (ESI-MS) experiments were performed on a Waters ACQUILITY UPLC SQ Detector. The Matrix-assisted laser desorption/ionization analysis (M@LDI TOF-TOF) were performed on AB SCIEX MALDI TOF-TOF 4800 Plus using *o*-Cyano-4-hydroxycinnamic acid as a matrix.

### Triethylene glycol-tosylate (2)

Triethylene glycol monomethyl ether (0.1 mol) and a water solution of potassium hydroxide (50 mL, 0.22 mol, 2.2 eq.) were added into 50 mL THF and cooled to  $0^\circ\text{C}$ . A solution -of p-tosyl chloride (0.12 mol, 1.2 eq.) in 100 mL of THF cooled at  $0^\circ\text{C}$  was then added dropwise over 30 min. The reaction was stirred at  $5^\circ\text{C}$  for 2h and at room temperature for an additional 18h. Reaction was quenched by addition of ethyl acetate (100 mL), and organic phases were collected, extracted with 75 mL portion of 6 N HCl, dried over  $\text{MgSO}_4$  and the solvent was removed by evaporation yielding 95% of desired product.

$^1\text{H}$  NMR (300 MHz,  $\text{CDCl}_3$ ):  $\delta$  (ppm) 3.30 (s, 3H,  $\text{CH}_3\text{OCH}_2$ ), 3.47 – 3.62 (m, 10H), 4.09 (s, 2H,  $\text{CH}_2\text{OSO}_2$ ), 7.29 (d, 2H,  $J = 7.2$  Hz, ArH), 7.73 (d, 2H,  $J = 7.4$  Hz, ArH),

ESI-MS:  $m/z$  341  $[\text{M}+\text{Na}]^+$ .

**Triethylene glycol-iodine (3)**

Triethylene glycol-tosylate **2** (0,05 mol) was dissolved in 50 mL of acetone and carefully added to a refluxing potassium iodide (0.18 mol, 3.6 eq.) in acetone and reacted for 16h. Afterwards, the acetone was removed under reduced pressure. The residue was dissolved in 100 mL of chloroform and extracted with 100 mL of water. The organic layers were washed with brine and dried over MgSO<sub>4</sub>. The solvent was removed by evaporation affording final product with yield of 92%.

<sup>1</sup>H NMR (400 MHz, CDCl<sub>3</sub>): δ (ppm) 3.23 (t, 3H, J = 6.9 Hz, CH<sub>3</sub>OCH<sub>2</sub>), 3.35 (s, 2H, OCH<sub>2</sub>CH<sub>2</sub>I), 3.52 (s, 2H, CH<sub>3</sub>OCH<sub>2</sub>), 3.64 (m, 6H), 3.72 (t, 2H, J = 8.8 Hz, OCH<sub>2</sub>CH<sub>2</sub>I)

ESI-MS: m/z 296 [M+Na]<sup>+</sup>.

**Triethylphosphite ethylene glycol (4)**

Compound **3** (25 mmol, 1 eq.) and triethyl-phosphite (30 mmol, 1,2 eq.) were placed into the vessel and reacted under microwave irradiation for 1h at 200°C. Subsequently, the mixture was extracted with H<sub>2</sub>O/AcOEt, and the collected organic fractions were washed with brine and dried over Na<sub>2</sub>SO<sub>4</sub> and solvent was removed by evaporation. The final product **4** was purified by vacuum distillation. Yield: 80%.

<sup>1</sup>H NMR (400 MHz, DMSO-*d*<sub>6</sub>): δ (ppm) 1.20 (t, 6H, J = 7.0 Hz, CH<sub>3</sub>CH<sub>2</sub>OP) 2.01 (m, 2H, CH<sub>2</sub>CH<sub>2</sub>P) 3.21 (s, 3H, CH<sub>3</sub>OCH<sub>2</sub>), 3.40 (m, 2H, CH<sub>3</sub>OCH<sub>2</sub>), 3.48 (s, 6H, CH<sub>2</sub>O), 3.53 (m, 2H, CH<sub>2</sub>CH<sub>2</sub>P), 3.97 (m, 4H, CH<sub>3</sub>CH<sub>2</sub>OP),

<sup>31</sup>P NMR (162 MHz, DMSO-*d*<sub>6</sub>) δ (ppm): 28.50 (s, 1P).

ESI-MS: m/z 306 [M+Na]<sup>+</sup>.

**Triethylene glycol phopshonic acid (5)**

Triethylphosphite ethylene (1,7 mmol, 1 eq.) and HCl 37% (7 mmol, 4 eq.) were placed into the vessel and reacted under microwave irradiation for 1,5h at 120°C. Subsequently, the mixture was extracted with H<sub>2</sub>O/DCM and H<sub>2</sub>O fractions were dried by evaporation. The product was purified by vacuum distillation. Yield: 98%.

**<sup>1</sup>H NMR** (400 MHz, DMSO-*d*<sub>6</sub>): δ (ppm) 1.84 (m, 2H, CH<sub>2</sub>CH<sub>2</sub>P) 3.23 (s, 3H, CH<sub>3</sub>OCH<sub>2</sub>) 3.41 (m, 2H, CH<sub>3</sub>OCH<sub>2</sub>), 3.50 (m, 6H, OCH<sub>2</sub>), 3.56 (m, 2H, CH<sub>2</sub>CH<sub>2</sub>P), 7.85 (s, 2H, HOP),

**<sup>31</sup>P NMR** (162 MHz, DMSO-*d*<sub>6</sub>) δ (ppm): 21.95 (m, 1P).

**ESI-MS:** m/z 251 [M+Na]<sup>+</sup>.

### Triethylene glycol phosphonic dichloride (6)

The triethylene glycol phosphonic acid **5** (0.65 mmol, 1 eq.), oxalyl chloride (6.5 mmol, 10 eq.) and dry CHCl<sub>3</sub> were added into the oven dried round-bottomed flask and stirred at 40°C for 1 night. Solvent was removed under vacuum and obtained solid was then dried under vacuum. Yield 35%.

**<sup>1</sup>H NMR** (400 MHz, CDCl<sub>3</sub>): δ (ppm) 2.5 (m, 2H, CH<sub>2</sub>CH<sub>2</sub>P) 3.34 (s, 3H, CH<sub>3</sub>OCH<sub>2</sub>) 3.58 – 4.00 (m, 10H, OCH<sub>2</sub>),

**<sup>31</sup>P NMR** (162 MHz, CDCl<sub>3</sub>) δ (ppm): 45.40 (m, 1P).

**ESI-MS:** Due to the fast hydrolysis of the compound mass was not detected.

### 3PO-Ph - 1PO-TEG Cavitand (10)

The freshly prepared triethylene glycol phosphonic dichloride **6** (11 mmol, 10 eq.), the 3P=O cavitand **9** (0.1 mmol, 1 eq.), *N*-methyl-pyrrolidinium (10 mmol, 10 eq.) and acetonitrile (20 mL) were added into a oven-dried round-bottomed flask, and stirred for 16h at 80°C. Subsequently, the mixture was extracted with H<sub>2</sub>O/DCM, and the organic layers were washed with brine and dried over Na<sub>2</sub>SO<sub>4</sub>. The solvent was removed by evaporation under reduced pressure. The product was purified by flash column chromatography yielding: 40%.

**<sup>1</sup>H NMR** (300 MHz, CDCl<sub>3</sub>): δ (ppm) 1.04 (t, 12H, J = 7.4 Hz, CH<sub>2</sub>CH<sub>2</sub>CH<sub>3</sub>). 1.41 (m, 8H, CH<sub>2</sub>CH<sub>2</sub>CH<sub>3</sub>), 2.34-2.20 (m, 8H, CH<sub>2</sub>CH<sub>2</sub>CH<sub>3</sub>), 4.81 (t, 4H, J = 7.4 Hz, ArCH), 6.51 (s, 4H, ArH<sub>up</sub>), 7.13 (s, 4H, ArH<sub>down</sub>), 7.52 (m, 8H, POArH<sub>m</sub>), 7.61 (m, 4H, POArH<sub>p</sub>), 8.09 (m, 8H, POArH<sub>o</sub>),

**<sup>31</sup>P NMR** (162 MHz, CDCl<sub>3</sub>) δ (ppm): 7.20 (s, 1P, PAr), 7.60 (s, 2P, PAr), 17.60 (s, 1P, PCH<sub>2</sub>CH<sub>2</sub>O).

**ESI-MS:** m/z 1167 [M+Na]<sup>+</sup>.

**Tetraglycol tetramethylene cavitand (12).**

The tetrabromo-tetramethylene cavitand (0.15 mmol, 1 eq.), NaH (1 mmol, 6.5 eq.) and TEG-OH (0.6 mmol, 4 eq.) were dissolved in THF (15 mL) and stirred 16h at RT. Subsequently, the reaction was quenched in water, extracted with DCM, organic fractions were washed with brine and dried over sodium sulphate. The solvent was removed by evaporation under reduced pressure. The product was purified by flash column chromatography yielding: 80%.

<sup>1</sup>H NMR (400 MHz, MeOD):  $\delta$  (ppm) 1.87 (d, 12H,  $J = 7.1$  Hz,  $\text{CH}_3\text{CHAr}$ ), 3.24 (s, 12H,  $\text{CH}_3\text{OCH}_2$ ), 3.57-3.70 (m, 48H,  $\text{CH}_2\text{O}$ ), 4.42 (d, 4H,  $J = 7.2$  Hz,  $\text{OCH}_2\text{O}_{\text{in}}$ ), 4.47 (s, 8H,  $\text{ArCH}_2\text{O}$ ), 5.05 (q, 4H,  $J = 7.1$  Hz,  $\text{ArCHAr}$ ), 5.94 (d, 4H,  $J = 7.0$  Hz  $\text{OCH}_2\text{O}_{\text{out}}$ ), 7.53 (s, 4H,  $\text{ArH}_{\text{down}}$ )

**ESI-MS:**  $m/z$  1318  $[\text{M}+\text{Na}]^+$ .

**Tetra PO-Et Tetra-Chloro cavitand (14)**

The tetrachloro-resorcinarene **13** (0.63 mmol, 1 eq.) and dichloroethylphosphine (2.6 mmol, 4.1 eq.) were dissolved in pyridine (20 mL) under Ar atmosphere and stirred at 70°C for 3h. Afterwards, the mixture was cooled to the RT and  $\text{H}_2\text{O}_2$  (20 mL) was added. The mixture was stirred for additional 30 min at RT, quenched in water and filtered. Collected white solid was dried under vacuum and purified by flash column chromatography. Yield 60%.

<sup>1</sup>H NMR (300 MHz,  $\text{CDCl}_3$ ):  $\delta$  (ppm) 1.46 (m, 12H,  $\text{CH}_3\text{CH}_2\text{P}$ ), 1.80 (t, 4H,  $J = 7.1$  Hz,  $\text{CHCH}_2\text{CH}_2$ ), 2.06 (s, 12H,  $\text{CH}_3\text{Ar}$ ), 2.17 (m, 8H,  $\text{CH}_3\text{CH}_2\text{P}$ ), 3.00 (bq, 8H,  $J = 5.2$  Hz,  $\text{CHCH}_2\text{CH}_2$ ), 3.72 (t, 8H,  $J = 7.1$  Hz,  $\text{CH}_2\text{CH}_2\text{Cl}$ ), 4.51 (t, 4H,  $J = 7.4$  Hz,  $\text{ArCH}$ ), 7.26 (s, 4H,  $\text{ArH}_{\text{down}}$ ).

<sup>31</sup>P NMR (162 MHz,  $\text{CDCl}_3$ )  $\delta$  (ppm): 23.3 (s, 4P).

**MALDI TOF-TOF:**  $m/z$  1169  $[\text{M}+\text{Na}]^+$ .

**Tetra PO-Et-Tetra-phthalimide cavitand (15).**

The tetrachloro-tetraPO-Et cavitand **14** (0.22 mmol, 1 eq.), KI (cat),  $\text{K}_2\text{CO}_3$  (1.81 mmol, 8 eq.) and phthalimide (1.81 mmol, 8 eq.) were dissolved in dry DMF (15 mL) and stirred at 90°C for 5h. Afterwards, the DMF was removed under vacuum, the residue was dissolved in DCM and extracted with  $\text{H}_2\text{O}$ . Collected organic fractions were dried over  $\text{Na}_2\text{SO}_4$  and white solid was purified by flash column chromatography yielding 50% of desired product.

**<sup>1</sup>H NMR** (400 MHz, CDCl<sub>3</sub>): δ (ppm) 1.40 (m, 12H, CH<sub>3</sub>CH<sub>2</sub>P), 1.80 (t, 4H, J = 7.3 Hz, CHCH<sub>2</sub>CH<sub>2</sub>), 2.07 (s, 12H, CH<sub>3</sub>Ar), 2.19 (m, 8H, CH<sub>3</sub>CH<sub>2</sub>P), 2.48 (q, 8H, J = 7.8 Hz, CHCH<sub>2</sub>CH<sub>2</sub>), 3.91 (t, 8H, J = 7.3 Hz, CH<sub>2</sub>CH<sub>2</sub>N), 4.61 (t, 4H, J = 7.6 Hz, ArCH), 7.26 (s, 4H, ArH<sub>down</sub>), 7.62-7.73 (m, 16H, NCAr).

**<sup>31</sup>P NMR** (162 MHz, CDCl<sub>3</sub>) δ (ppm): 24.2 (s, 4P).

**ESI-MS:** m/z 1627 [M+K]<sup>+</sup>.

#### **Tetra PO-Et-Tetra-amino cavitand (16)**

Tetra PO-Et-Tetra-phthalimide cavitand **15** (0.078 mmol, 1 eq.) was dissolved in CHCl<sub>3</sub> (10 mL) and hydrazine in methanol (3.91 mmol, 50 eq.) was added at once and mixture was stirred at 60°C for 4h. The solution was cooled to the room temperature, filtered and solid was washed three times with CHCl<sub>3</sub>. The white solid was redissolved in water with 1N HCl, sonicated and vacuum dried. Yield 70%.

**<sup>1</sup>H NMR** (400 MHz, DMSO-*d*<sub>6</sub>): δ (ppm) 1.33 (m, 12H, CH<sub>3</sub>CH<sub>2</sub>P), 1.47 (bs, 4H, CHCH<sub>2</sub>CH<sub>2</sub>), 2.07 (s, 12H, CH<sub>3</sub>Ar), 2.26 (m, 8H, CH<sub>3</sub>CH<sub>2</sub>P), 2.63 (bs, 8H, CHCH<sub>2</sub>CH<sub>2</sub>), 2.85 (bt, 8H, CH<sub>2</sub>CH<sub>2</sub>N), 4.09 (bs, 8H, CH<sub>2</sub>NH<sub>2</sub>), 4.44 (bs, 4H, ArCH), 7.75 (bs, 4H, ArH<sub>down</sub>).

**<sup>31</sup>P NMR** (162 MHz, CDCl<sub>3</sub>) δ (ppm): 24.2 (s, 4P).

**<sup>1</sup>H NMR** (400 MHz, D<sub>2</sub>O): δ (ppm) 1.34 (m, 12H, CH<sub>3</sub>CH<sub>2</sub>P), 1.58 (bs, 4H, CHCH<sub>2</sub>CH<sub>2</sub>), 2.02 (s, 12H, CH<sub>3</sub>Ar), 2.33 (m, 8H, CH<sub>3</sub>CH<sub>2</sub>P), 2.63 (m, 8H, CHCH<sub>2</sub>CH<sub>2</sub>), 2.99 (t, 8H, CH<sub>2</sub>CH<sub>2</sub>N), 4.56 (bs, 4H, ArCH), 7.49 (s, 4H, ArH<sub>down</sub>).

**<sup>31</sup>P NMR** (162 MHz, D<sub>2</sub>O) δ (ppm): 28.4 (s, 4P).

**ESI-MS:** m/z 1091 [M+Na]<sup>+</sup>.

## 4.8. References.

---

<sup>1</sup> IUPAC. Compendium of Chemical Terminology, 2nd ed. (the "Gold Book") **2012**, p.1397.

<sup>2</sup> Szejtli, J.; Osa, T. *Cyclodextrins*, Pergamon, Oxford, **1996**, Vol. 3.

<sup>3</sup> Diederich, F. *Cyclophanes: Monographs in Supramolecular Chemistry*, The Royal Society of Chemistry, Cambridge, UK, **1991**.

<sup>4</sup> Murakami, Y.; Hayashida, O. *Comprehensive Supramolecular Chemistry*, Pergamon, Oxford, **1996**, Vol. 2, p. 4198.

<sup>5</sup> a) Duan, Q.; Cao, Y.; Li, Y.; Hu, Y.; Xiao, T.; Lin, C.; Pan, Y.; Wang, L. *J. Am. Chem. Soc.* **2013**, *135*, 10542,

<sup>6</sup> a) Pinalli, R.; Suman, M.; Dalcanale, E. *Eur. J. Org. Chem.* **2004**, 451.; b) Pinalli, R.; Dalcanale, E.; *Acc. Chem. Res.* **2013**, *46*, 399.; c) Kwang, S. et al.; *Chemical Society Reviews* **2006**, *35*, 355.; d) Schierbaum, K. D.; Weiss, T.; Thoden van Velzen, E. U.; Engbersen, J. F. J.; Reinhoudt, D. N.; Goepel, W.; *Science* **1994**, *256*, 1413.

<sup>7</sup> a) Timmerman, P.; Verboom, W.; Reinhoudt, D. N. *Tetrahedron* **1996**, *52*, 2663-2704. b) Moran, J. R.; Karbach, S.; Cram, D. J. *J. Am. Chem. Soc.* **1982**, *104*, 5826-5828.

<sup>8</sup> a) Tucker, J. A.; Knobler, C. B.; Trueblood, K. N.; Cram, D. J. *J. Am. Chem. Soc.* **1989**, *111*, 3688.; b) Careri, M.; Dalcanale, E.; Mangia, A.; Ruffini, M. *Anal. Comm.* **1997**, *34*, 13.

<sup>9</sup> Thoden van Velzen, E. U.; Engbersen, J. F. J.; de Lange, P. J.; Mahy, J. W. G.; Reinhoudt, D. N. *J. Am. Chem. Soc.* **1995**, *117*, 6853.

<sup>10</sup> Fraser, J. R.; Borecka, B.; Rotter, J.; Sherman, J. C. *J. Org. Chem.* **1995**, *60*, 1207.

- 
- <sup>11</sup> Park, S. J.; Hong, J.-I. *Tetrahedron Lett.* **2000**, *41*, 8311.
- <sup>12</sup> Sebo, L.; Diederich, F. *Helv. Chim. Acta.* **2000**, *83*, 93.
- <sup>13</sup> a) Haino, T.; Rudkevich, D. M.; Rebek, Jr.; J. *J. Am. Chem. Soc.* **1999**, *121*, 11253.; b) Hof, F.; Trembleau, L.; Ullrich E. C.; Rebek, Jr., *J. Angew. Chem. Int. Ed.* **2003**, *42*, 3150.
- <sup>14</sup> Liu, S.; Gibb, B. *Chem. Commun.* **2008**, 3709.
- <sup>15</sup> Dionisio, M.; Oliviero, G.; Menozzi, D.; Federici, S.; Yebeutchou, R. M.; Schmidtchen, F. P.; Dalcanale, E.; Bergese, P. *J. Am. Chem. Soc.* **2012**, *134*, 2392.
- <sup>16</sup> ATLAS on Substance Use (2010) - *Resources for the prevention and treatment of substance use disorders*, World Health Organisation, **2011**
- <sup>17</sup> Sreekumar, A.; Poisson, L. M.; Rajendiran, T. M.; Khan, A. P.; Cao, Q.; Yu, J.; Laxman, B.; Mehra, R.; Lonigro, R. J.; Li, Y.; Nyati, M. K.; Ahsan, A.; Kalyana-Sundaram, S.; Han, B.; Cao, X.; Byun, J.; Omenn, G. S.; Ghosh, D.; Pennathur, S.; Alexander, D. C.; Berger, A.; Shuster, J. R.; Wei, J. T.; Varambally, S.; Beecher, C.; Chinnaiyan, A. M. *Nature* **2009**, *457*, 910.
- <sup>18</sup> Von Bohlen; Halbach, O.; Dermietzel, R. *Neurotransmitters and Neuromodulators: Handbook of receptors and Biological Effects*; Wiley-VCH, Weinheim **2006**.
- <sup>19</sup> Minaker, S. A.; Daze, K. D.; Ma, M. C. F.; Hof, F. *J. Am. Chem. Soc.*, **2012**, *134*, 11674.
- <sup>20</sup> Florea, M.; Kudithipudi, S.; Rei, A.; Gonzalez-Alvarez, M. J.; Jeltsch, A.; Nau, W. M. *Chem. Eur. J.* **2012**, *18*, 3521.

<sup>21</sup> McGovern, R. E.; Fernandes, H.; Khan, A. R.; Power, N. P.; Crowley, P. B. *Nature Chemistry* **2012**, *4*, 527.

<sup>22</sup> a) Varier, R. A.; Timmers, H. T. *Biochim. Biophys. Acta.* **2011**, *1815*, 75.; b) Ellinger, J.; Kahl, P.; von der Gathen, J.; Rogenhofer, S.; Heukamp, L. C.; Gütgemann, I.; Walter, B.; Hofstädter, F.; Büttner, R.; Müller, S. C.; Bastian, P. J.; von Ruecker, A. *Prostate* **2010**, *70*, 61.

<sup>23</sup> Thomas, S. N.; Funk, K. E.; Wan, Y.; Liao, Z.; Davies, P.; Kuret, J.; Yang, A. J. *Acta Neuropathol.* **2012**, *123*, 105.

<sup>24</sup> Picture reprintem from: <http://www.epizyme.com/>

<sup>25</sup> Biavardi, E.; Tudisco, C.; Maffei, F.; Motta, A.; Massera, C.; Condorelli, G. G.; Dalcanale, E. *Proc. Natl. Acad. Sci. U.S.A.* **2012**, *109*, 2263.

<sup>26</sup> Cantadori, B.; Betti, P.; Boccini, F.; Massera, C.; Dalcanale, E., *Supramol. Chem.* **2008**, *20*, 29.

<sup>27</sup> Gibson, M. S.; Bradshaw, R. W., *Angew. Chem. Int. Ed.* **1968**, 919.



# Lanthanides inclusion in molecular containers\*

# 5

*These work reported in this chapter has been carried out in the frame of FP7 ITN "FINELUMEN" project.*

## 5.1 Introduction.

Luminescence is a phenomena, that always has fascinated man-kind.<sup>1</sup> During the 19<sup>th</sup> century scientist like Wiedemann, Stokes, Becquerel and others commenced the exploration of this untouched field, opening it for further investigation. Over the years the study of luminescence has led to many inventions such as fluorescence microscopy, fluorescent tubes, plasma screens, fluorescent and phosphorescent paints, phosphorescent labels or safety signs.<sup>2</sup> In particular, lanthanides present very good emission profiles upon external stimuli and their complexes with suitable ligands have been extensively studied. Lanthanides can be complexed by a ligand in two ways: covalently and non-covalently. While the first type of complexes are more stable, the non-covalent ones present better luminescent properties, but their stability is highly affected by the type of ligand used and the local environment. Many approaches have been proposed to enhance the stability of these luminescent complexes.<sup>3</sup>

In this chapter the work based on the luminescent and non luminescent lanthanide complexes encapsulation into molecular containers will be depicted.

## 5.2 Principles of luminescence.

Luminescence is defined as an emission of electromagnetic radiation beyond thermal equilibrium,<sup>4</sup> and can be classified according to the stimulus promoting light emission as follow:

- Chemiluminescence – light emission as a result of a chemical reaction
- Mechanoluminescence – light emission upon mechanical action (stress) directly on solids
- Electroluminescence – light emission as a result of current or strong electric field
- Bioluminescence – light emission as a result of a chemiluminescent reactions in living systems
- Radioluminescence – light emission as a result of radioactive decay
- Photoluminescence – light emission as a result of light adsorption`

In photoluminescence, the light (mostly wavelength ranges in the infrared, ultraviolet and visible light spectrum) interacts with the matter which absorbs it and subsequently, due to an electron excitation, another portion of light is emitted. In particular cases, light adsorption can reach up to 95%, thus becoming a very sensitive and efficient process. Figure 1 shows a typical diagram of excitation and emission of a luminescent dye. Excitation promotes the transfer of an electron from the ground state to the excited state. Therefore, luminescence is strongly correlated with photon energy and purity of a phosphor.

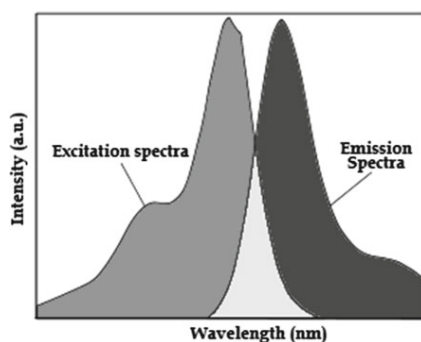


**Figure 1.** A general diagram presenting excitation and emission of a fluorophore.

Light absorption promotes significant physical changes inside the molecule. Excitation of the electronic cloud of a molecule after photon absorption, entails the change of the electron density and the change of the molecule geometry affecting in particular the distances between the carbon atoms. Electronic excitation, rotational excitation, nuclear spin inversion and bond deformations represent some of the possible excitation modes giving fluorescence or phosphorescence. Fluorescence is defined as a photoluminescence emission, from the singlet electronic state, upon excitation of the matter by a light source, while phosphorescence is a process affecting the triplet electronic state as depicted in Figure 2. Due to longer emission, phosphorescence can be visible by eye also after excitation by light.

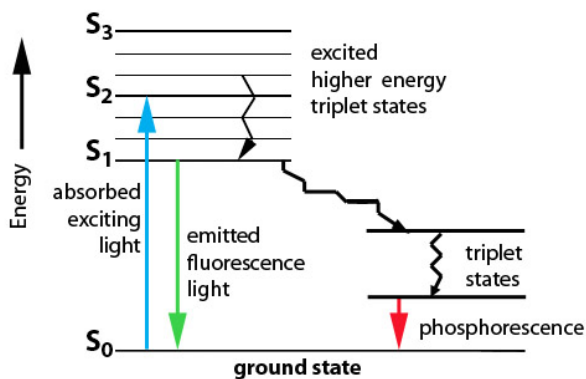


**Figure 2.** Jablonski diagram demonstrating the differences between fluorescence and phosphorescence.

### 5.2.1 The Lanthanide ions main properties.

Lanthanides (Ln) are situated at the bottom of the periodic table ranging from lanthanum ( $Z = 57$ ) to lutetium ( $Z = 71$ ) and are commonly named as "lanthanide series". The first scientific explanations of some properties of Lanthanides were given in the course of the development of quantum mechanics already in the 20<sup>th</sup> century.<sup>5</sup> It became apparent that the dominant oxidation state of Lanthanides is (III) and that the electronic configuration of a trivalent lanthanide ion is  $[Xe]4f^n$  ( $n=0-14$ ); this means that the f orbital electrons are shielded by the 5s and 5d orbitals making them "inner" electrons. Thus, lanthanides are f-block elements (apart from Lu which is a d-block element) characterized by the filling of the 4f electron shell. The f-electrons in most of lanthanide complexes are considered to have properties which are close to those of isolated ions. The direct excitation of the inner f orbital is strictly forbidden, making the direct photoexcitation of the lanthanide ions very difficult.

The most extensive measurements of energy levels of  $4f^n$  configuration of lanthanide ions were carried out by Dieke and co-workers.<sup>6</sup> Most of the lanthanide ions show luminescence in the visible region of the optical spectrum and the lines generated from the different lanthanides have been well established. In Figure 3, the so-called Dieke diagram for several lanthanide ions

is depicted. In the diagram the allowed optical transitions are plotted as energies for different ions. This energy level diagram is useful because it plays an important role to design suitable materials for phosphors.

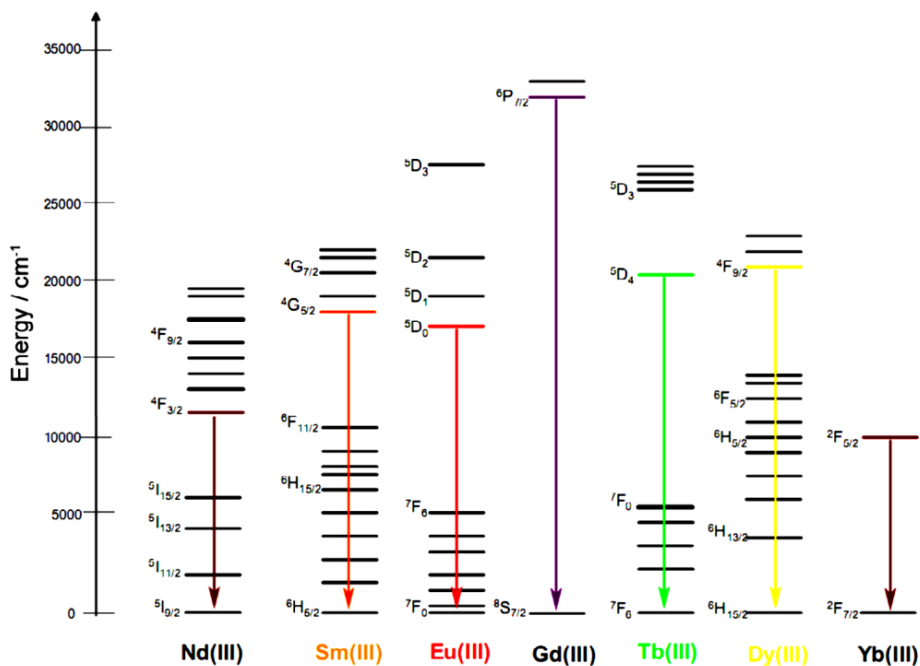


**Figure 3.** The Dieke energy level diagram of interesting lanthanide ions presenting their emitting levels.

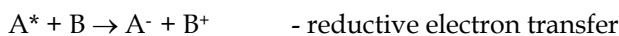
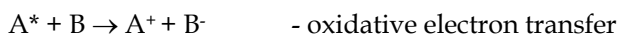
At the beginning of the 1930's many physicists believed that the sharp lines of absorption and emission may be due to electronic transitions within the 4f electron shells<sup>7</sup> rather than to the alternative transitions from the inner 4f shell to the outer 5d – 6s shells.<sup>8</sup>

The excitation and emission spectra of Ln-containing compounds show sometimes broad bands which can be explained by assuming charge transfer (CT) transitions between the Ln dopant and a host ion or between the host ions themselves. Energy transfer between Lanthanides and their ligands is a well-known example, which can enhance the complex luminescence.

Several types of energy transfer within  $\text{Ln}^{3+}$  dopants and hosts have been described:<sup>9</sup>

- Resonant energy transfer between ions of same energy level
- Spectral diffusion
- Energy donation
- Sensitizer's transfer
- Quenching centres transfer
- Charge transfer

In general, the energy transfer takes place between different kinds of orbitals, or different ions. In solution, where the lifetime of the excited state is long enough, an excited molecule  $A^*$  has a chance to encounter another molecule B. This leads to two types of interaction: electron transfer and charge transfer.<sup>10</sup>



Electron and charge transfers can be used to quench an electronically excited state preventing luminescence and/or intramolecular reactivity. By dint of this interactions some chemical species, which do not absorb light, assisted by charge transfer become luminescent. The lanthanide ions are well known to be very efficient in absorbing energy, and in transferring it to another ion, promoting the energy emission. This process is called "Activation" and the Ln ion is called "Activator". When the energy is transferred from the ligand to the Ln core, the process is called "Sensitization", and the Ln ion "Sensitizer". These processes promotes luminescence. The importance of the luminescence of the Ln ions is related to its peculiar characteristics, e.g. long lifetime and line-like emission bands, which make those ions unique among the species, which are known to be luminescent. Such characteristics are due to the fact that the emitting excited state and the ground state have the same  $f^n$  electronic configuration and that the f orbitals are shielded from the environment by the outer s and p electrons, as already discussed. Coordinating environment

together with the nature of the ligand, strongly affects the complex luminescence intensity and lifetime. Proper ligand choice helps to modulate competition between radiative and non-radiative deactivation of the luminescence, affecting the efficient light absorption by the Ln ion.

### 5.2.2. The antenna effect.

Poor adsorption coefficients of Lanthanides in the visible and UV spectral region are well known.<sup>11</sup> To overcome this problem, a ligand which presents a good adsorption profile, should be incorporate into the system. In complexes of lanthanide ions with encapsulating ligands, an intense luminescence may, in principle, be obtained by the “antenna effect”<sup>12</sup>, which is defined as a light conversion process via an absorption-energy transfer-emission sequence involving distinct absorbing (ligand, light collector) and emitting (metal ion) components (Figure 4). In such a process, the quantities that contribute to the luminescence intensity are (i) the intensity of the ligand absorption, (ii) the efficiency of the ligand-to-metal energy transfer, and (iii) the efficiency of the metal luminescence.

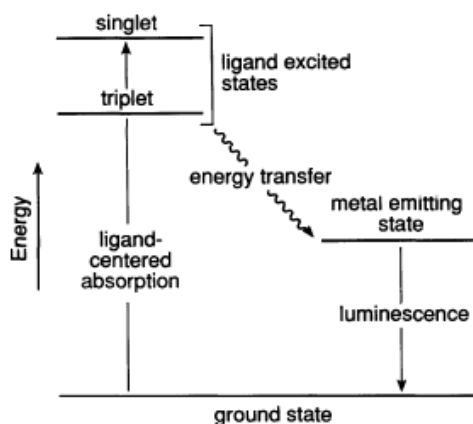


**Figure 4.** Antenna effect involving ligands and emitting metals.

Due to the limited exhibition of coordination ability towards Ln ions, conventional ligands are unable to give inert complexes, especially in aqueous media where water tends to occupy all coordination spheres. Therefore, the use

of organic ligands having strong affinity for lanthanide ions and high antenna effect is essential.

Lanthanide complexes with  $\beta$ -diketonate ligands are the most investigated,<sup>13</sup> thanks to their commercial availability, relatively easy synthesis and very good luminescent properties.<sup>14</sup> In Figure 5, three main types of  $\beta$ -diketonate complexes with Ln are shown.

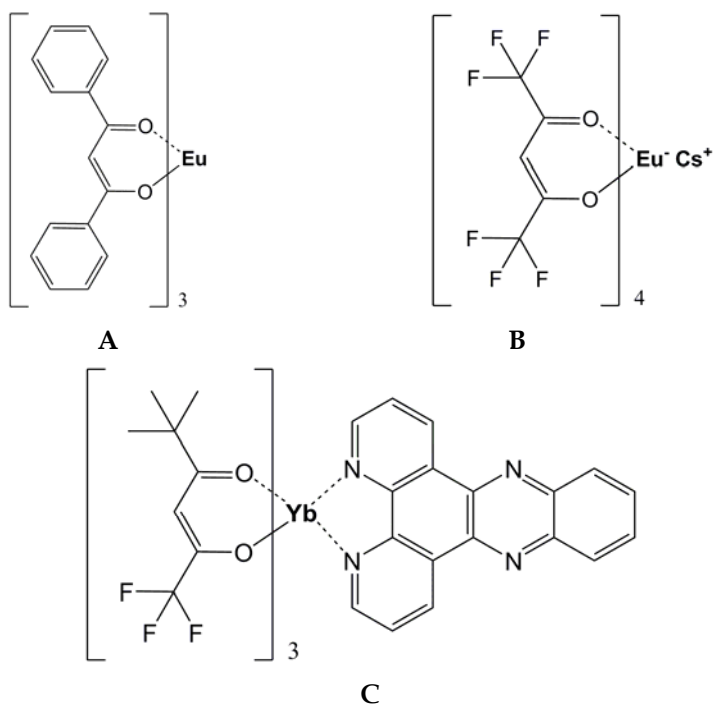


**Figure 5.** Tris  $\beta$ -diketonate Europium complex (A), Europium tetrakis  $\beta$ -diketonate complex (B), Ytterbium Lewis base adduct complex (C).

In the neutral tris  $\beta$ -diketonate complex (A), the Lanthanide ion coordinates three  $\beta$ -diketonate ligands; in the charged complex (B) the Ln ion coordinates four  $\beta$ -diketonates and could coordinate either an alkali metal ion (e.g.  $\text{Li}^+$ ,  $\text{Na}^+$ ,  $\text{K}^+$ ,  $\text{Cs}^+$ ,  $\text{Rb}^+$ ) or a protonated organic base (e.g. pyridinium  $\text{H}^+$ , piperidinium  $\text{H}^+$ , etc.), or a quaternary ammonium ion (e.g.  $\text{Et}_4\text{N}^+$ ,  $\text{Bu}_4\text{N}^+$ , etc.). The complex C is formed by the neutral complex A, which due to the unsaturated



coordination sphere of the Lanthanide can still attach Lewis-base co-ligands, such as: water, 1,10-phenantroline, 2,2'-bipyridine, etc..

Most lanthanide ions ( $\text{Eu}^{3+}$ ,  $\text{Sm}^{3+}$ ,  $\text{Dy}^{3+}$ ) present good luminescence upon  $\beta$ -diketonate complex formation. Terbium presents very low or absent luminescence at room temperature, because the triplet level of the  $\beta$ -diketonate ligands with aromatic substituents is below the  $^5\text{D}_4$  resonance level of the Terbium ion. No metal-centered photoluminescence can be observed for Gadolinium complexes, due to the very high energy level of the 4f shell.

### 5.2.3. The supramolecular approach.

Supramolecular chemistry offers the opportunity to design stable lanthanide complexes for efficient light absorption and luminescence emission,<sup>15</sup> involving different ligands like carboxylic acid derivatives<sup>16</sup>, terphenyl ligands<sup>17</sup>, proteins<sup>18</sup> etc.. These Lanthanide-based supramolecular complexes can be obtain *via* molecular recognition events or self-assembly of well-designed, preorganized systems. Different structures like balls, capsules, dendrimers or polymers held by weak interactions based on lanthanide chemistry have been synthesized.<sup>19</sup>

The strong coordination ability of lanthanides is widely use in organic synthesis. Lanthanides as coordinating metals are more powerful than alkaline metals and they are widely used as templating agents in organic synthesis. The formation of flatten macrocyclic structures as well as more complicated sphere-shaped complexes is fostered by the use of Lanthanide ions.<sup>20</sup> Some examples of those complexes are shown by Raymond and co-workers who reported kinetically inert lanthanide complexes encapsulated in an amine macrocyclic structure.<sup>21</sup> Moreover, Sessler and co-workers reported the formation of a "texaphyrin", an expanded porphyrin based on pyrrole units built around a Lanthanum core as reported in figure 6.<sup>22</sup>

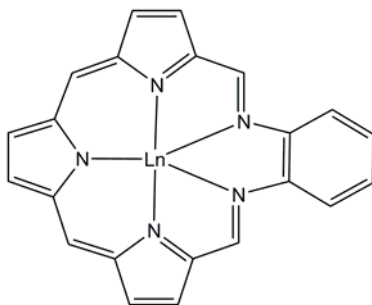


**Figure 6.** General scheme of the Texapirine@Lanthanide complex.

The 1,4,7,10-tetraazacyclododecane-1,4,7,10-tetraacetic acid (DOTA) is one of the most studied macrocyclic structures for the coordination of Lanthanide ions (Figure 7.).

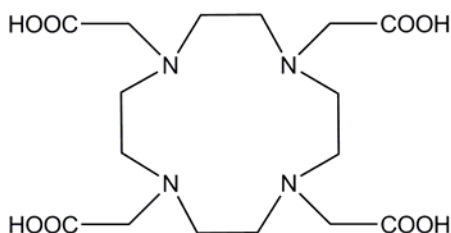


**Figure 7.** Structure of 1,4,7,10-tetraazacyclododecane-1,4,7,10-tetraacetic acid (DOTA).

The ligand is widely used as chelating agent thanks to its octadentate coordination character.<sup>23,24</sup> Yttrium<sup>3+</sup> and Gadolinium<sup>3+</sup> DOTA complexes were found to be very efficient, stable and non-toxic contrast agents.<sup>25</sup> The efficiency of these Ln@DOTA complexes can be enhanced by the introduction of new functional groups into the aza moiety.<sup>25</sup>

The employment of 2,2'-bipyridine cryptates as multivalent ligands (Figure 8) brings to the formation on sphere-like complexes, as reported by Ralpa et al.<sup>26</sup>

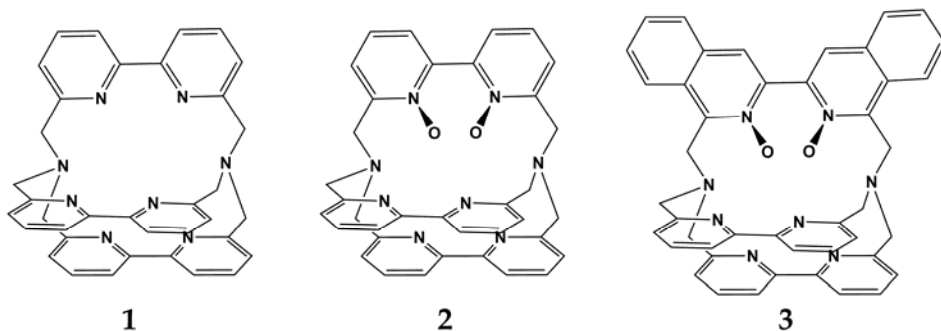


**Figure 8.** Cryptate ligands used in lanthanide complexation.

Cryptate ligands showed high absorption energy and resulted to be kinetically inert in aqueous environment. The emission quantum yields of complex  $[1@Ln]^{3+}$  ( $Ln = Eu^{3+}, Tb^{3+}$ ) upon energy transfer process was found to be rather low. The nitrogen oxidation of one of the 2,2'-bipyridinium units in ligand (2) and one of the 3,3'-biisoquinoline units of ligand (3) brought an energy transfer enhancement.<sup>27</sup> In complexes 2 and 3 the included cation is better protected from the interaction with water than in the case of the  $[1@Ln]^{3+}$  cryptate, and these complexes present a significant gain in light-conversion efficiency over  $1@Ln$  cryptates. In fact, it is known that the coordinated water molecules quench the light emission *via* non-radiative deactivation through O-H vibrations. Moreover, the lower distances between the Ln ions and the chelating units (2 and 3) permit an efficient charge transfer from the antenna unit to the lanthanide core.

Calyx[ $n$ ]arenes are known to be very efficient in Ln(III) ions coordination.<sup>28</sup> In 2000, Raston and co-workers reported the use of a combinatorial approach for the synthesis of a complex based on molecular capsules employing Y(III) ions, *p*-sulfonatocalix[4]arene as receptor and a crown ether at the core of the capsule, held in the hydrophobic capsule interior.<sup>29</sup> In their study the Y(III) ions coordinate to the oxygen of the sulfonate groups and to 7 water molecules, in a calix-SO $\cdots$ Y $\cdots$ HOH $\cdots$ OS-calix motif. The capsule formation is boosted both through the direct interaction of the sulfonate groups with the surrounding water molecules, and by the presence of the crown ether (Figure 9). The crown

ether is the primary building component around which the capsule is formed, avoiding the Y(III) complexation.

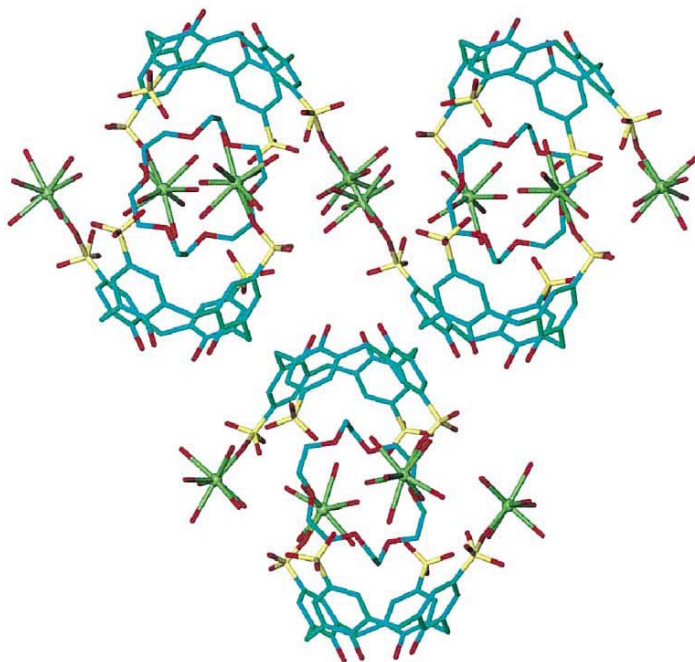


**Figure 9.** Yttrium coordination in the *p*-sulfonatocalix[4]arene-18-crown-6 complex.<sup>26</sup>

The coordination of Lanthanide ions *via* supramolecular weak non-covalent interactions afforded the formation of versatile macrostructures. The strong affinity of flatten as well as spherical scaffolds has been proven.

### 5.3. Results and discussions.

The aim of this work was to investigate the capability of molecular containers to encapsulate luminescent and non-luminescent lanthanide complexes. Inclusion into cages could change the luminescent properties of the complexes, potentially enhancing their stability and emission. Different strategies have been undertaken to promote Ln complex encapsulation, namely hydrophobic driven encapsulation, crystal engineering and solvent free encapsulation.

### 5.3.1. Hydrophobic driven encapsulation.

The rationale behind this approach is to produce a protocol where the luminescent guest is directly encapsulated during the self-assembly of the cage. The driving force for encapsulation is the hydrophobicity of the Ln complex, which should prefer capsule inclusion to water solvation; to this purpose, water soluble capsule components are needed. The octaacid cavitand shown in Figure 10, kindly provided by Prof. Gibb, forms a capsule in water at pH8.9. The basic conditions are necessary to the capsule formation since the water solubilising groups are carboxylates at the periphery of the cavitand.

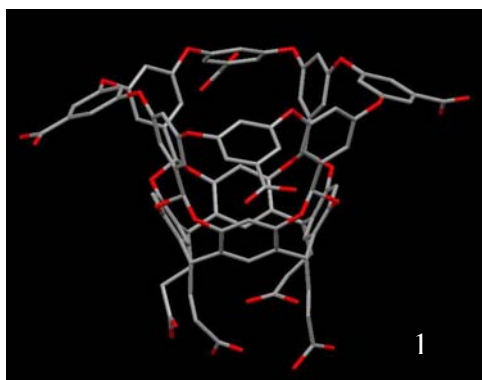


**Figure 10.** X-Ray structure of Gibb's octa-carboxylic acid cavitand (**1**).

Its hydrophilic character is due to the presence of an external hydrophilic coat formed by four carboxylates placed on the upper rim of the cavity, and by another four at the lower rim.

The octaacid cavitand through its deep ( $8 \times 8 \text{ \AA}$ ) and hydrophobic cavity, is capable to host a wide range of organic compounds, like steroids<sup>30</sup>, naphthyl derivatives<sup>31</sup>, olefins<sup>32</sup>, aliphatic hydrocarbons<sup>33</sup> etc.. The use of a guest with proper size and shape triggers the formation of the capsule, which is held together by  $\pi$ - $\pi$  weak interactions between the aromatic walls of the two cavitands and by additive host-guest interactions (Figure 11).<sup>34</sup>

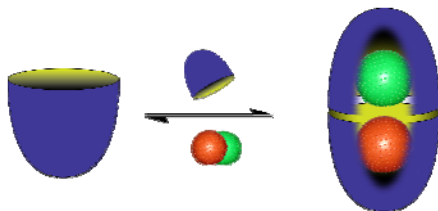


**Figure 11.** *Octaacid cavitand capsule formation upon guest(s) encapsulation.*

We performed complexation experiments using the octaacid cavitand as host and the three complexes depicted in Figure 12, as guests. Guests A and C were provided by the group of Prof. M. Pietraszkiewicz from the Polish Academy of Science in Warsaw, FINELUMEN partner, while complex B was purchased as ACS grade from Strem Chemicals Inc. A and C are highly luminescent Eu (III) complexes, while B does not present luminescent properties.

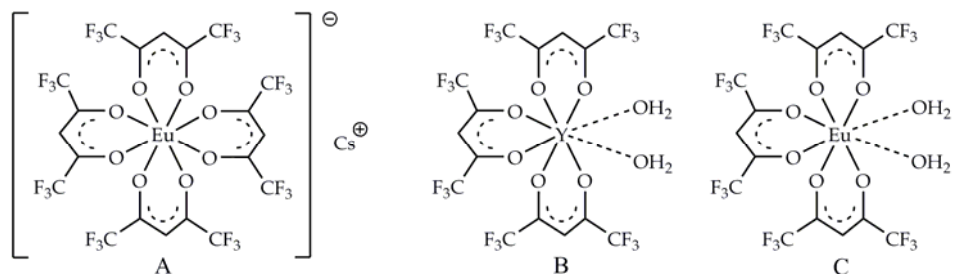


**Figure 12.** *Lanthanide complexes used for the complexation experiments.*

Computer modelling studies show that complex **A** fits very well in the cavity of the capsule formed by two octaacid molecules, while solvation studies show that the water solubility as well as the luminescent properties are maintained upon complexation (Figure 13).

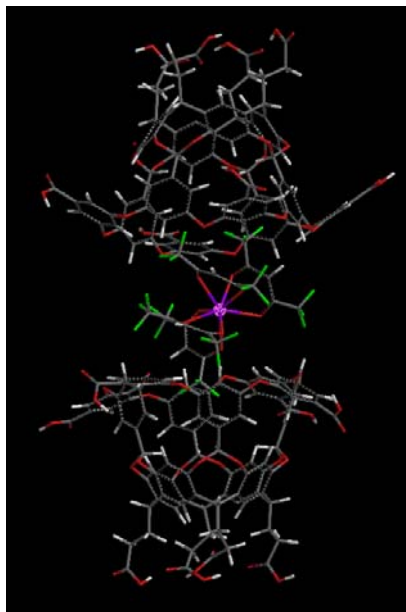


**Figure 13.** *In-silico simulation of capsule formation upon complexation of the Cs Eu (hfac)<sub>4</sub> complex.*

The computer modelling results encouraged us to perform experimentally the complexation of complexes A, B and C into the capsule formed by the two octaacid cavitands. Being A and C paramagnetic, we monitored their encapsulation only through <sup>19</sup>F NMR spectroscopy, while encapsulation of complex B was followed also by <sup>1</sup>H NMR spectroscopy. A D<sub>2</sub>O buffer solution (50mM NaCl + 10mM borate buffer pH 8,9) was used as solvent both for the guests and the host, and the NMR tubes were filled under inert Ar atmosphere in order to avoid any disturbances.

Figure 14, shows the <sup>19</sup>F NMR titration between the octaacid host cavitands and complex A [Cs·Eu (hfac)<sub>4</sub>] as guest.

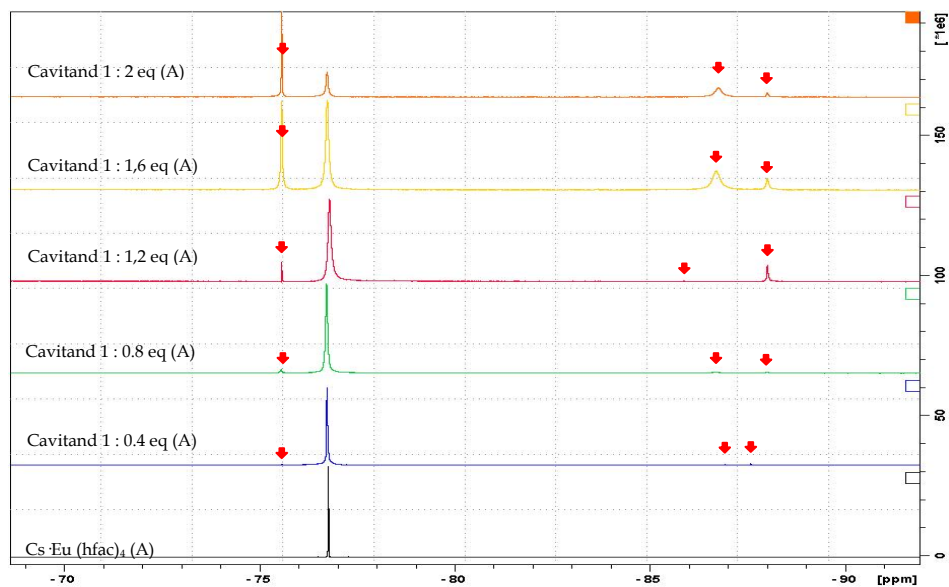


**Figure 14.**  $^{19}\text{F}$  NMR titration between Gibb's cavitand and  $[\text{Cs}\cdot\text{Eu}(\text{hfac})_4]$  in  $\text{D}_2\text{O}$  buffer.

The titration was performed adding portions of 0.4 equivalents of cavitand into a  $\text{D}_2\text{O}$  buffer solution of complex A. The black bottom spectrum presents the europium complex **A** in freshly prepared  $\text{D}_2\text{O}$  buffer (-76.8 ppm). Being the complex instable in water, the spectrum was recorded immediately after the preparation to avoid complex destruction. The blue spectrum was recorded after addition of 0.4 equivalent of octaacid cavitand. As shown in the figure, three small peaks start to appear, highlighted by the red arrows: one at lower field (-75.7 ppm) and two at higher field (-81.6 and -83 ppm). The peaks at lower field could be consistent with the guest encapsulation. The addition of 4 portions of cavitands, lead to the intensity enhancement of the peaks at -75.7, -81.6 and -83 ppm, and to an intensity decrease of the peak at -76.8 ppm, diagnostic for the complex. Each addition caused the formation of a white precipitate inside the NMR tube and subsequent decrease of the luminescence until complete quenching after addition of 2 eq. of the cavitand. The decrease and broadening of the complex diagnostic peak followed by the appearance of three new peaks at -75.7, -81.6 and -83 ppm, could be consistent with the



possible complex destruction due to coordination of the Eu (III) to the water or to the acid moieties of the host, and not with the encapsulation of the guest into the capsule.

The solid formed into the NMR tube after the titration was recovered and analysed through  $^1\text{H}$  and  $^{19}\text{F}$  ( $\text{DMSO } d_6$ ) NMR, and ESI-MS. The analyses revealed that the precipitate was neither consistent with the formed capsule nor with the complex. The same NMR experiment was performed using complexes B and C. The results of the titration were similar to the results obtained with complex A. No evidence of cavitand dimerization upon complex encapsulation was observed.

### 5.3.2. The phosphonate cavitands as potential ligands for lanthanide complexation.

The unique sensing properties of phosphonate cavitands were already described in Chapter 1 and 4. The initial inspiration to investigate the capability of these molecular receptors in lanthanides complexation came from the knowledge that phosphonates groups bind lanthanides efficiently. Recently Vasudevan and co-workers reported examples of coordination complexes between Europium (III) and R-P=O as ligand.<sup>35</sup>

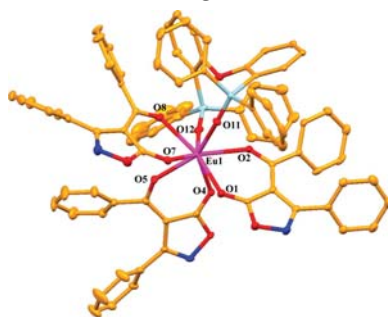


**Figure 15.** X-Ray molecular structure of the Eu (III) complex in which the metal (violet) is coordinated by the three  $\beta$ -diketonate ligands and two P=O units (light blue). All hydrogen atoms have been omitted for clarity.<sup>36</sup>

In a previous work, Dalcanale's group reported examples of supramolecular capsules based on a tetraphosphonate cavitand coordinating metals like: Ba(II),

Ca(II) and Zn(II).<sup>36</sup> In all three cases the cage complexes were formed, but the number of  $\text{P}=\text{O}$  groups directly involved in the complexation with the metal, spanned from three  $\text{P}=\text{O}$  in the case of Ba, to zero  $\text{P}=\text{O}$  for Zn. In the latter case the cavitands behave mainly as second sphere ligand, making a network of H-bonds with the water molecules directly coordinated to the metal ions. The reason for this behavior can be ascribed to the very high rigidity and preorganization of the tetraphosphonate cavitands, which, in this specific case, are detrimental to the correct positioning of the  $\text{P}=\text{O}$  ligands around the cations (Figure 16).



**Figure 16.** Cage formation according to the size of the metal guest.

Following the previously obtained results, crystal engineering studies were undertaken in order to see the capability of mono-, di- and tetraphosphonate cavitands to coordinate different Ln (III) ions. Therefore, different phosphonate cavitands were synthesized and tested.

We started from the mono-phosphonate cavitands, reported in Figure 17.

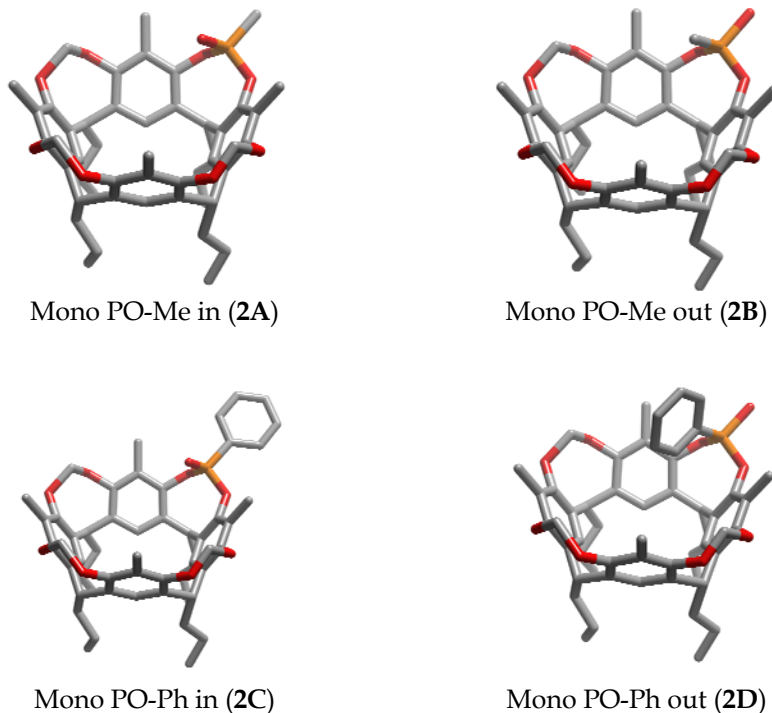


**Figure 17.** The 3D models of monophosphonate cavitands used in the crystal engineering studies. The in or out is relative to the position of the  $\text{P}=\text{O}$  group with respect to the cavity.

Two different substituents on the  $\text{P}=\text{O}$  group, namely methyl and phenyl, were used, in order to investigate their influence on the coordination properties of the cavitands (Figure 17). In particular, the electron rich phenyl group is expected to help the lanthanide ion coordination due to the well-known interactions with rare earth metals like caesium picrate.<sup>37</sup>

All the cavitands were synthesized according to reported procedures.<sup>38,40</sup> The coordination studies were performed employing both inorganic (Figure 18) and organic (Figure 19) lanthanide complexes (the Lanthanum trifluoromethanesulfonate complex was purchased from Sigma-Aldrich and

used as received, the Europium complexes were synthesised by group of Prof. Pietraszkiewicz).

In the experiments where inorganic salts were used as guests, the host cavitand was dissolved in DCM and then a water solution of the inorganic lanthanide salt was added. In order to obtain a homogeneous solution, TFE was added to the biphasic mixture. The obtained solution was left to crystallize by slow evaporation.

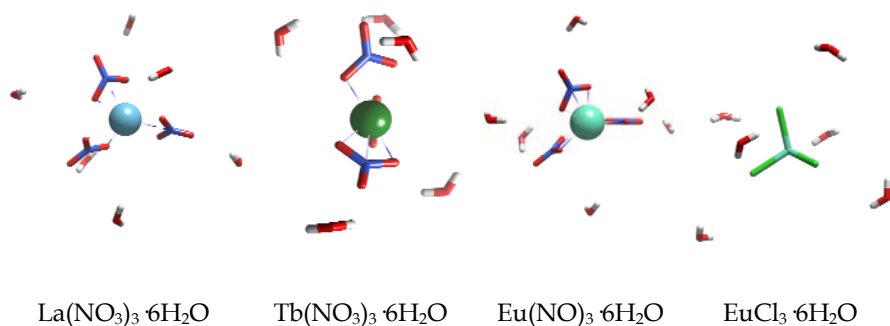


**Figure 18.** 3D figures of inorganic lanthanides compounds used for cavitand complexation.

Unfortunately we were not able to obtain any crystals of the desired complex between the monophosphonate cavitand and the inorganic Ln complexes. Only an amorphous precipitate, not suitable for X-Ray analysis, was formed. In order to boost the crystal formation, different techniques like slow diffusion, gel crystallization or low temperature crystallization were employed, without success.

In the second set of experiments, the organic salts were dissolved in DCM, acetone or in a mixture of DCM/Acetone (8:2) and added to a DCM solution of the cavitand. In this case the use of TFE was not necessary. As in the previous experiment, the DCM solution was left to crystallize by slow evaporation.

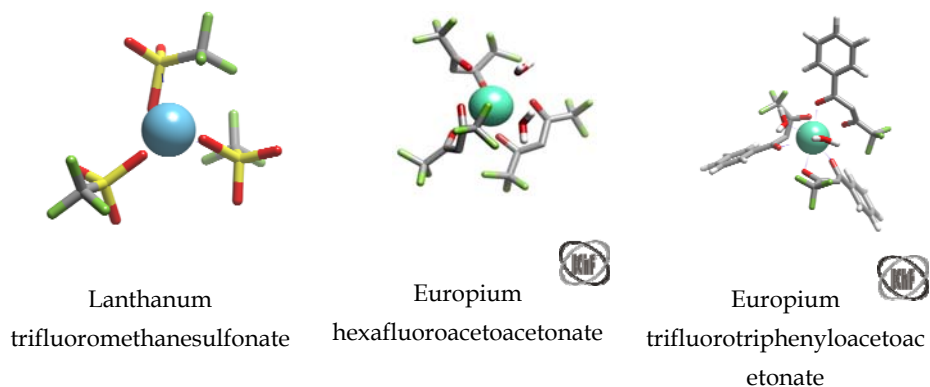
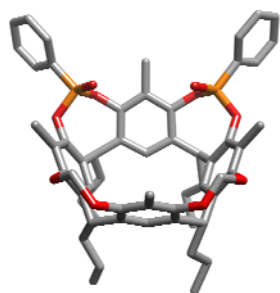


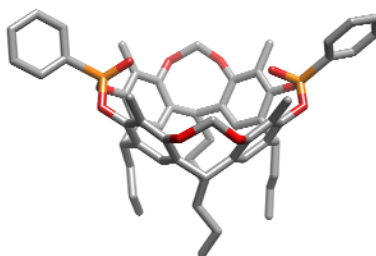
**Figure 19.** 3D figures of organic lanthanide compounds used for cavita $\tilde{d}$  complexation.

Also in this case we didn't obtain any crystals suitable for X-Ray diffraction analysis. Analyzing the three solutions at the UV lamp, we observed that the luminescence of the complexes was quenched. This was probably due to the destruction of the fragile Europium complexes.

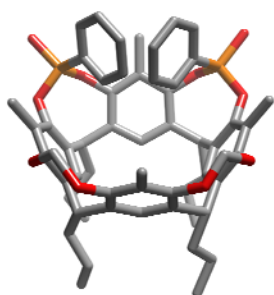
Following these experiments, we decided to move to the di-**P=O** cavita $\tilde{d}$ s (Figure 20), to see if the additional **P=O** group could enhance the cavita $\tilde{d}$  performances in coordinating the La (III) complexes. The synthesis of the di-phosphonate cavita $\tilde{d}$ s leads to the formation of six isomers, depending on the relative position of the two **P=O** groups and their orientation with respect to the cavity (Figure 20).<sup>39</sup> All the six possible isomers were tested in the crystallization experiments, employing the same Ln complexes used in the case of the mono **P=O** cavita $\tilde{d}$ s.



Di AB PO-Ph in-in (3A)



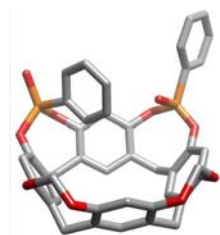
Di AC PO-Ph in-in (3B)



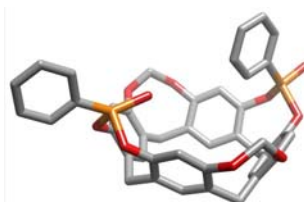
Di AB PO-Ph out-out (3C)



Di AC PO-Ph out-out (3D)



Di AB PO-Ph in-out (3E)



Di AC PO-Ph in-out (3F)

**Figure 20.** 3D figures of AB and AC (in and out) cavitand isomers.

For the inorganic La (III) salts, the same conditions reported for the previous set of experiments were used, while in the case of the organic La (III) complexes, both the salts and the cavitands were dissolved in different solvent mixtures, as reported in Table 1.

Solvent	Ratio
DCM	
Acetone	
TFE	
DCM/Acetone	8:2
DCM/TFE	3:7
DCM/TFE	5:5
DCM/THF	5:5

**Table 1.** Mixture of solvents (with their molar ratio) used for the crystallization experiments.

In the case of the di AC PO-Ph in-in and di AB PO-Ph in-in cavitands with  $\text{La}(\text{NO}_3)_3 \cdot 6\text{H}_2\text{O}$  and  $\text{Eu}(\text{NO}_3)_3 \cdot 6\text{H}_2\text{O}$ , the crystals obtained turned out to be just the empty cavitands, without coordinated metal. Other crystal growing techniques such as low temperature, solvent diffusion and gel crystallization were employed, but no appreciable results were obtained.

The coordination of Eu (III) and La (III) by 8  $\text{P}=\text{O}$  groups are known in the literature.<sup>40</sup> Therefore, the attempt to coordinate Ln salts employing a tetrakisphosphonate cavitand with all the four  $\text{P}=\text{O}$  groups orientated inward the cavity (**Tiiii**) was made. Two different cavitands were synthesised: one with four methyl substituents on the  $\text{P}=\text{O}$  moieties and one with four phenyl groups (Figure 21).

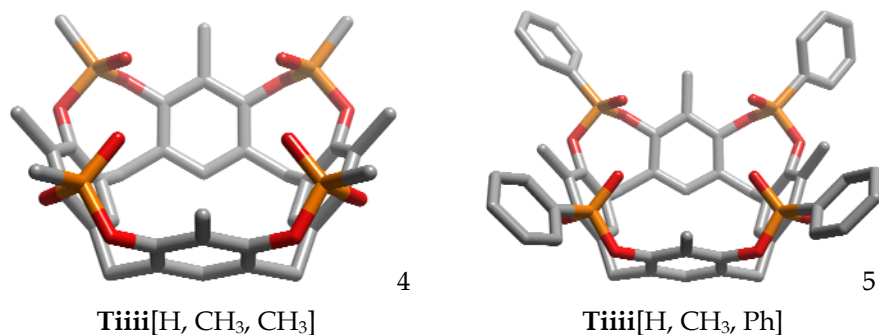


**Figure 21.** The X-Ray molecular structure of the **Ti(III)** cavitanths.

The same inorganic La(III) complexes of the previous experiments were tested. The tetraphosphonate **P=O** cavitanths were dissolved in different solvent mixtures, as reported in Table 2, and they were added to the inorganic salts dissolved in water/TFE (2/8).

Solvent	Ratio
DCM	
ACN	
TFE	
DCM/Acetone	8:2
DCM/TFE	3:7
DCM/TFE	5:5
DCM/THF	5:5
CHCl <sub>3</sub> /TFE	5:5
DMC/ACN	8:2
TFE/H <sub>2</sub> O	8:2

**Table 2.** Mixtures of solvents used for the complexation studies with **Ti(III)** cavitanths.

Besides the organic complexes used previously, six new Ln (III) salts were employed as reported in Figure 25. The new three picrates complexes were synthesized according to reported procedure.<sup>41</sup>



For the crystal growth, all the organic complexes were dissolved in pure DCM or in DCM/ TFE (8/2) or DCM/Acetone (8/2). The solution containing the complexes **6**, **7**, and **7** resulted to be at pH~6, due to the presence of the picric acid as a counter ion. Neutralization with Et<sub>3</sub>N was made to standardize the conditions to pH~7.

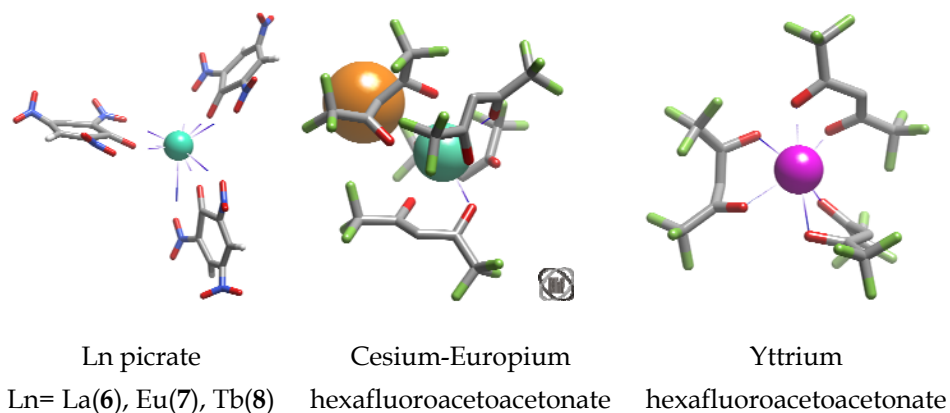


**Figure 22.** 3D figures of organic lanthanide compounds used for the complexation experiments.

In the case where the inorganic Ln salts were employed, the crystals obtained resulted to be the empty **Tiiii** cavitand. In the cases of the solutions containing **6**, **7** and **8**, the X-Ray diffraction analysis on the crystals obtained revealed the presence of free cavitands and picric acid units forming  $\pi$ - $\pi$  stacking with the cavitand skeleton.

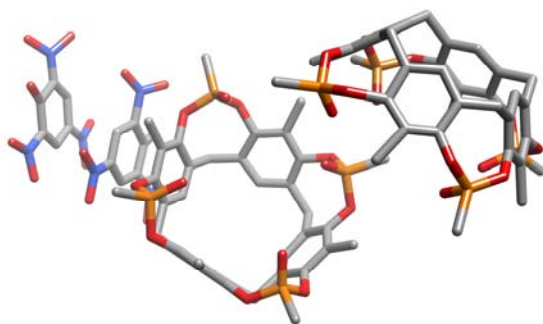


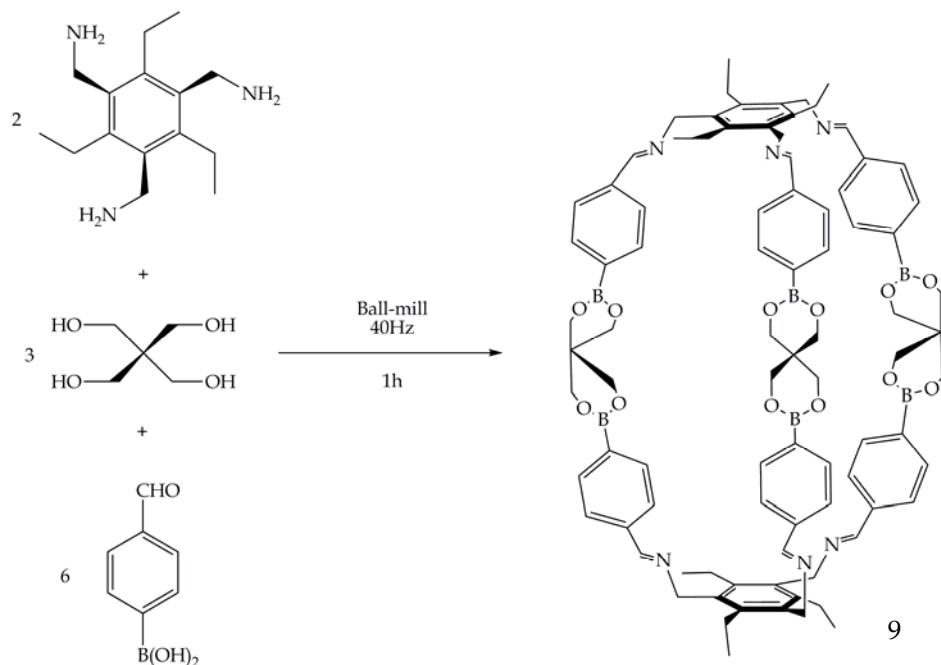
**Figure 23.** *The X-Ray molecular structure of the crystals obtained mixing **Tiii** [H, CH<sub>3</sub>, CH<sub>3</sub>] and complex **8**. (The data were not good enough to allow a complete structural refinement).*

In the case of the experiments involving the other organic complexes (Cesium-Europium hexafluoroacetoacetate, Yttrium and Europium hexafluoroacetoacetate, Europium t trifluorotriphenylacetoacetate) only the free tetraphosphonate cavitands were obtained upon crystallization.

### 5.3.3. Solvent free encapsulation in coordination cages.

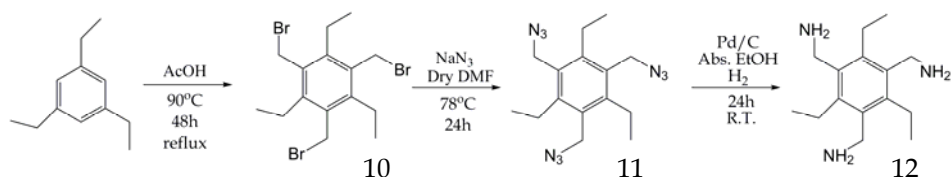
The results obtained in the previous studies showed that Lanthanide complexes are not very stable in solution. The possibility to encapsulate Ln-complexes into a molecular container in absence of solvent was therefore explored.

In 2009 Kay Severin and co-workers reported the solvent free preparation of a nanosize cage formed by reaction between the three different components shown in Scheme 1.<sup>42</sup>



**Scheme 1.** Solvent free synthesis of a nano-size cage.

The same protocol of Severin was repeated in our lab using Mini-Mill PULVERISETTE 23 ball mill as reactor. The first step of the procedure was the synthesis of 1,3,5-triaminomethyl-2,4,6-triethylbenzene (**12**), following Scheme 2.



**Scheme 2.** Synthesis of 1,3,5-triaminomethyl-2,4,6-triethylbenzene.

Commercial 1,3,5-triethylbenzene was reacted with Zn powder, HBr and formaldehyde under acidic conditions for 2 days leading to the bromurated product **10**, which was successively reacted with  $\text{NaN}_3$  in DMF obtaining the

tetraaza product **11**. As last step, the reduction of the azide groups was carried out using Pd/C under H<sub>2</sub> atmosphere, leading to 1,3,5-triaminomethyl-2,4,6-triethylbenzene (**12**).

Compound **12** (2 eq) was reacted with pentaerythriol (3 eq) and 4-formylphenylboronic acid (6 eq) into a stainless-steel jar equipped with five stainless-steel balls (1 cm of diameter) for 1h with different milling amplitudes starting from 5 Hz to 40 Hz. The milling process causes the increase of the reaction temperature. After 1h, the reaction was left to cool down to room temperature, and the product was dried under vacuum to remove the water, by-product of the reaction. The crude was then dissolved in CHCl<sub>3</sub> and washed with water. The organic phase was dried under vacuum and the obtained product was characterized via <sup>1</sup>H NMR and ESI-MS. The characterization confirmed the cage formation. Docking experiments based on the data of the cage crystal structure were done with Spartan. Ferrocene and Y(hfac)<sub>3</sub>(H<sub>2</sub>O)<sub>2</sub> were used as guest models and their fitting into the cavity explored. Ferrocene was chosen to see if a smaller guest could better fit into the cage, while the diamagnetic Yttrium complex, suitable for NMR complexation experiments, was chosen as model guest because structurally similar to our target luminescent complex Eu (hfac)<sub>3</sub>. The results show that both the guests can fit into **9**; in particular, ferrocene is encapsulated in a rather loose way (Figure 24), and Y (hfac)<sub>3</sub>(H<sub>2</sub>O)<sub>2</sub> in a tighter mode.

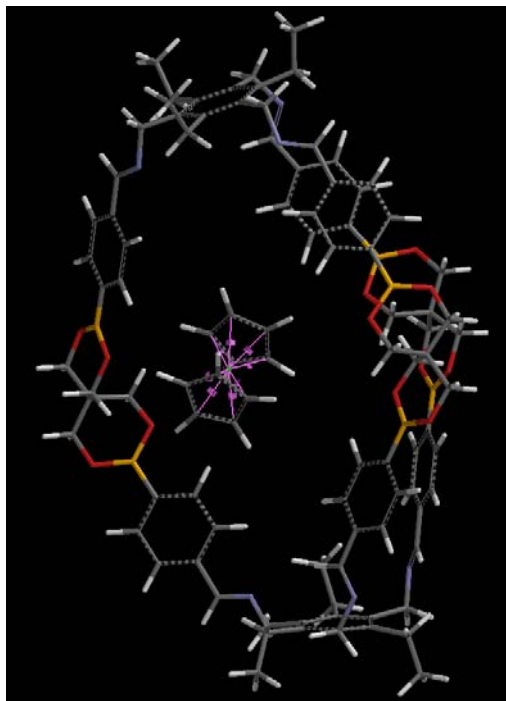


**Figure 24.** *Spartan modelling of ferrocene inclusion into the cage.*

The synthesis of the cage was performed using the same procedure described above, and adding into the ball mill also  $\text{Y}(\text{hfac})_3 \cdot 2\text{H}_2\text{O}$  as guest. The stability of the Yttrium complex under the high milling strength conditions was explored before, confirming its resistance for chosen conditions. A 3:6:2:1 stoichiometric mixture of pentaerythritol, 4-formylphenylboronic acid, 1,3,5-triaminomethyl-2,4,6-triethylbenzene and  $\text{Y}(\text{hfac})_3(\text{H}_2\text{O})_2$  was mixed together in the ball mill jar. Different conditions of time and frequency were tested. In all the cases the product recovered was the empty cage. Both ESI-MS and  $^1\text{H}$  NMR characterization showed no inclusion of the Yttrium complex.

Following the unsuccessful approach with compound **9**, our attention turned to cavitand-based molecular containers.<sup>31,32,35</sup> In 2007, the group of Warmuth reported the formation of a sphere-shaped molecular container formed by four, six and eight tetraformyl cavitands linking together through amino aliphatic

spacers. In particular, the scaffold formed by six cavitands linked together by twelve di-aminoaliphatic chains is the thermodynamic favourite product, and it is obtained with 90% yield (Figure 25).<sup>43</sup> In their study, the researchers demonstrated the capability of this macromolecule to form 1:1 and 2:1 complexes with  $R_4N^+Br^-$  salts ( $R = n$ -pentyl,  $n$ -hexyl,  $n$ -heptyl) in organic solvents.<sup>44</sup>

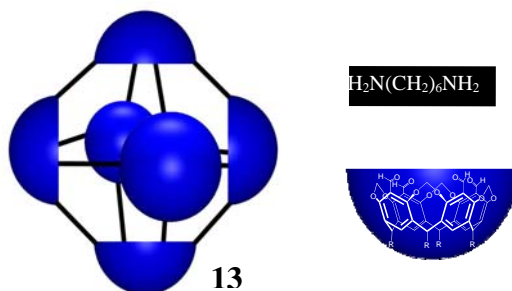
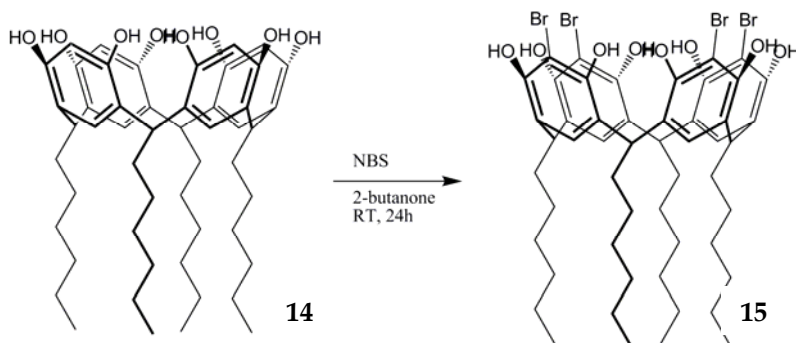


**Figure 25.** The molecular container formation employing tetraformyl cavitand (blue) and diamino linker (black).

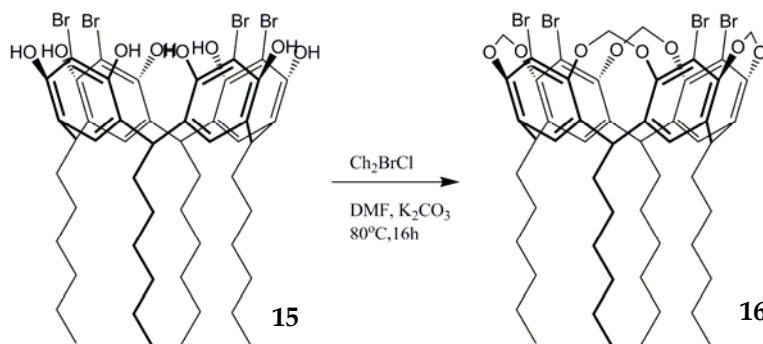
For this reason we decided to use the same scaffold for our La complexes inclusion experiments. The tetraformyl cavitand was synthesized in 4 steps starting from the synthesis of resorcinarene **14** following the standard procedure described previously. The apical position tetra bromination of **15** was performed in 2-butanone using freshly crystallized NBS as brominating reagent (Scheme 3).



**Scheme 3.** Cavitand bromination in apical position.

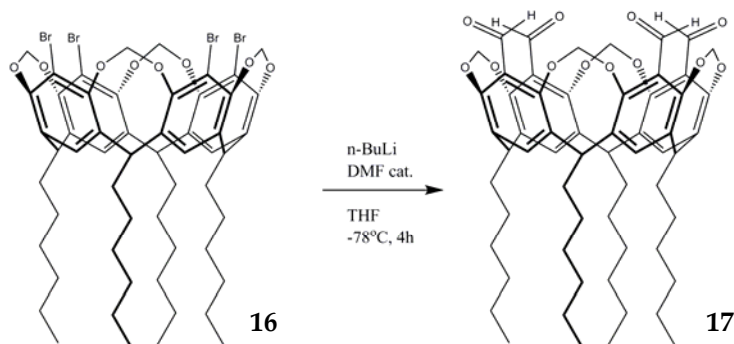
The reaction was carried under anhydrous Ar conditions at room temperature for 24 hrs. The reaction was quenched in water and the obtained precipitate was purified by filtration, fully characterised and used directly in the next step.

The bridging reaction was performed under dry conditions. Resorcinarene **15** was reacted at 80°C with BrCH<sub>2</sub>Cl in presence of K<sub>2</sub>CO<sub>3</sub> as a base and DMF as solvent for 16 hrs (Scheme 4). Cavitant **16** was obtained in excellent yield (92%) after purification by flash column chromatography.



**Scheme 4.** *Synthesis of cavitant 16.*

Formylation reaction was performed employing a well-known procedure based on the use of n-BuLi (Scheme 5). Being this reaction exothermic, the addition of n-BuLi was performed at very low temperature, to avoid destruction of the desired cavitant. The THF solution of cavitant **16** was stirred at -78°C, and a solution of n-BuLi in hexane was added dropwise. The reaction was stirred for 30 min at -78°C and additional 16 hrs at room temperature. The reaction was quenched by addition of a 5% solution of NH<sub>4</sub>Cl, extracted with EtOAc and the product was purified by flash column chromatography. **17** was obtained in good yield and characterized via <sup>1</sup>H NMR and ESI-MS.



**Scheme 5.** Synthesis of the tetraformyl cavitand **17**.

The cage synthesis was performed in absence of solvent using the procedure described before for the formation of cage **9**. The tetraformyl cavitand **17** was reacted with 1,6-diaminohexane into the ball mill jar for 1h at 40Hz, under argon atmosphere. Unfortunately, in spite several attempts, we were not able to synthesise the desired cage. No evidence of the molecular container formation was detected neither by  $^1\text{H}$  NMR or ESI-MS spectrometry. The unreacted cavitand and linker were recovered. Probably the absence of a condensation initiator like TFA<sup>41</sup> precludes the cage formation.

## 5.4. Conclusions.

The goal of this study was the self-assembly of supramolecular cages incorporating luminescent lanthanide complexes. Potentially, the inclusion into cages could change the luminescent properties of the lanthanide complexes, enhancing their stability and emission. So far, the only way to control guest inclusion in cavitand-based coordination cages and capsules is based on solvation, provided that the guest can fit into the inner cavity. In general, if the guest is poorly solvated by the chosen solvent it will prefer to be included, otherwise the cavity will be filled by the solvent. Since the chosen lanthanide complexes to be included do not present specific groups on the periphery suitable for specific binding by the cavity, we decided to play with the solvent effect to induce guest inclusion.



Several approaches have been undertaken along this line:

1. The use of a water soluble cavitand-based capsules held together by hydrophobic interactions. For this purpose we decided to use the water soluble cavitand capsule **1**. This capsule is water soluble only under basic conditions, because the water solubilizing groups are carboxylates at the periphery of the capsule. Since the inner cavity of **1** is hydrophobic, the driving force for encapsulation would have been the hydrophobicity of the lanthanide complexes, which should prefer capsule inclusion to water solvation. In silico modelling provided evidence of the possible inclusion of lanthanide complexes into such capsules. Despite the large effort carried out in this direction, we were unable to encapsulate any luminescent guest inside the water soluble cage, mainly because of the instability of the Ln complexes in water.

2. Solid state studies were performed using mono-, di- and tetraphosphonate cavitands as ligands for inorganic and organic lanthanide complexes. Many attempts to growth crystals of the desired coordination complexes were made, employing different Ln complexes and solvents under various crystallization conditions. Unfortunately, in all attempts, only the free di- or tetraphosphonate cavitands were obtained, proving their inefficiency as ligands for lanthanide complex coordination.

3. Since the first approach turned out to be unfeasible due to the instability of luminescent Ln complexes in solution, we turned our attention to solvent free inclusion using cages **9** and **13**. The idea behind this approach is to facilitate the inclusion of the lanthanide complexes during the preparation of the covalent cages in a solvent free environment, so to avoid solvent competition for the cavity. Cage **9** was prepared under ball mill reaction conditions. With this procedure, the cage assembly was performed in the presence of different lanthanide complexes. No inclusion of the lanthanide guest was ever observed. The synthesis of cage **13** under the same ball mill reaction conditions turned out to be unsuccessful, probably due to the absence of a condensation initiator.

## **5.5. Acknowledgements.**

Special thanks to Dr. Chiara Massera (University of Parma, Italy) for X-Ray studies, to Prof. Bruce Gibb (Tulane University, New Orleans, USA) for providing the cavitand, to Prof. Marek Pietraszkiewicz (Polish Academy of Science, Warsaw) for the synthesis of luminescent complexes, to Prof. Franco Uguzzoli (University of Parma, Italy) for the computer modelling simulations.

## 5.6. Experimental section.

**General Methods.** All commercial reagents were ACS reagent grade and used as received. Solvents were dried and distilled using standard procedures.  $^1\text{H}$  NMR spectra were recorded on Bruker Avance 300 (300 MHz), the  $^1\text{H}$  NMR and  $^{31}\text{P}$  NMR spectra were recorded on Bruker Avance 400 (400 MHz) spectrometers. All chemical shifts ( $\delta$ ) were reported in parts per million (ppm) relative to proton resonances resulting from incomplete deuteration of NMR solvents.  $^{31}\text{P}$  NMR spectra were recorded on Avance 400 (162 MHz) and all chemical shifts were reported to external 85%  $\text{H}_3\text{PO}_3$  at 0 ppm. Electrospray ionization mass spectrometry (ESI-MS) experiments were performed on a Waters ACQUILITY UPLC SQ Detector. The solvent free reactions were performed in FRITSCH Mini-Mill PULVERISETTE 23 ball mill apparatus using stainless steel 15 mL grinding jar equipped with five stainless steel balls (1cm  $\varnothing$ ).

The octaacid cavitand **1** was kindly provided by Prof. B. Gibb; for the synthesis see ref: 30 and 31.

For the synthesis of the cavitands **2** (A, B, C and D) and **3** (A, B, C, D, E and F) see ref 40.

### Cavitand Tiiii [ $\text{H}$ , $\text{CH}_3$ , $\text{CH}_3$ ] (**4**)

Dichloromethylphosphate (1.46 mL, 16.17 mmol) and N-methylpyrrolidine (432  $\mu\text{L}$ , 4.15 mmol) were added, under nitrogen, to a suspension of resorcinarene (2.0 g, 3.67 mmol) in 100 mL of anhydrous dichlorobenzene. The mixture was stirred at 140°C for 24 hours. After evaporation of the solvent, the crude product was purified by flash-column chromatography to give the desired compound as white solid (0.81 g, 28%).

$^1\text{H}$  NMR ( $\text{CDCl}_3/\text{MeOD}$ , 300 MHz):  $\delta$  (ppm) 1.81 (d, 12H,  $J=6.8$  Hz,  $\text{POCH}_3$ ), 1.98 (s, 12H,  $\text{ArCH}_3$ ), 3.36 (d, 4H,  $J=7.1$  Hz,  $\text{Ar}_2\text{CH}_{2ax}$ ), 4.19 (d, 4H,  $J=7.2$  Hz,  $\text{ArCH}_{2eq}$ ), 6.99 (s, 4H,  $\text{ArH}_{down}$ )

**<sup>31</sup>P NMR** (CDCl<sub>3</sub>/MeOD, 162 MHz):  $\delta$  (ppm) 22.03 (s, 4P, POCH<sub>3</sub>). **ESI-MS**: m/z 785.3 [M+H]<sup>+</sup>

### **Cavitand Tiiii [C<sub>3</sub>H<sub>7</sub>, H, Ph] (5)**

Resorcinarene [C<sub>3</sub>H<sub>7</sub>, H] (517 mg, 0.80 mmol) was dissolved in freshly distilled pyridine (20 mL), and the dichlorophenylphosphine (0.447 mL, 3.39 mmol) was added slowly, at room temperature. After 3 hours of stirring at 80°C, the solution was allowed to cool to RT; then a solution of 35% H<sub>2</sub>O<sub>2</sub> (8 mL) and CHCl<sub>3</sub> (1:1) was added. The mixture was stirred for 30 minutes at room temperature and the solvent was removed under reduced pressure. The water was added, and the precipitate was filtered and purified by flash column chromatography. The product was obtained as a fine white powder with a yield of 95%.

**<sup>1</sup>H NMR** (300 MHz, CDCl<sub>3</sub>):  $\delta$  (ppm) 1.04 (t, 12H, J = 7.4 Hz, CH<sub>2</sub>CH<sub>2</sub>CH<sub>3</sub>), 1.41 (m, 8H, CH<sub>2</sub>CH<sub>2</sub>CH<sub>3</sub>), 2.34-2.20 (m, 8H, CH<sub>2</sub>CH<sub>2</sub>CH<sub>3</sub>), 4.81 (t, 4H, J = 7.4 Hz, ArCH), 6.51 (s, 4H, ArH<sub>up</sub>), 7.13 (s, 4H, ArH<sub>down</sub>), 7.52 (m, 8H, POArH<sub>m</sub>), 7.61 (m, 4H, POArH<sub>p</sub>), 8.09 (m, 8H, POArH<sub>o</sub>).

**<sup>31</sup>P NMR** (162 MHz, CDCl<sub>3</sub>)  $\delta$  (ppm): 4.02 (s, 4P).

**ESI-MS**: m/z 1167.3 [M+Na]<sup>+</sup>.

### **Lanthanum, Europium, Terbium Picrate complexes (6, 7 and 8)**

**General procedure:** Ln<sub>2</sub>O<sub>3</sub> (1.42 mmol) was dissolved into an aqueous solution of HCl 5N. The solution was evaporated to dryness, the residue taken up in water (40 mL) and dissolved into a solution of NaOH 2N. After vigorous stirring, a gelatinous precipitate was formed. The precipitate was filtered and thoroughly washed with water. The solid was then suspended in water and stirred at 80°C. A water suspension of picric acid (8.52 mmol) was added into the hot slurry in small portions till almost completely dissolved. A saturated solution of picric acid in water (5 mL) was then added in order to dissolve the last traces of Ln<sub>2</sub>O<sub>3</sub>. The hot solution was stirred for 15 minutes and then filtered. The obtained solution was acidified to pH 4 by adding a saturated aqueous solution of picric acid. The final solution was cooled in an ice bath to facilitate the crystallization of the final product. The yellowish elongated crystalline plates were filtered and washed first by ice-cold water and then by 3

portions ( 10 mL) of dichloromethane. The crystals were left to dry on air for 2 days. Yield 60%.

**6 - ESI-MS:** La(pic)<sub>3</sub> · 6H<sub>2</sub>O - m/z 968 [M+K]<sup>+</sup>

**7 - ESI-MS:** Eu(pic)<sub>3</sub> · 9H<sub>2</sub>O - m/z 521 [M+2Na]<sup>+</sup>

**8 - ESI-MS:** Tb(pic)<sub>3</sub> · 11H<sub>2</sub>O - m/z 1027 [M+2K+H]<sup>+</sup>

### Ball Mill cage (9)

1,3,5-triaminomethyl-2,4,6-triethylbenzene (0,233 mmol), 4-formylphenylboronic acid (0.7 mmol) and pentaerythritol (0,350 mmol) were placed into an oven-dried stainless-steel grinding jar and reacted for 1h at 20 Hz. After cooling down to RT, the residue was transferred into a flask, dried under vacuum at 80°C for 2h and extracted 3 times by dry CHCl<sub>3</sub> (3x5 mL). The product was obtained as pink solid with a yield of 90%..

**<sup>1</sup>H-NMR** (400 MHz, CDCl<sub>3</sub>): δ (ppm) 1.30 (t, 18H, CH<sub>3</sub>CH<sub>2</sub>Ar, *J*= 7.3Hz), 2.71 (q, 12H, CH<sub>3</sub>CH<sub>2</sub>Ar, *J*= 7.4 Hz), 4.06 (s, 24H, CCH<sub>2</sub>O), 4.99 (s, 12H, NCH<sub>2</sub>Ar), 7.70 (d, 12H, *J*= 7.7 Hz, phenyl), 7.82 (d, 12H, *J*= 7.9 Hz, phenyl), 8.15 (s, 6H, imine)

**ESI-MS:** m/z 752 [M+H+Na]<sup>2+</sup>

### 1,3,5-tribromomethyl-2,4,6-triethylbenzene (10)

Zn (6,11 mmol) powder was suspended into AcOH (160 mmol) and a solution of HBr in AcOH (33%, 44 mmol) was added dropwise in 30 min. The mixture was stirred until the Zn powder was dissolved. Successively, 1,3,5-triethylbenzene (6,12 mmol), paraformaldehyde (66 mmol) and HBr in AcOH (33%, 130 mmol) were added and the mixture was heated at 90°C for 48h. After two days, the reaction was cooled down to RT. A white precipitate was formed. The solid was filtrated, washed with water and dried under vacuum. The product was obtained with a yield of 40%.

**<sup>1</sup>H-NMR** (300 MHz, CDCl<sub>3</sub>): δ (ppm) 1.30 (t, 9H, CH<sub>3</sub>CH<sub>2</sub>Ar, *J*= 7.6 Hz), 2.92 (q, 6H, CH<sub>3</sub>CH<sub>2</sub>Ar, *J*= 7.6 Hz), 4.54 (s, 6H, BrCH<sub>2</sub>Ar)

**ESI-MS:** m/z 460 [M+Na]<sup>+</sup>

Mp. 151°C

**1,3,5-triazidomethyl-2,4,6-triethylbenzene (11)**

To a solution of 1,3,5-tribromomethyl-2,4,6-triethylbenzene (2,26 mmol), in DMF (25 mL) the  $\text{NaN}_3$  (13,5 mmol) was added in small portions over 30 min. The mixture was stirred for 24h at RT. The reaction was quenched by addition of DCM and the excess of  $\text{NaN}_3$  was filtered off through celite. The organic phase was washed with  $\text{H}_2\text{O}$ , dried over  $\text{Na}_2\text{SO}_4$ , filtered, and dried under reduced pressure. **11** was collected as a white solid with a yield of 80%.

$^1\text{H-NMR}$  (300 MHz,  $\text{CDCl}_3$ ):  $\delta$  (ppm) 1.20 (t, 9H,  $\text{CH}_3\text{CH}_2\text{Ar}$ ,  $J= 7.6$  Hz), 2.83 (q, 6H,  $\text{CH}_3\text{CH}_2\text{Ar}$ ,  $J= 7.6$  Hz), 4.46 (s, 6H,  $\text{N}_3\text{CH}_2\text{Ar}$ )

**ESI-MS:**  $m/z$  350  $[\text{M}+\text{Na}]^+$

Mp. 60°C

**1,3,5-triaminomethyl-2,4,6-triethylbenzene (12)**

1,3,5-triazidomethyl-2,4,6-triethylbenzene (1 mmol) was dissolved in absolute ethanol (25 mL) and placed into a hydrogenation flask and 1 spatula of Pd/C was added successively. The reactor was placed in a Parr apparatus under  $\text{H}_2$  atmosphere (3bar) and the solution was mixed for 12h. Afterwards, the reaction was filtered through celite to remove unreacted Pd/C and the solvent was removed under reduced pressure affording quantitatively the desired product **12**.

$^1\text{H-NMR}$  (300 MHz,  $\text{CDCl}_3$ ):  $\delta$  (ppm) 1.24 (t, 9H,  $\text{CH}_3\text{CH}_2\text{Ar}$ ,  $J= 6.9$  Hz), 1.43 (bs, 9H,  $\text{NH}_2\text{CH}_2\text{Ar}$ ), 2.86 (q, 9H,  $\text{CH}_3\text{CH}_2\text{Ar}$ ,  $J= 6.9$  Hz), 3.87 (s, 6H,  $\text{NH}_2\text{CH}_2\text{Ar}$ )

**ESI-MS:**  $m/z$  272  $[\text{M}+\text{Na}]^+$

Mp. 130°C

For the synthesis of resorcinarene  $[\text{C}_6\text{H}_{13}, \text{H}]$  (**14**) see Chapter 2.

**Resorcinarene  $[\text{C}_6\text{H}_{13}, \text{Br}]$  (15)**

Resorcinarene  $[\text{C}_6\text{H}_{13}, \text{H}]$  (5,1mmol) was dissolved in 2-butanone (30 mL) into an oven-dried three-necked round bottomed flask equipped with a thermometer and the mixture was cooled in an ice-bath to 5°C. NBS was added in small portions over 30 min at a temperature below 10°C and the flask was covered by aluminium sheet and stirred for 16h at RT. The mixture was

quenched by water and the precipitate was filtered, washed with water and dried under vacuum. The product was obtained as a white solid with a yield of 40%.

$^1\text{H-NMR}$  (400 MHz,  $\text{DMSO-}d_6$ ):  $\delta$  (ppm) 0.83 (t, 12H,  $\text{CH}_3\text{CH}_2\text{CH}_2$ ,  $J= 6.5$  Hz), 1.18-1.33 (m, 32H,  $-\text{CH}_2-$ ), 2.15 (q, 8H,  $\text{CH}_2\text{CHAr}$ ,  $J= 6.8$  Hz), 4.35 (t, 8H,  $\text{CH}_2\text{CHAr}$ ,  $J= 7.6$  Hz), 7.34 (s, 4H,  $\text{ArH}_{\text{down}}$ ), 9.08 (s, 8H,  $\text{ArOH}$ )

**ESI-MS:**  $m/z$  1169  $[\text{M}+\text{Na}]^+$

### **MeCav** [ $\text{C}_6\text{H}_{13}$ , Br] (**16**)

Product **10** (0.87 mmol) was dissolved in dry DMF (25 mL) in an oven dried schlenk under Ar atmosphere and  $\text{K}_2\text{CO}_3$  (8,77 mmol) and  $\text{CH}_2\text{Br}_2$  (4,35 mmol) were added. The mixture was stirred at  $90^\circ\text{C}$  for 16h. The reaction was cooled to RT, quenched by  $\text{H}_2\text{O}$ , filtered and dried under vacuum. The collected solid was purified by flash chromatography obtaining the desired product as a white solid with a yield of 92%.

$^1\text{H-NMR}$  (400 MHz,  $\text{CDCl}_3$ ):  $\delta$  (ppm) 0.89 (t, 12H,  $\text{CH}_3\text{CH}_2\text{CH}_2$ ,  $J= 7.2$  Hz), 1.32-1.57 (m, 32H,  $-\text{CH}_2-$ ), 2.23 (q, 8H,  $\text{CH}_2\text{CHAr}$ ,  $J= 6.9$  Hz), 4.42 (d, 4H,  $\text{CH}_2\text{OAr}$ ,  $J= 7.2$  Hz), 4.84 (t, 4H,  $\text{CH}_2\text{CHAr}$ ,  $J= 8$  Hz), 5.97 (d, 4H,  $\text{CH}_2\text{OAr}$ ,  $J= 7.2$  Hz), 7.05 (s, 4H,  $\text{ArH}_{\text{down}}$ )

**ESI-MS:**  $m/z$  1223  $[\text{M}+\text{K}]^+$

### **MeCav** [ $\text{C}_6\text{H}_{13}$ , COH] (**17**)

Compound **11** (0.42 mmol) was dissolved in THF (10 mL), cooled to  $-78^\circ\text{C}$  a 2.5 M solution of  $n\text{-BuLi}$  in hexane (2,52 mmol) was added dropwise and the reaction was stirred for 20 min. The mixture was warmed up to  $0^\circ\text{C}$  and stirred for an additional 30 min. The ice-bath was successively replaced by an acetone bath and dry DMF (16,8 mmol) was added into the reaction leaving it at  $-78^\circ\text{C}$  for 10 min. Afterwards, the reaction was warmed to RT and stirred for 1h. The reaction was quenched by a 5% solution of  $\text{NH}_4\text{Cl}$  and extracted with  $\text{EtOAc}$  (2x). The organic fraction collected was washed with saturated  $\text{NaHCO}_3$  (1x), brine (1x), dried over  $\text{MgSO}_4$  and the solvent was removed under reduced pressure. The crude was purified by flash chromatography leading to the desired product with a yield of 50%

<sup>1</sup>H-NMR (400 MHz, CDCl<sub>3</sub>): δ (ppm) 0.93 (t, 12H, CH<sub>3</sub>CH<sub>2</sub>CH<sub>2</sub>, J= 6.6Hz), 1.26-1.46 (m, 32H, -CH<sub>2</sub>-), 2.26 (q, 8H, CH<sub>2</sub>CHAr, J= 6.7Hz), 4.48 (d, 4H, CH<sub>2</sub>OAr, J= 7.5Hz), 4.92 (t, 4H, CH<sub>2</sub>CHAr, J= 8.1Hz), 5.93 (d, 4H, CH<sub>2</sub>OAr, J= 7.5Hz), 7.3 (s, 4H, ArH<sub>down</sub>), 10.27 (s, 4H, HCAr)

ESI-MS: m/z 1006 [M+Na]<sup>+</sup>

### Container 13

Cavitand [C<sub>6</sub>H<sub>13</sub>, COH, CH<sub>2</sub>] (**18**) (0.203 mmol) and 1,6-diaminohexane (0.40 mmol) were placed into an oven-dried stainless-steel grinding jar and reacted for 1h at 20 Hz. After cooling down to RT, the residue was transferred into a flask, dried under vacuum at 80°C for 2h and extracted 3 times by dry CHCl<sub>3</sub> (3x5 mL). The product was not isolated. Only the unreacted cavitand **18** and the diaminohexane linker were detected.



## 5.7 References.

---

- <sup>1</sup> Valeur, B.; Berberan-Santos, M. N. J. *Chem. Educ.* **2011**, 731.
- <sup>2</sup> Valeur, B. *Molecular Fluorescence. In Encyclopædia of Applied Spectroscopy*, Wiley-VCH: Weinheim, **2009**; 477.
- <sup>3</sup> a) Dong, Y. B.; Wang, P.; Ma, J. P.; Zhao, X. X.; Wang, H. Y.; Tang, B.; Huang, R. Q. *J. Am. Chem. Soc.* **2007**, 129, 4872; b) Sabbatini, N.; Guardigli, M.; Manet, I.; Ungaro, R.; Casnati, A.; Ziesel, R.; Ulrich, G.; Asfari, Z.; Lehn, J.-M. *Pure Appl. Chem.* **1995**, 67, 135.
- <sup>4</sup> Braslavsky, S. E. *Glossary of Terms used in Photochemistry, 3rd edition (IUPAC recommendations 2006)*, *Pure Appl. Chem.* **2007**, 79, 293-465.
- <sup>5</sup> a) Freed S. *Phys. Rev.*, **1931**, 38, 2122.; b) Tomaschek R, *Physik. Z.* **1932**, 33, 878.; c) van Vleck, J. H. J. *Phys. Chem.* **1937**, 41, 67.
- <sup>6</sup> Dieke, G. H. *Spectra and energy levels of rare earth ions in crystals*, Interscience Publishers, New York **1968**.
- <sup>7</sup> a) Kleinerman, M., *J. Chem. Phys.* **1969**, 51, 2370.; b) Kleinerman, M.; Choi Sang-I. *J. Chem. Phys.* **1968**, 49, 3901.; c) Bakker, B. H.; Goes, M.; Hoebe, N.; van Ramesdonk, H. J.; Verhoeven, J. W.; Werts, M. H. V.; Hofstraat, J. W. *Coord. Chem. Rev.* **2000**, 208, 3.; d) Blasse, G. *Struct. Bonding* **1976**, 26, 45.
- <sup>8</sup> Chen, F. F.; Bian, Z. Q.; Liu, Z. W.; Nie, D. B.; Chen Z. Q.; Huang, C. H. *Inorg. Chem.* **2008**, 47, 2507.
- <sup>9</sup> Shinde, K. N. *Phosphate Phosphors for Solid State Lighting*, Springer-Verlag; Berlin, **2013**, 42.
- <sup>10</sup> Balzani, V. *Top Curr. Chem.*, Springer-Verlag; Berlin, **2007**, 1.

- <sup>11</sup> Camall, W.T. *Handbook on the Physics and Chemistry of Rare Earths*, Vol. 3, North-Holland, Amsterdam, **1979**, 171.
- <sup>12</sup> Sabbatini, N.; Guardigli, M.; Lehn, J.-M. *Coord. Chem. Rev.* **1993**, 123, 201.
- <sup>13</sup>a) Binnemans, K., et al. *Handbook on the Physics and Chemistry of Rare Earths* Elsevier: Amsterdam, **2005**; 35, 225, 107; b) de Sa, G. F.; Malta, O. L.; Donega, C. D.; Simas, A. M.; Longo, R. L.; Santa-Cruz, P. A.; da Silva, E. F. *Coord. Chem. Rev.* **2000**, 196, 165.; c) Yanagida, S.; Hasegawa, Y.; Murakoshi, K.; Wada, Y.; Nakashima, N.; Yamanaka, T. *Coord. Chem. Rev.* **1998**, 171, 461.
- <sup>14</sup>a) Melby, L. R.; Rose, N. J.; Abramson, E.; Caris, J. C. *J. Am. Chem. Soc.* **1964**, 86, 5117; b) Bauer, H.; Blanc, J.; Ross, D. L. *J. Am. Chem. Soc.* **1964**, 86, 5125.
- <sup>15</sup> a) Lenaerts, P.; Driesen, K.; Van Deun, R.; Binnemans, K. *Chem. Mater.* **2005**, 17, 2148.; b) van Bekkum, H., Flanigen, E. M., Jansen, J. C., Eds. *Introduction to Zeolite Science and Practice*; Elsevier: Amsterdam, **1991**.; c) Bekiari, V.; Lianos, P. *Adv. Mater.* **1998**, 10, 1455.; d) Xu, Q. H.; Li, L. S.; Li, B.; Yu, J. H.; Xu, R. R., *Microporous-Mesoporous Mater.* **2000**, 38, 351.
- <sup>16</sup> de Sa', G. F.; Nunes, L. H. A.; Wang Z.-M.; Chopin, G. R. *J. Alloys Comp.* **1993**, 196, 17.
- <sup>17</sup> Petoud, S.; Bunzli, J.-C. G.; Schlenk, K. J.; Piruet, C. *Inorg. Chem.* **1997**, 36, 1345.
- <sup>18</sup> Horrocks De Jr., W. W.; Bolender, P.; Smith, W. D.; Supkowski, R. M. *J. Am. Chem. Soc.* **1997**, 119, 5972.
- <sup>19</sup> Prodi, L.; Maestri, M.; Balzani, V.; Lehn, J.-M.; Roth, C. *Chem. Phys. Lett.* **1991**, 180, 45.
- <sup>20</sup> Alexander, V. *Chem. Rev.* **1995**, 95, 273.

- 
- <sup>21</sup> Smith, P. H.; Reyes, Z. E.; Lee, C.-W.; Raymond, K. N. *Inorg. Chem.* **1988**, *27*, 4154.
- <sup>22</sup> a) Sessler, J. L.; Murai, T.; Hemmi, G. *Inorg. Chem.* **1989**, *28*, 3390.; b) Sessler, J. L.; Mody, T. D.; Hemmy, G. W.; Lynch, V. *Inorg. Chem.* **1993**, *32*, 3175.
- <sup>23</sup> Delgado, R.; Frausto de Silva, J. J. R. *Talanta* **1982**, *29*, 850.
- <sup>24</sup> a) Desreux, J. F. *Inorg. Chem.* **1980**, *19*, 1319.; b) Cacheris, W. P.; Nickle, S. K.; Sherry, A. D. *Inorg. Chem.* **1987**, *26*, 958.; c) Loncin, M. F.; Desreux, J. F.; Merciny, E. *Inorg. Chem.* **1986**, *25*, 2646.
- <sup>25</sup> a) Aime, S.; Botta, M.; Ermondi, G.; Fedeli, F.; Uggeri, F. *Inorg. Chem.* **1992**, *31*, 1100.; b) Lazar, I.; Hrcir, D. C.; Kim, W.-D.; Kiefer, G. E.; Sherry, A. D. *Inorg. Chem.* **1992**, *31*, 4422.; c) Morrow, J. R.; Chin, K. O. A. *Inorg. Chem.* **1993**, *32*, 3357.
- <sup>26</sup> Ralpha, B.; Ballardini, R.; Balzan, V.; Lehn, J.-M.; Perathoner, S.; Sabbatini, N. *Photochem. And Photobiol.* **1990**, *52*, 299.
- <sup>27</sup> Prodi, L.; Maestri, M.; Balzani, V.; Lehn, J.-M.; Roth, C. *Chem. Phys. Lett.* **1991**, *180*, 45.
- <sup>28</sup> Bünzli, J.-C. G.; Froidevaux, P.; Harrowfield, J. M. *Inorg. Chem.* **1993**, *32*, 3306.
- <sup>29</sup> a) Hardie, M. J.; Johnson, J. A.; Raston, C. L.; Webb, H. R. *Chem. Commun.* **2000**, 849.; b) Drljaca, A.; Hardie, M. J.; Johnson, J. A.; Raston, C. L.; Webb, H. R. *Chem. Commun.* **1999**, 1135.
- <sup>30</sup> Gibb, C. L. D.; Gibb, B. C., *J. Am. Chem. Soc.* **2004**, *126*, 11408.
- <sup>31</sup> Kaanumalle, L. S.; Gibb, C. L. D.; Gibb, B. C.; Ramamurthy, V. *Org. Biomol. Chem.* **2007**, *5*, 236.

- <sup>32</sup>Natarajan, A.; Kaanumalle, L. S.; Jockusch, S.; Gibb, C. L. D.; Gibb, B. C.; Turro, N. J.; Ramamurthy, V. J. *Am. Chem. Soc.* **2007**, *129*, 4132.
- <sup>33</sup> Lui, S.; Gibb, B. C. *Chem. Comm.* **2008**, 3709.
- <sup>34</sup> Gibb, B. C. *Nano-capsules assembled by the hydrophobic effect, in Organic nanostructures*, John Wiley and Sons, New York, USA, **2007**.
- <sup>35</sup> Biju, S.; Reddy, M. L. P.; Cowley A. H.; Vasudevan, K. V. *Crystal Growth & Design* **2009**, *9*, 3562.
- <sup>36</sup> Melegari, M.; Massera, C.; Ugozzoli, F.; Dalcanale E., *CrystEngComm* **2010**, *12*, 2057.
- <sup>37</sup> Chun-Hui Huang, *Rare earth coordination chemistry*, Wiley, **2010**.
- <sup>38</sup> Pinalli, R.; Nachtigall, F. F.; Ugozzoli, F.; Dalcanale, E. *Angew. Chem. Int.* **1999**, *38*, 2377.
- <sup>39</sup> Dalcanale, E.; Jacopozi, P.; Ugozzoli, F.; Mann, G. *Supramol. Chem.* **1998**, *9*, 305.
- <sup>40</sup> Harrowfield, J. *JCS, Dalton Trans.* **1996**, *8*, 1687.
- <sup>41</sup> Harrowfield, J. M.; Lu, W. M.; Skelton, B. W.; White, A. H. *Aust. J. Chem.* **1994**, *47*, 321.
- <sup>42</sup> Severin, K. J. *Am. Chem. Soc.* **2009**, *131*, 3154.
- <sup>43</sup> Liu, H.; Warmuth, R. *Nature Protocols* **2007**, *5*, 1288.
- <sup>44</sup> Liu, H.; Liu, Y.; Warmuth, R. *Supramol. Chem.* **2008**, *1-2*, 41.



## Appendix A

### X-Ray data analysis

**Table Z1.** Crystallographic data and refinement details for **QxBox@benzene** and **QxBox@toluene**

	<b>QxBox@benzene</b> <b>2QxBox 13C<sub>6</sub>H<sub>6</sub> 3DMSO</b>	<b>QxBox@toluene</b> <b>QxBox C<sub>7</sub>H<sub>8</sub> 10DMSO</b>
Formula	C <sub>268</sub> H <sub>272</sub> N <sub>16</sub> O <sub>35</sub> S <sub>3</sub>	C <sub>119</sub> H <sub>156</sub> N <sub>8</sub> O <sub>26</sub> S <sub>10</sub>
Formula	4373.20	2435.12
Crystal system	Orthorhombic	Triclinic
Space group	<i>Pna21</i>	<i>P-1</i>
<i>a</i> /Å	35.074(2)	13.8189(6)
<i>b</i> /Å	17.240(1)	20.9182(9)
<i>c</i> /Å	38.079(2)	22.3304(9)
α/°	-	82.233(1)
β/°	-	78.896(1)
γ/°	-	83.447(1)
<i>V</i> /Å <sup>3</sup>	23025(2)	6250.2(5)
<i>Z</i>	4	2
<i>D<sub>c</sub></i> /g cm <sup>-3</sup>	1.262	1.294
<i>F</i> (000)	9280	2588
μ/mm <sup>-1</sup>	0.109	0.249
θ <sub>min,max</sub> /°	1.07, 26.45	0.94, 28.76
Reflections	258223	91044
Independent	47230 (Rint = 0.0757)	32404 (Rint = 0.0363)
Observed	29493	21241
Data/restr./pa	47230 / 13 / 2433	32404 / 1 / 1448
<i>R</i> [Fo>4σ(Fo)] <sup>a</sup>	0.0983	0.0749
w <i>R</i> <sub>2</sub> <sup>a</sup>	0.1369	0.2358
Δρ <sub>min,max</sub> /e Å <sup>-3</sup>	-0.736, 1.122	-0.866, 2.128
<i>S</i> <sup>b</sup>	1.036	1.020

<sup>a</sup>*R*<sub>1</sub> = Σ || Fo| - |Fc|| / Σ|Fo|, w*R*<sub>2</sub> = [Σ w(Fo<sup>2</sup>-Fc<sup>2</sup>)<sup>2</sup> / ΣwFo<sup>4</sup>]<sup>1/2</sup>. <sup>b</sup>Goodness-of-fit *S* = [Σw(Fo<sup>2</sup>-Fc<sup>2</sup>)<sup>2</sup> / (n-p)]<sup>1/2</sup>, where *n* is the number of reflections and *p* the number of parameters.

**Table Z2.** Crystallographic data and refinement details for **QxBox@o-xylene** and **QxBox@p-nitrotoluene**

	<b>QxBox@o-xylene</b> <b>QxBox C<sub>8</sub>H<sub>10</sub> ·10DMSO</b>	<b>QxBox@p-nitrotoluene</b> <b>QxBox C<sub>7</sub>H<sub>7</sub>NO<sub>2</sub> ·10DMSO</b>
Formula	C <sub>120</sub> H <sub>158</sub> N <sub>8</sub> O <sub>26</sub> S <sub>10</sub>	C <sub>119</sub> H <sub>155</sub> N <sub>9</sub> O <sub>28</sub> S <sub>10</sub>
Formula	2449.14	2480.12
Crystal	Triclinic	Triclinic
Space group	<i>P</i> -1	<i>P</i> -1
<i>a</i> /Å	13.831(1)	13.782(2)
<i>b</i> /Å	20.861(2)	21.118(3)
<i>c</i> /Å	22.329(2)	22.256(3)
α/°	82.246(1)	82.608(3)
β/°	78.873(1)	80.567(3)
γ/°	83.335(1)	83.776(3)
<i>V</i> /Å <sup>3</sup>	6236.7(9)	6311.(2)
<i>Z</i>	2	2
<i>D<sub>c</sub></i> /g cm <sup>-3</sup>	1.304	1.305
<i>F</i> (000)	2604	2632
μ/mm <sup>-1</sup>	0.250	0.249
θ <sub>min,max</sub> /°	0.94, 28.37	0.98, 24.86
Reflections	88528	11151
Independent	31077 ( <i>R</i> <sub>int</sub> = 0.0419)	21793 ( <i>R</i> <sub>int</sub> = 0.0550)
Observed	19961	13545
Data/restr./p	31077 / 0 / 1458	21793 / 0 / 1491
<i>R</i>	0.0736	0.0746
w <i>R</i> <sub>2</sub> <sup>a</sup>	0.2301	0.2126
Δρ <sub>min,max</sub> /e Å <sup>-3</sup>	-1.355, 1.789	-0.288, 0.423
<i>S</i> <sup>b</sup>	1.081	1.031

<sup>a</sup>*R*<sub>1</sub> = Σ || *F*<sub>o</sub>|-|*F*<sub>c</sub>||/Σ|*F*<sub>o</sub>|, w*R*<sub>2</sub> = [Σ w(*F*<sub>o</sub><sup>2</sup>-*F*<sub>c</sub><sup>2</sup>)<sup>2</sup>/ Σw*F*<sub>o</sub><sup>4</sup>]<sup>1/2</sup>. <sup>b</sup>Goodness-of-fit *S* = [Σw(*F*<sub>o</sub><sup>2</sup>-*F*<sub>c</sub><sup>2</sup>)<sup>2</sup>/ (*n*-*p*)]<sup>1/2</sup>, where *n* is the number of reflections and *p* the number of parameters.

**Table Z3.** Crystallographic data and refinement details for **QxCage@benzene** and **MeQxBox@benzene**

	<b>QxCage@benzene</b> <b>QxCage C<sub>6</sub>H<sub>6</sub></b>	<b>MeQxBox@benzene</b> <b>MeQxBox 2C<sub>6</sub>H<sub>6</sub> ·CHCl<sub>3</sub></b>
Formula	C <sub>98</sub> H <sub>94</sub> N <sub>8</sub> O <sub>16</sub>	C <sub>101</sub> H <sub>93</sub> N <sub>8</sub> O <sub>36</sub> Cl <sub>3</sub>
Formula	1639.81	1781.18
Crystal system	Triclinic	Triclinic
Space group	<i>P</i> -1	<i>P</i> -1
<i>a</i> /Å	14.133(1)	15.781(1)
<i>b</i> /Å	14.130(1)	16.535(1)
<i>c</i> /Å	21.787(2)	17.268(1)
α/°	103.903(2)	93.524(2)
β/°	103.877(2)	98.392(2)
γ/°	94.547(2)	100.530(2)
<i>V</i> /Å <sup>3</sup>	4056.6(6)	4364.5(5)
<i>Z</i>	2	2
<i>D<sub>c</sub></i> /g cm <sup>-3</sup>	1.342	1.355
<i>F</i> (000)	1732	1868
μ/mm <sup>-1</sup>	0.092	0.180
θ <sub>min,max</sub> /°	1.00, 24.49	1.20, 27.32
Reflections	13398	57191
Independent	13398 ( <i>R</i> <sub>int</sub> = 0.0000)	19622 ( <i>R</i> <sub>int</sub> = 0.0635)
Observed	10137	10200
Data/restr./pa	13398 / 0 / 1095	19622 / 0 / 1103
<i>R</i> [F <sub>o</sub> >4σ(F <sub>o</sub> )] <sup>a</sup>	0.0471	0.0683
w <i>R</i> <sub>2</sub> <sup>a</sup>	0.1083	0.1733
Δρ <sub>min,max</sub> /e Å <sup>-3</sup>	-0.394, 0.420	-0.588, 1.259
<i>S</i> <sup>b</sup>	1.050	1.024

<sup>a</sup>*R*<sub>1</sub> = Σ || F<sub>o</sub>|-|F<sub>c</sub>||/Σ|F<sub>o</sub>|, w*R*<sub>2</sub> = [Σ w(F<sub>o</sub><sup>2</sup>-F<sub>c</sub><sup>2</sup>)<sup>2</sup>/ ΣwF<sub>o</sub><sup>4</sup>]<sup>1/2</sup>. <sup>b</sup>Goodness-of-fit *S* = [Σw(F<sub>o</sub><sup>2</sup>-F<sub>c</sub><sup>2</sup>)<sup>2</sup>/ (*n*-*p*)]<sup>1/2</sup>, where *n* is the number of reflections and *p* the number of parameters.





## *The author*



- 08/1985 Born in Częstochowa, Poland.
- 09/2007 Bachelor in Biotechnology, Jan Długosz University in Częstochowa, Poland. Referent: Dr. M. Myga
- 02/2009-08/2009 Student Exchange with A.- C. Gaumont, ENSICAEN - University of Caen, France
- 09/2009 Master in Chemistry, Jan Długosz University in Częstochowa, Poland. Referent: Dr. J. Peszke
- 03/2010-12/2010 Post-Graduate Research, University of Parma, Italy. Advisor: Prof. E. Dalcanale
- 01/2010-12/2013 Doctoral Research with Prof. E Dalcanale University of Parma, Italy
- 09/2012 Research Exchange with Prof. D. Bonifazi University of Namur, Belgium

Parma, January 2014

Jakub Waldemar Trzciński